VOLUME CHANGE AND SWELLING PRESSURE OF EXPANSIVE CLAY IN THE CRYSTALLINE SWELLING REGIME

A Thesis presented to the Faculty of the Graduate School
University of Missouri

In Partial Fulfillment
of the Requirements for the Degree

Ph.D. Civil & Environmental Engineering

by
ALEXANDRA WAYLLACE
Dr. William Likos, Thesis Supervisor

MAY 2008

The undersigned, appointed by the Dean of the Graduate School, have examined the thesis entitled

VOLUME CHANGE AND SWELLING PRESSURE OF EXPANSIVE CLAY IN THE CRYSTALLINE SWELLING REGIME

Presented by Alexandra Wayllace

A candidate for the degree of Doctor of Philosophy of Civil & Environmental Engineering

And hereby certify that in their opinion it is worthy of acceptance.

_____

Professor William Likos

_____

Professor John Bowders

_____

Professor Erik Loehr

_____

Professor Stephen Anderson

_____

Professor Michael Underwood

To my family…

ACKNOWLEDGEMENTS

I would like to thank first and foremost my advisor, Dr. William Likos. His advice, guidance and support were invaluable throughout my graduate studies and in the completion of this research.

Thanks are also due to the other members of my graduate committee, Dr. John Bowders, Dr. Erik Loehr, Dr. Stephen Anderson, and Dr. Michael Underwood. They helped me analyze my research from different perspectives.

I would also like to thank the Civil & Environmental Division of Engineering of the University of Missouri-Columbia for supporting my studies during the major part of my graduate studies. Financial support was also provided by the American Chemical Society (Petroleum Research Fund) and the Portland Cement Association Education Foundation.

Special thanks are due to Mr. Robert Maytag for first giving me the opportunity to study in this country. Finally, I want to thank my family and friends for their continuous support and encouragement.

TABLE OF CONTENTS

LIST OF FIGURES

LIST OF TABLES

ABSTRACT

A significant amount of research has been carried out to characterize expansive clay behavior from either microstructural or macrostructural perspectives; however, there exists a current gap in our knowledge about the basic mechanisms that relate one structural level to another. This research works to fill the gap between our understanding of expansive clay behavior at a microstructural (particle and fabric scale) level with our understanding at the bulk (engineering) scale.

The main objectives of the work are: 1) to qualitatively examine how clay particle fabric, stress paths, water potential, and mineralogy affect the translation of crystalline interlayer swelling to bulk volume change and swelling pressure; 2) to quantify these effects by defining curves describing constitutive surfaces for the behavior of smectite in the crystalline swelling regime under free swell and constant strain (zero volume change) boundary conditions; 3) to interpret the experimental observations in the context of existing conceptual models, including the porosity evolution model (Likos & Lu, 2006) and the Barcelona Basic Model (BBM) (Gens & Alonso, 1992); and (4) to develop and evaluate a new conceptual model for examining microstructural changes in fabric associated with crystalline interlayer swelling.

Three types of clay were selected for testing: Na-smectite, Ca-smectite, and a Ca-exchanged form of the Na-smectite. Results obtained include: SEM imaging of Na and Ca smectite, void ratio as a function of compaction pressure, water vapor sorption isotherms, axial deformation vs. relative humidity (RH) during wetting and drying for free swelling boundary conditions, and swelling pressure vs. RH for constant strain boundary conditions.

Three scale-level porosities were identified; this work focused on the interaction between the interlayer (e_{IL}) and the inter-particle (e_{IP}) void spaces. Sorption isotherms follow a wavy behavior, with the steeper portions of the curve corresponding to the one and two layer hydration states. Bulk volume change and swelling pressure response reflected this behavior, especially for RH corresponding to the 1-to-2 hydration layer transition. Initial density has a significant effect on bulk volume change and swelling pressure for RH equal or greater than that corresponding to the second hydration layer; interlayer swelling for denser specimens is more effectively upscaled to bulk response. During the first layer transition, most of the crystalline swelling was absorbed into the inter-particle void space. Clay mineralogy and exchange cation identity are also important variables. Ca-smectite exhibits larger bulk volume changes and swelling pressures than Na-smectite for tests under the same stress conditions. For the Ca-exchanged smectite, the cation affects sorption response but it does not affect the volume change response. Hysteresis in the volume change response is more evident for denser specimens, and is larger for Na-smectite. Stress history is also an important factor. The ratio of macrostructural strains to microstructural strains ($\varepsilon^{P}_{VM}/\varepsilon_{vm}$) decreases with lower values of maximum past pressure (p_o) for all suction values during wetting; as suction decreases, the $\varepsilon^{P}_{VM}/\varepsilon_{vm}$ ratio is larger in magnitude, and it becomes more sensitive to p_o.

With better knowledge of how microstructural swelling translates to macroscopic behavior and what mechanisms and variables are important, the geotechnical engineering community will be more equipped to approach and resolve the several problems involving expansive clays. Likewise, numerous applications in industry can use expansive clays more effectively if quantitative values provide a guideline of what

combinations of normal stress, void ratio, and water content of a soil within the crystalline swelling regime have a significant effect in the soil performance.

CHAPTER I

INTRODUCTION

1.1 Background

Predicting volume change and swelling pressures in expansive clay minerals is of great importance for numerous engineering and industrial applications. Damage per year caused by expansive soils, for example, has been reported to cost more than all other natural hazards combined, including earthquakes, fires, floods, and tornadoes (Chen, 1988). In industry, engineered clay barriers used for waste disposal take advantage of the swelling properties of clays, their ability to self-seal, and their corresponding low conductivity to water and contaminants.

A significant amount of research has been conducted to characterize expansive clay behavior from both microstructural and macrostructural perspectives. Investigations of particle-scale dynamics and clay-water-electrolyte systems have contributed to the progress of studies at a microstructural scale. Techniques such as microscale imaging, X-ray diffraction (XRD), and others have enabled scientists to obtain insight into basic mechanisms related to the adsorption and desorption of water (and other sorbates) on mineral surfaces at the particle and sub-particle (mineral interlayer) scale. Macroscopic studies, on the other hand, have been primarily conducted for the purpose of expansive soil identification, classification, and hazard mitigation, and have primarily fallen within the purview of the geotechnical engineering community. Prediction methods for ground movements and swelling pressures are mostly empirical or semi-empirical (Hunt, 1986; Nolson & Miller, 1992), where most predictive methodologies are derived from experimental tests that are relatively easy and inexpensive. Studies developed in effort to

predict the swelling of clays include, for example, Warketin et. al. (1957), Kjellander et. al, (1988), Delville & Laszlo (1990), and Yong (1999), among many others.

While studies of expansive clay behavior exist at both the micro and macro scale, there are currently very few that address the inherent coupling between the micro- and macro-levels of scale. As a consequence, there exists a gap in our basic understanding of the mechanisms that relate one level of scale to another. Our basic understanding of how the microstructural (particle and interlayer scale) changes that occur when expansive clay minerals adsorb or desorb water translate, or "upscale," to corresponding changes in macroscopic behavior (swelling pressure, volume change) remains relatively poor.

Two basic types of swelling processes in expansive clay-water-ion systems have been identified: crystalline swelling and osmotic swelling (see Chapter 2). The former occurs at relatively low water content (less than ~20%) primarily as a consequence of the initial hydration of interlayer exchangeable cations. Swelling occurs as water enters the mineral interlayer as a sequence of successive molecular layers, which results in a step-wise separation of the interlayer for up to three or four layers of water. Osmotic swelling occurs at higher water contents and is associated with continuing interlayer separation that develops from movement of water into the interlayer due to the difference in ion concentration within the interlayer and within the bulk pore water. Interlayer separation proceeds beyond the three or four water layers associated with crystalline swelling, ultimately leading to partial or complete disassociation of the interlayers and the formation of a hydrated solid or gelled state.

The macroscopic volume change and swelling pressure behavior of expansive clay has been studied a great deal in the osmotic swelling regime (e.g., for specimens upon

complete inundation with water). Very few studies have investigated swelling behavior within the crystalline swelling regime. Bulk swelling pressures associated with crystalline swelling, however, have been measured to be as much as 13% of pressures associated with osmotic swelling for specimens confined at constant volume (Villar et. al, 2004), and thus may be significant. There is consequent motivation to better understand the crystalline swelling process in general, and how the microstructural volume changes associated with crystalline swelling translate to bulk volume changes and swelling pressures in particular.

With better knowledge of how microstructural swelling translates to macroscopic behavior and what mechanisms and variables are important, the geotechnical engineering community will be more equipped to approach and resolve the several problems involving expansive clays. Likewise, numerous applications in industry can use expansive clays more effectively if quantitative values provide a guideline of what combinations of normal stress, void ratio, and water content of a soil within the crystalline swelling regime have a significant effect in the soil performance.

1.2 Objectives

As illustrated on Figure 1.1, this research works to fill the gap between our understanding of swelling clays at a microstructural level with understanding of swelling clays at a macroscopic level. How do volume changes occurring on the interlayer scale upscale to volume change and swelling pressure for bulk particle systems? How do variables such as void ratio, compaction conditions, particle and pore fabric, confining conditions, initial conditions, pore fluid chemistry, and clay chemistry govern this

upscaling process? What models are available to quantify these effects? Specific objectives within this general framework that are addressed in this work are:

- To qualitatively examine how clay fabric, stress paths, water potential and mineralogy (exchange cation) affect the translation of interlayer swelling to macroscopic volume change and swelling pressure.
- To quantify these effects by obtaining functions describing constitutive surfaces for expansive clay behavior in the crystalline swelling regime under free swell and constant strain (zero volume change) boundary conditions.
- To interpret the experimental observations in the context of existing conceptual models, including the multi-scale porosity evolution model described by Likos & Lu (2006) and the Barcelona Basic Model (BBM) described by Gens & Alonso (1992).
- To develop and evaluate a new conceptual model for quantifying microstrucutral changes in fabric associated with crystalline interlayer swelling.

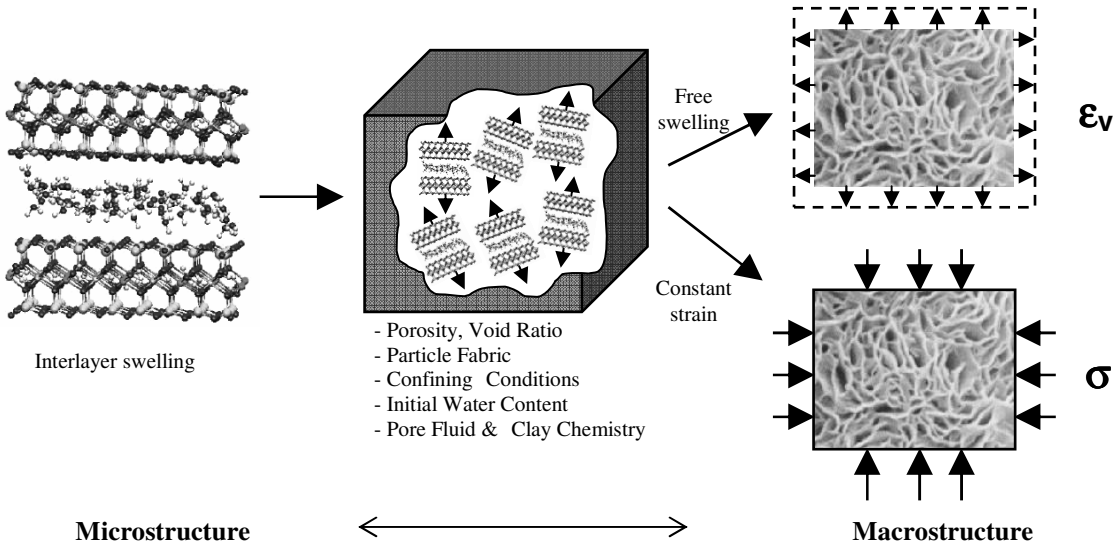

Figure 1.1. Translation of crystalline swelling to macroscopic volume change and swell pressure

1.3 Scope and organization of thesis

A comprehensive literature review was carried out and is summarized in Chapter II. The objective was to obtain a state of the art understanding of the microstructure of expansive clays, water-mineral interaction and water adsorption mechanisms, and the influences of clay fabric and stress paths on macroscopic swelling behavior. Existing conceptual frameworks for describing micro-macro fabric interactions in expansive clays were reviewed and used to help design the experimental portion of the research. These frameworks were subsequently considered to assist in the rationalization of patterns observed in previous investigations, and in the current experimental investigation.

Chapter III describes the methods and materials used in this study. Index properties, cation exchange capacity (CEC) and X-ray diffraction patterns for sodium and calcium smectite used in the experimental program are provided and analyzed. Specimen preparation (compaction of cylindrical "cakes") using a 1-D load frame is explained in detail. Experimental techniques were developed to quantify: gravimetric water content for different hydration levels, bulk volume change under free swelling conditions, and bulk swelling pressures for constant volume boundary conditions. Three experimental systems for testing under free swelling or constant strain boundary conditions are described. This includes an approach for measuring specimen volume change (axial strain) under free swell conditions in a controlled relative humidity (RH) environment using an osmotic (salt solution) control technique and approaches using two computer-controlled environmental chambers where volume change and/or swelling pressures can be measured under controlled RH for either a) free swelling, b) constant strain, or c) constant stress boundary conditions.

Results from the experimental portion are presented in Chapter IV. Scanning Electron Microscope (SEM) images, relationships between void ratio and compaction pressure, sorption isotherms, bulk volume change response as a function of RH and initial void ratio, and swelling pressures measured are presented. The primary experimental observations are summarized.

Interpretation of the experimental results in light of three conceptual models is presented in Chapter V. A new microstructural fabric model for upscaling interlayer volume changes is developed and evaluated using data obtained for specimens hydrated under free swelling conditions. A second conceptual framework (Likos and Lu, 2006) is considered to interpret interactions between interlayer and interparticle porosities for clays at different water potentials for both free swelling and constant strain boundary conditions. Finally, a third framework (Gens & Alonso, 1992) is considered to interpret macroscopic swelling behavior as a result of the stress paths for a specimen at both the microstructural and macrostructural levels. Chapter VI summarizes the conclusions obtained in this study and points to additional paths for future study.

CHAPTER II

LITERATURE REVIEW

Accomplishing the goals of this research requires a good understanding of the general structure of swelling clay minerals, short- and long-range water adsorption mechanisms, swelling mechanisms, and the influences of particle and pore fabric in swelling behavior. This chapter summarizes these aspects of expansive clays and reviews several previous studies that focus on the influences of clay mineralogy and clay fabric to bulk swelling behavior. Emphasis is placed on studies that have attempted to link the microstructure of hydrating clay mineral systems to their macroscopic swelling pressure and volume change response. Conceptual frameworks forming the basis of these studies, most notably the porosity evolution model described by Likos and Lu (2006) and the Barcelona Basic Model (BBM) described by Gens and Alonso (1992), are subsequently considered in Chapter VI to interpret the observations made during the present experimental investigation.

2.1. Smectite mineralogy

Most expansive soils contain minerals of the smectite group or vermiculite because only these minerals have an expandable interlayer and a specific surface area large enough to produce unsatisfied water adsorption forces in their naturally occurring state (Mitchell, 1993). Among swelling clays, combinations of sodium and calcium smectite are mostly studied because of their high natural occurrence and their relatively well-characterized nature. There exist both dioctahedral and trioctahedral varieties of smectite; each variety includes several specific minerals (montmorillonite, beidellite,

nontronite, saponite, etc). Materials used in this research are assumed to consist mainly of montmorillonite.

A schematic diagram of the structure of smectite is provided in Figure 2.1. An octahedral sheet is placed between two tetrahedral or silica sheets to form a 2:1 repeating lattice (Newman, 1987; Mitchell, 1993); the oxygens in the tips of the tetrahedra are common to the octahedra sheet as well, interconnecting both layers permanently. Silica tetrahedra ideally consist of silicon coordinated tetrahedrally with four oxygens, while the octahedral sheet is composed of aluminum ions coordinated octahedrally with six oxygens or hydroxyls. In smectites, isomorphous substitution for silicon or aluminum may take place (e.g., Mg^{2+} for Al^{3+} and Al^{3+} for Si^{4+}), which results in an electrical charge deficiency of 0.5 to 1.2 per unit cell, and cation exchange capacities ranging from 80 to 150meq/100g. To satisfy electrical neutrality, exchangeable cations such as Na or Ca are absorbed between the mineral layers in the pore space referred to herein as the interlayer space. Bulk swelling occurs when water penetrates between the 2:1 structural units, hydrates the interlayer cations, and forces the interlayers apart. The efficiency with which the swelling process occurring at the interlayer scale translates to bulk volume change or swelling pressure depends on the larger scale features of the particle groups and pore fabric.

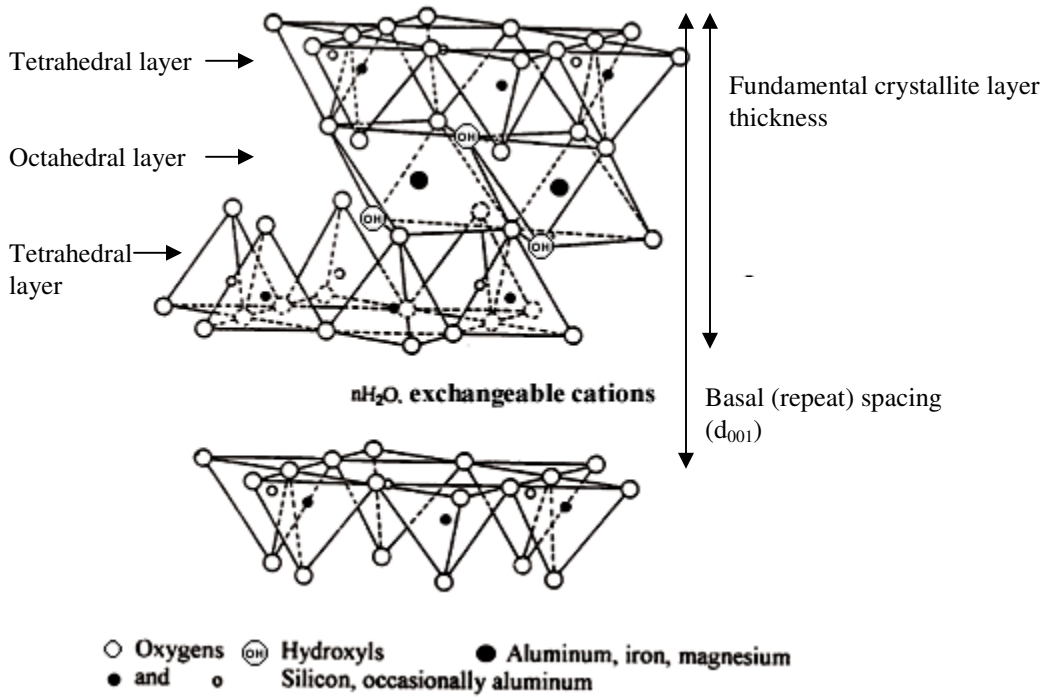

Figure 2.1. Schematic diagram for smectite structure (after Mitchell, 1993)

2.2. Water adsorption mechanisms

Three microscale mechanisms for water adsorption are important in expansive soil behavior: hydration, capillarity, and osmosis. Of these, hydration and osmosis play a key role in the two main clay swelling processes: crystalline and osmotic swelling (Marshall, 1949; van Olphen, 1977; Madsen and Muller-Vonmoos, 1989). Capillary mechanisms, which occur primarily in pore spaces associated with larger scales, are more likely to act only as a mode of providing water for the other more predominant and short-ranged water adsorption mechanisms (Snethen et. al., 1977; Miller, 1996). A typical soil water characteristic curve (SWCC) for an expansive clay with the different water adsorption regimes conceptually identified in it is presented in Figure 2.2.

The focus of this research remains within the crystalline swelling regime, which is driven primarily by the energy associated with the hydration of exchangeable interlayer cations and attraction associated with solid-liquid interactions occurring in the immediate vicinity of the clay particle surfaces. This process is explained in more detail later.

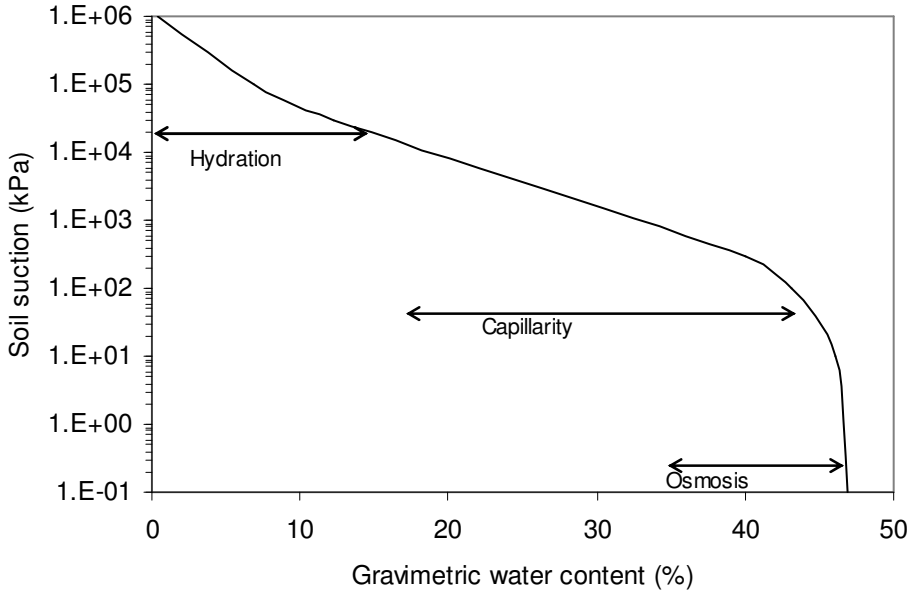

Figure 2.2. Typical water retention curve (SWCC) for clay showing adsorption regimes

2.2.1. Mineral surface hydration

Hydration of the clay mineral surface originates as a result of short-range attractive forces developed on the negatively charged clay particle and interlayer surfaces due to hydrogen bonding, charged surface-dipole attraction, or a combination of both (Mitchell, 1993). Water molecules may form hydrogen bonds with exposed oxygens or hydroxyls on tetrahedral layer surfaces. Cation hydration, which is likely to dominate over particle surface hydration, results in an increase of the ionic radii of the cation, an

increase of the interlayer pore space, and an overall volume change of the soil mass. Because exchangeable cations are associated with the mineral surface, their water of hydration may also be considered associated with the mineral surface. Surface and cation hydration is predominant in the 20,000 kPa – 550,000 kPa suction regime, with corresponding gravimetric water contents for the soil-water system of less than 30% (Israelachvili, 1992, Mitchell, 1993). Because short-range hydration mechanisms in soils are associated with the particle surfaces rather than the particle fabric, water adsorption in this unsaturated regime is relatively unaffected by disturbances such as compaction.

2.2.2. Capillarity

Capillarity originates from the curvature of air-water interfaces within the porous soil fabric. Water adsorption driven by capillarity depends largely on the geometric features of the larger scale interparticle pore space and thus is sensitive to disturbance associated with compaction. Capillarity may be defined in terms of matric suction, and depends on the surface tension of the pore fluid, the degree of saturation, and capillary radius. As saturation increases, the pore-water menisci are enlarged and matric suction decreases. This mechanism is primarily important for suctions ranging from 0 kPa to 10,000 kPa.

2.2.3. Osmosis

Figure 2.3 shows a conceptual distribution of ions near a negatively charged clay mineral surface. As the affinity for the cations is greatest at the clay mineral surface, cations are concentrated near the surface and tend to be diffuse as distance from the clay mineral surface increases. The well-known model proposed by Guoy-Chapman can

explain this phenomenon through the theory of diffuse double layer (DDL), where the decay of electrical potential is modeled as a one-dimensional exponential function (Mitchell, 1993).

Osmotic water adsorption results from concentration differences of dissolved ions between the interlayer pore water (overlapping double layers) and the free (bulk) water. It is a long-range interaction, which mostly depends on ionic concentration, the type of exchangeable ion (e.g., Ca vs. Na), pH of the pore water, and clay mineralogy (van Olphen, 1977). Corresponding osmotic swelling results from the balance of attractive and repulsive forces that develop between overlapping electrical double layers. Osmotically driven water adsorption is primarily important for total suctions less than about 800 kPa, which generally occurs at gravimetric water contents of around 40% for soil systems with expansive clay minerals.

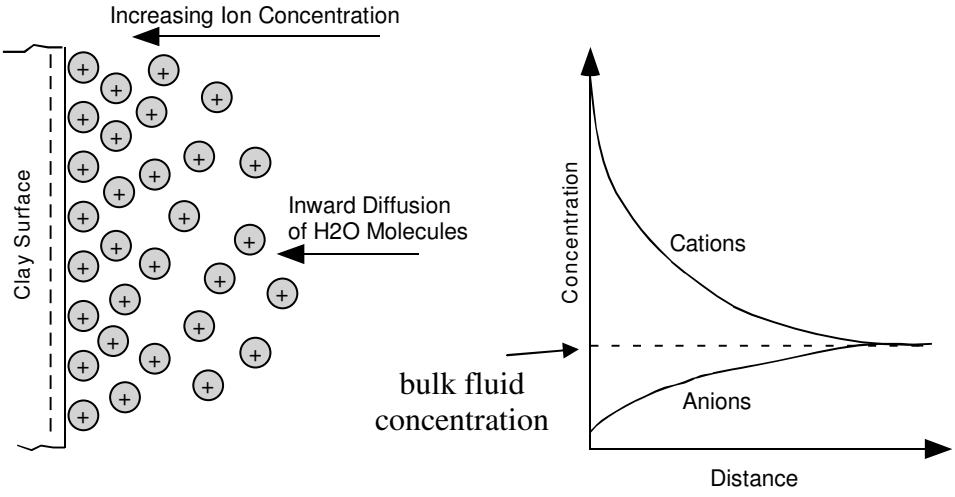

Figure 2.3. Distribution of ions adjacent to a clay surface (after Mitchell, 1993)

2.3. Crystalline swelling

Crystalline swelling, or "Type I" swelling, is a process by which initially dry expansive clay minerals intercalate one, two, three, or four discrete layers of water between the mineral interlayers (Norrish, 1954). This process, which occurs before osmotic or "Type II" swelling, is driven primarily by the energy associated with the hydration of exchangeable interlayer cations and attraction associated with solid-liquid interactions occurring in the immediate vicinity of the clay particle surfaces (short range hydration mechanisms).

The basic crystalline swelling process is conceptually illustrated in Figure 2.4. In this figure, an expansive smectite particle comprised of two unit layers undergoes four successive stages of hydration, starting with a completely dry system and hydrating up to three molecular layers of water. As water is adsorbed in the interlayer, the mineral basal spacing makes a transition to the next hydrate state. According to previous experimental and theoretical studies (e.g., Chipera et. al, 1997; Barshad, 1949; Karaborni et. al, 1996), the basal spacing of smectite proceeds from 9.7Å to 12 Å upon transitioning from the zero-layer to one-layer hydrate, from 12 Å to 15.5 Å during the one-layer to two-layer transition, and from 15.5 Å to 18.3 Å from the two-layer to three-layer transition. For hydrating sodium smectite, relative humidity values (RH) corresponding to the successive hydration regimes range from approximately 30% to 60% for stability of the one-layer hydrate state, and 75% and greater for the two-layer hydrate state. In the case of calcium smectite, the 0-to-1 layer hydration transition occurs at RH less than 1%, and the 1-to-2 layer transition corresponds to a RH range of 15% to 85% (Chipera et. al,

1997; Likos, 2004). Table 2.1 summarizes the approximate ranges of RH for stability of the various hydration states during both adsorption and desorption.

The net work required for removing or adding a water layer in the interlayer space can be obtained from water vapor desorption and adsorption isotherms. To obtain associated swelling pressures, the work may be divided by the change in distance that occurs in the interlayer ($2.6x10^{-8}$cm for one layer of water). For example, Van Olphen (1963) calculated that for calcium montmorillonite, the pressure associated with removing the water from the fourth, third, second, and first hydration states were 20,000 kPa, 125,000 kPa, 250,000 kPa, and 600,000 kPa respectively.

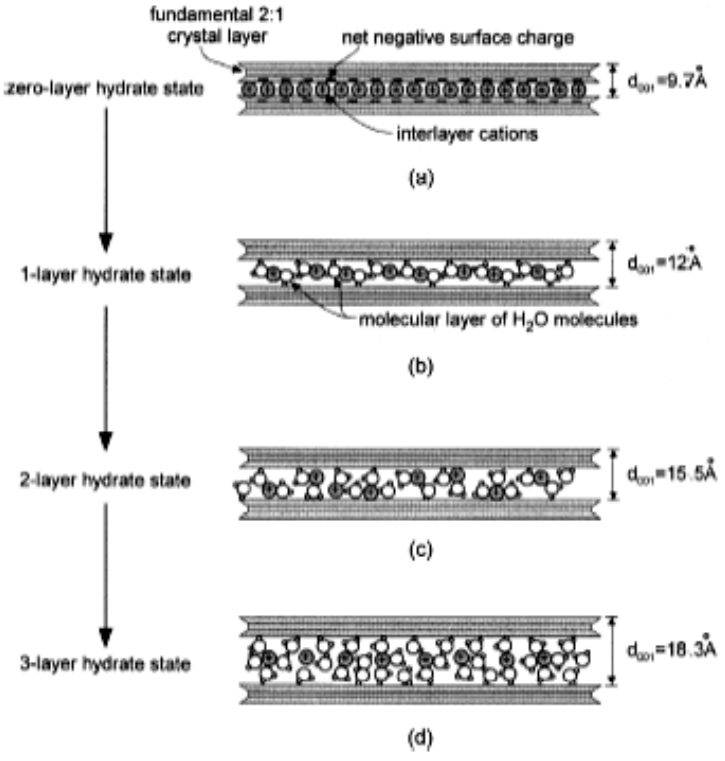

Figure 2.4. Conceptual illustration of the sequential crystalline swelling process for smectite (Likos, 2004)

Table 2.1 Approximate relative humidity ranges for stable hydration states of Ca and Na smectite (interpreted from Chipera et. al, 1997)

	Hydration state	Stable RH during wetting	Stable RH during drying
Calcium smectite	zero layer (~9.7Å)	not present	not present
	one layer (~12Å)	<1%	<1%
	two layer (~15.5Å)	15%-85%	15%-85%
Sodium smectite	zero layer (~9.7Å)	0%-12.5%	<5%
	one layer (~12Å)	38%-100%	10%-55%
	two layer (~15.5Å)	>75%	>65%

2.4. Role of particle and pore properties on swelling behavior

This section summarizes the role that particle and pore fabric, interlayer cation, and initial compaction play in influencing macroscopic swelling behavior.

2.4.1. Particle and pore fabric

The fabric of compacted swelling clays has been actively studied and shown to have critical influence in bulk swelling behavior (Pusch, 1982; Gens & Alonso, 1992; Rizzi et. al, 1996; Lloret et. al., 2003). Results of mercury intrusion porosimetry (MIP) tests generally show two dominant pore sizes in compacted clay systems, often referred to as those associated with the inter-aggregate and inter-particle porosities, respectively (e.g., Figure 2.5). If such measurements were capable of measuring pore diameters in the order of 0.001 μm, it is likely that a third significant pore size corresponding to the inter-layer porosity would be observed. As shown on Figure 2.5, the pore volume corresponding to the inter-aggregate porosity is significantly affected with the change in dry density of the samples (i.e. loosely compacted sample exhibits a much higher pore volume at a pore diameter around 100 μm). The pore volume associated with the inter-

particle void space is relatively unaffected by compaction of the specimens. Thus, compaction by the application of external stress acts largely to compact and remove the larger inter-aggregate pores, but has relatively little effect on the smaller intra-aggregate pores. Gens and Alonso (1992) stated that "only at dry densities of 1.84 and 1.95 Mg/m^3 bigger pores tend to disappear, and the structure becomes largely matrix dominated."

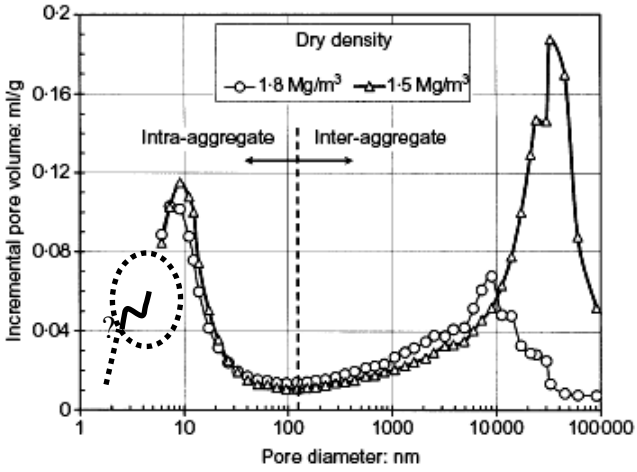

Figure 2.5. Pore size distribution by Mercury Intrusion Porosimetry (MIP) measurement for swelling clay (Lloret et. al, 2003).

Previous studies aimed at resolving the links between expansive clay microstructure and corresponding macroscopic behavior have focused on different levels of structure. Some authors have focused on two levels of scale (e.g., Gens & Alonso, 1992, Cui et. al, 2001; Xie et. al, 2006) while others have considered three levels of pore scale: inter-aggregate, intra-aggregate (or inter-particle), and interlayer (Likos and Lu, 2006). Here, inter-aggregate porosity accounts for the pore space between particles and/or relatively large aggregates; void spaces are observed at a scale of around 100 μm. Zooming in to a scale of 0.01 μm, the intra-aggregate or inter-particle porosity is observed. Finally, interlayer porosity, which comprises the space between the mineral

layers, is observed at a scale of 0.001 μm (Figure 2.6). The current research strives to gain a better understanding on how the interaction between the inter-particle and inter-layer porosities upscale to macroscopic behavior.

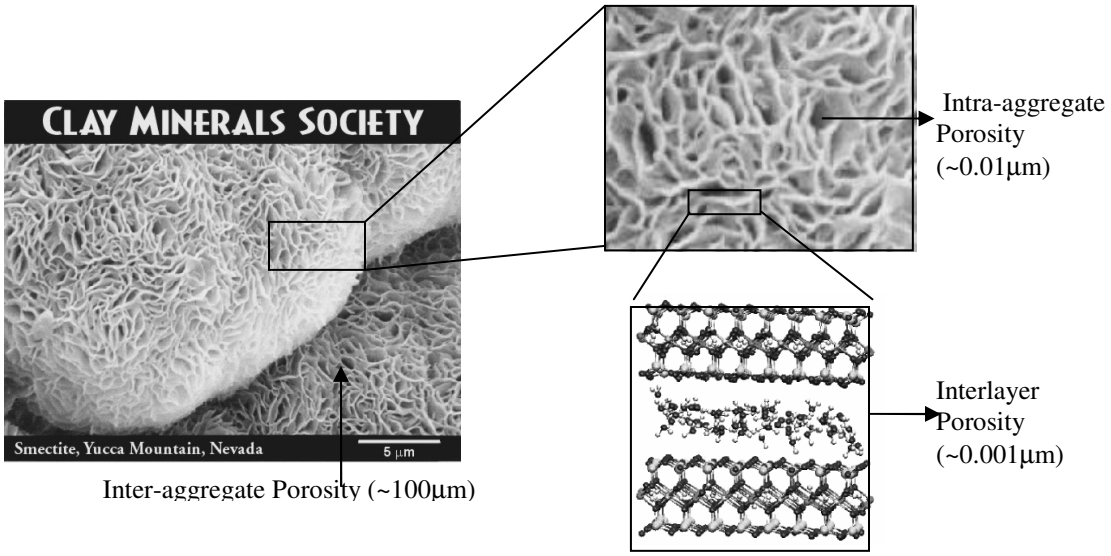

Figure 2.6. Multi-scale levels of pore fabric: inter-aggregate, intra-aggregate, & inter-layer porosity.

2.4.2. Effect of interlayer cation

Previous microscale imaging studies using scanning electron (SEM) and transmission electron (TEM) microscopy indicate that the fabric of expansive clay minerals is generally in the form of colloidal size tactoids with lamellar nature. These tactoids form parallelepiped-like micropores (Quirk, 1986; Tessier, 1990; Tuller & Or, 2002). Each tactoid consists of essentially parallel clay lamellas or mineral layers and the spacing between lamellas constitutes the interlayer space (Figure 2.7).

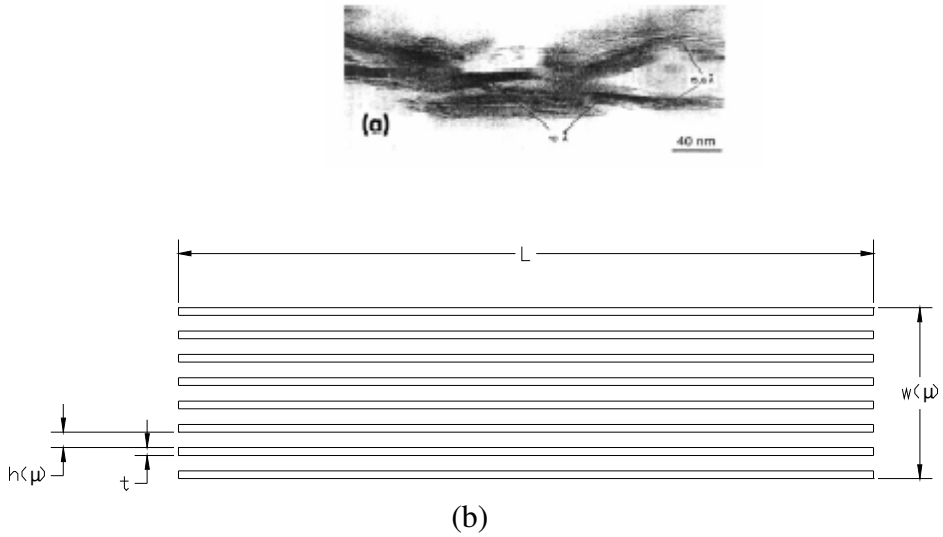

(b)

Figure 2.7. (a) Scanning Electron Micrograph (SEM) of smectite showing arrangement of tactoids (Tessier, 1990), and (b) Idealized tactoid geometry

The clay mineral type, the predominant exchangeable cation, and the mineral's sorption history have an effect on the thickness (t), length (L), and number of lamellas per tactoid (n). Sodium smectite, for example, is composed of relatively thin quasicrystals (n~20) with lamella thickness of 9.7 Å and length ranging from 1000Å to 3000Å. In contrast, calcium smectite may be composed of around 400 lamellas per tactoid, with t=9.7Å and L of about 2000Å (Tessier, 1990) (Figure 2.8). The separation distance between the individual layers (h(μ)) and the overall thickness of the quasicrystal (W(μ)) vary as a function of the water potential (μ). Due to the thicker nature of quasicrystals, calcium smectite exhibits larger bulk volume change within the crystalline swelling regime because more molecular water layers hydrate the tactoid at a given water potential (Likos and Lu, 2006).

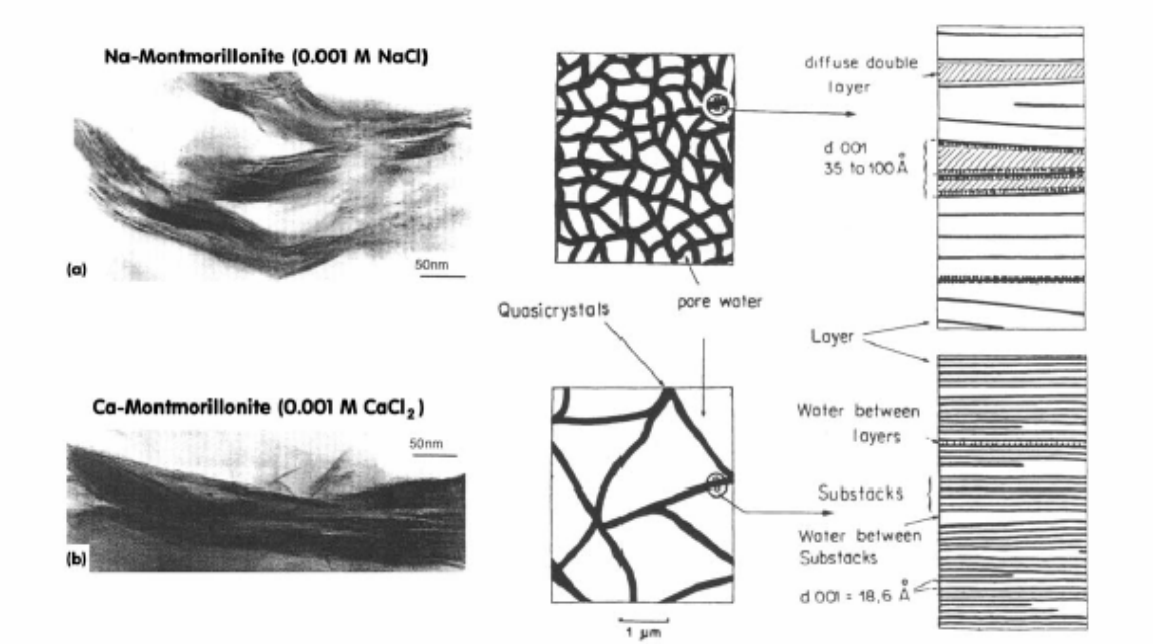

Figure 2.8. Clay fabric microstructure as affected by solution composition (Tessier, 1990).

2.4.3. Effect of compaction

The initial void ratio of expansive soils has a profound influence on corresponding swelling pressure and volume change associated with the adsorption and desorption of water. Upscaling of the inter-layer and inter-particle swelling to macroscopic behavior is a function of the clay fabric; thus, initial void ratio and stress history are key variables in this study. Previous works have documented that cylindrical specimens compacted at a lower density undergo less total axial strain when following a wetting path. Likos and Lu (2006), for example, measured axial strain of 10 Na and Ca smectite specimens compacted to different initial void ratios and hydrated within the crystalline swelling regime. Unconfined specimens were subjected to an RH increase from 0% to 92.3%. Corresponding axial strain (1-D swell) under the free swell conditions were recorded at equilibrium (Figure 2.9). The results showed that for an identical change in RH, initially denser specimens swelled more than initially loose specimens. Results were interpreted to

reflect an inefficient translation of interlayer swelling to bulk swelling for loosely compacted specimens that arises because the interlayer volume changes occurring on the particle scale are internally adsorbed by the larger scale pores. Conversely, densely compacted specimens exhibit more efficient translation from particle-scale swelling to bulk-scale swelling because the interlayer volume changes are less well accommodated by the internal pores. The fact that Ca-smectite exhibits higher volume changes than Na-smectite reflects the greater number of unit layers comprising each tactoid and the overall differences between the fabric of Ca and Na-smectite.

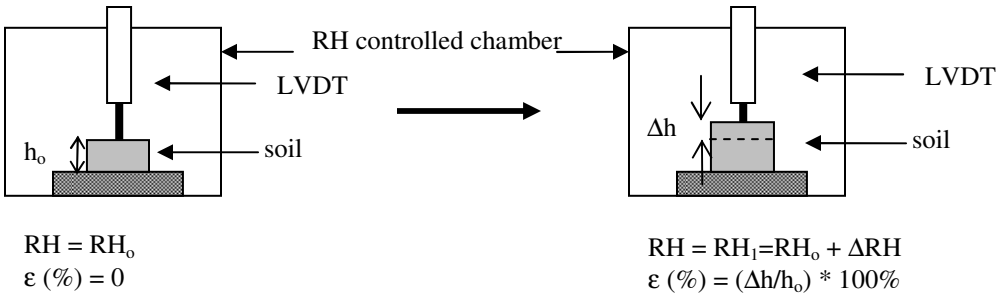

(a)

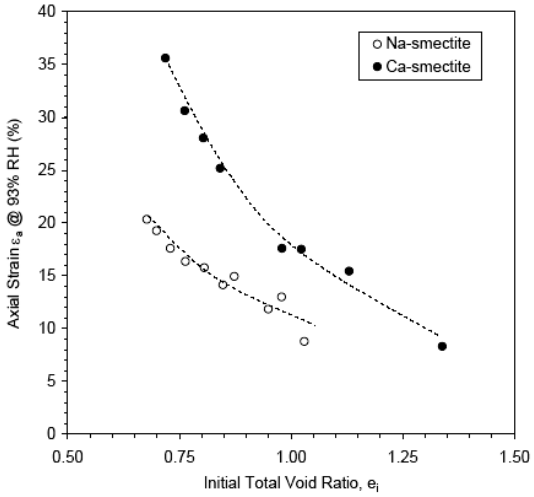

Figure 2.9. a) Schematic diagram of axial strain measurement, b)Axial strain at 93% RH as a function of initial total void ratio from a single-step testing series (after Likos and Lu, 2006).

2.5. Suction control methods

Typical suction values within the crystalline swelling regime range from 20MPa (RH= 86%) to 550MPa (RH= 1.7%). Applicable suction measurement methods for this range include filter paper and psychrometer techniques; however, they are not very accurate and require a long testing time. A good alternative for examining crystalline swelling behavior is to control relative humidity (RH) in a closed chamber and relate it directly to total suction (ψ_t) through Kelvin's equation:

$$\psi_t = -\frac{RT}{v_{w0}\omega_v}\ln(RH) \tag{2.1}$$

where ψ_t is in MPa, R is the universal gas constant (R= 8.314 J/mol*K), T is absolute temperature (K), v_{wo} is the specific volume of water (m^3/kg) and ω_v is the molecular mass of water vapor (ω_v= 18.016 kg/kmol). Figure 2.10 shows a plot of equation 2.1 for T=293.16K; total suction is zero at RH=100%. The following sections describe methodologies for control of RH using saturated salt solutions (2.5.1) and in an automated system based on proportioned mixing of wet (vapor saturated) and dry air (2.5.2). Both methods were adopted for the current experimental program.

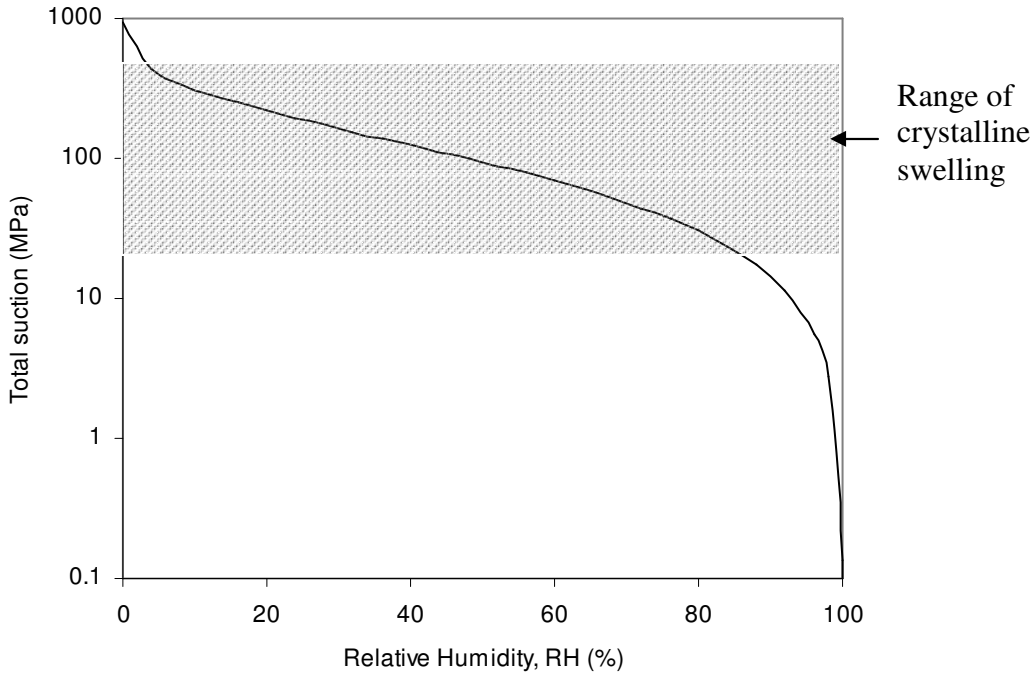

Figure 2.10. Theoretical relationship between total suction and RH (T=293.16K)

2.5.1. Saturated salt solutions

Relative humidity can be controlled using saturated or unsaturated salt or acid solutions (Young, 1967) by letting them reach thermodynamic equilibrium in closed environmental cells. Temperature changes must be accounted for, and equilibration times are relatively long. Saturated salt solutions can liberate or absorb some water without a significant effect on the equilibrium RH. A summary of several saturated salt solution properties is provided in Table 2.2. Water vapor sorption measurements may be made by placing a clay specimen in the headspace over one such solution and measuring the equilibrium water content of the specimen corresponding to the controlled RH.

Table 2.2. Saturated salt solution properties for RH control (Young 1967)

Salt Solution	Temp. (°C)	RH at 25°C	d(RH)/dT %/°C from 25°C
$NaOH \cdot H_2O$	15 - 25	7.0	0
$LiCl \cdot H_2O$	20 - 70	11.3	-0.01
$MgCl_2 \cdot 6H_2O$	10 - 50	32.7	-0.06
$NaI \cdot 2H_2O$	5 - 35	39.2	-0.32
KNO_2	20 - 40	48.2	-0.18
$Mg(NO_{3)} \cdot 6H_2O$	0 - 50	52.8	-0.29
$Na_2Cr_2O_7 \cdot 2H_2O$	0 - 50	53.7	-0.27
$NaBr \cdot 2H_2O$	-10 - 35	58.2	-0.28
$NaNO_2$	20 - 40	64.4	-0.19
$CuCl_2 \cdot 2H_2O$	10 - 30	68.4	0
NaCl	5 - 60	75.1	-0.02
$(NH_4)_2SO_4$	25 - 50	80.2	-0.07
KCl	5 - 40	84.2	-0.16
K_2CrO_4	20 - 40	86.5	-0.06
$BaCl_2 \cdot 2H_2O$	5 - 60	90.3	-0.08
$(NH_4)H_2PO_4$	20 - 45	92.7	-0.12
K_2SO_4	15 - 60	97.0	-0.05
$CuSO_4 \cdot 5H_2O$	25 - 40	97.2	-0.05

2.5.2. Automated humidity control system

Likos and Lu (2003) describe a testing system where RH in a closed environmental chamber is controlled by proportioned mixing of dry (RH~0%) and wet (RH~100%) air (Figure 2.11). Dry and wet gas flow rates are set at a combined flow rate of 500 cm^3/min into the environmental chamber. Dry and wet air are simultaneously obtained by flowing supply air through desiccant and a gas-washing bottle, respectively, using individual mass flow controllers. The ratio of dry air flow to wet air flow is selected depending on the RH desired. The controllable range of the system is approximately 0.5% to 90% RH, which corresponds to total suction ranging from approximately 717 MPa to 14 MPa and thus within the range of interest for crystalline swelling (Figure 2.10). The volume change (axial strain) and moisture content of

compacted clay specimens is monitored as a function of the applied RH and logged directly into a computer to obtain water vapor sorption or desorption isotherms and corresponding bulk volume change behavior.

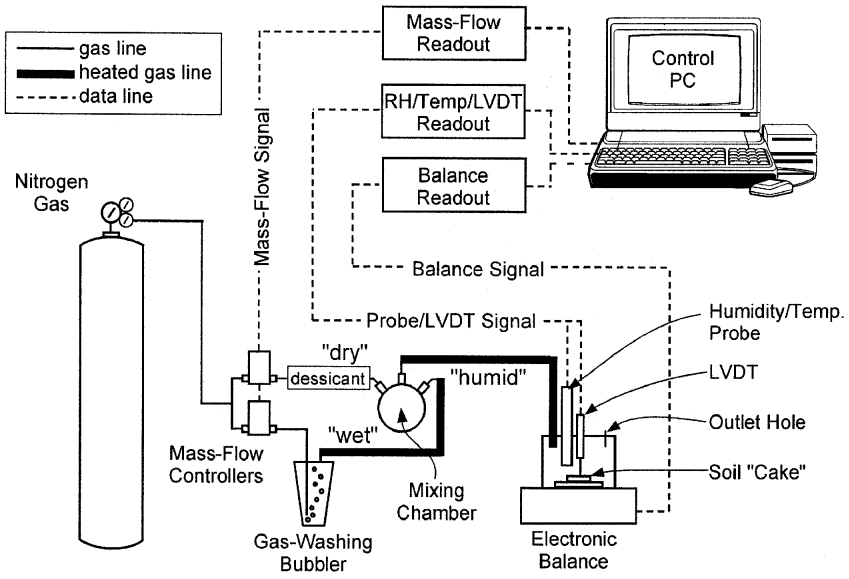

Figure 2.11. Automated relative humidity control system (Likos and Lu, 2003)

2.6. Typical water vapor sorption behavior for smectite

Water vapor sorption isotherms obtained for Na and Ca smectite specimens have been documented to have a wavy behavior that correspond well with the transitions of hydration states during crystalline swelling (Mooney et al., 1952; Collis-George, 1955; Van Olphen, 1965, Chipera et. al, 1997). Likos and Lu (2006), for example, used the system described above to obtain sorption isotherms and axial deformation for Na and Ca smectite with initial void ratio of 0.77 (Figure 2.12). Axial deformation reflects the wavy behavior of sorption isotherms. Transitions from zero-to-one and one-to-two layers are observed for the Na smectite sample at RH of 30%-45% and 60%-70% respectively. Interlayer spacing is more stable for the Ca smectite sample, where the first water layer is

retained at RH close to 0%, the two-layer state occurs at RH of around 25%, and basal spacing remains stable up to about 90% of RH.

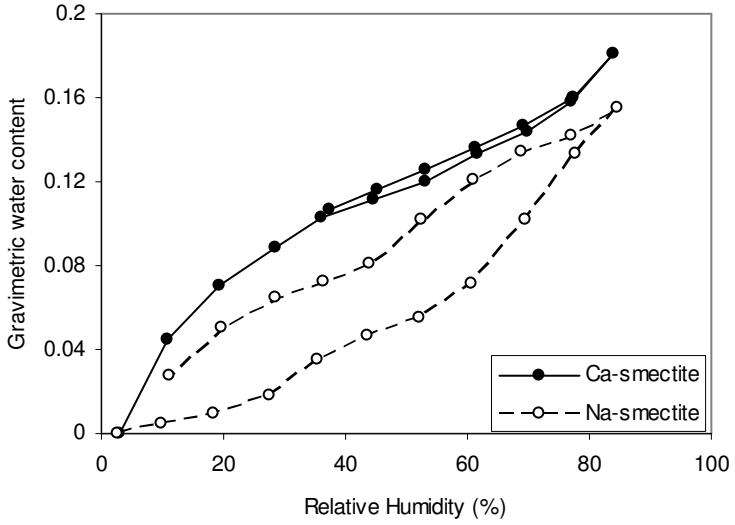

(a)

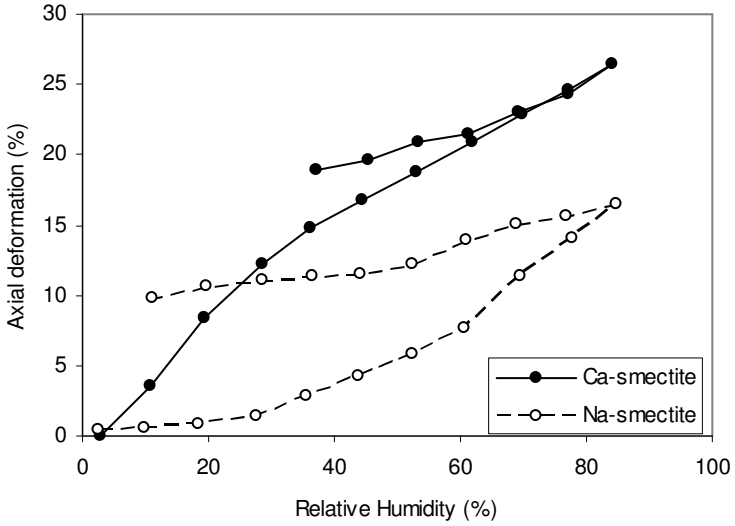

(b)

Figure 2.12. a) Sorption isotherms, b) Steady state axial strain measured during a multi-step wetting-drying cycle (Likos and Lu, 2006)

Hysteresis is more evident for the Na smectite, which is consistent with the sorption behavior. In both cases axial strain during drying is larger than during wetting at the same RH, which indicates plastic deformation sustained along drying paths.

2.7. Pore-scale porosity evolution model

Likos and Lu (2006) developed a porosity evolution model to quantitatively assess the relative changes in the interlayer and inter-particle void volume during the hydration of Na and Ca-smectite systems. Quantitative analysis of the changes in the inter-particle and inter-layer void ratios (e_{IP} and e_{IL}) was investigated by considering that the total void ratio (e_T) is comprised of an interparticle (e_{IP}) component and an interlayer (e_{IL}) component:

$$e_T = e_{IP} + e_{IL} \quad (2.2)$$

where e_{IL} may be quantified using the ratio between the interlayer separation (2δ) and the lamella thickness (t):

$$e_{IL} = 2\delta/t \quad (2.3)$$

$$\text{Thus, } e_{IP} = e_T - e_{IL} \quad (2.4)$$

which may be written in incremental form:

$$\Delta e_T = \Delta e_{IP} + \Delta 2\delta / t \quad (2.5)$$

The change in interparticle and interlayer void ratios for Na and Ca smectite as a function of RH was analyzed by placing the specimens in the automated humidity control system and monitoring the total void ratio as a function of RH. Changes in interlayer void ratio were computed from interlayer separations (δ) using humidity-controlled XRD results obtained on similar materials by Chipera et. al (1997).

Results obtained for a Na-smectite sample considering interlayer and interparticle void ratios are portrayed in Figure 2.13. Interlayer volume at RH=0% is zero, increasing at the one and two-layer hydration states at RH of 10%-30% and 60%-80%. During the first hydration transition, bulk volume changes are small, which is reflected by a decrease of the interparticle void ratio and interpreted to indicate that the particle scale volume changes are being adsorbed by the larger scale pores. After the second hydration layer transition, both interlayer and interparticle void ratios increase, resulting in a large increase of bulk volume change. Hysteresis was explained by observing that during drying, the interparticle void ratio remained fairly constant, which means the pore structure remains expanded upon drying once it is expanded during initial wetting (i.e., the deformation of the larger scale pores is plastic).

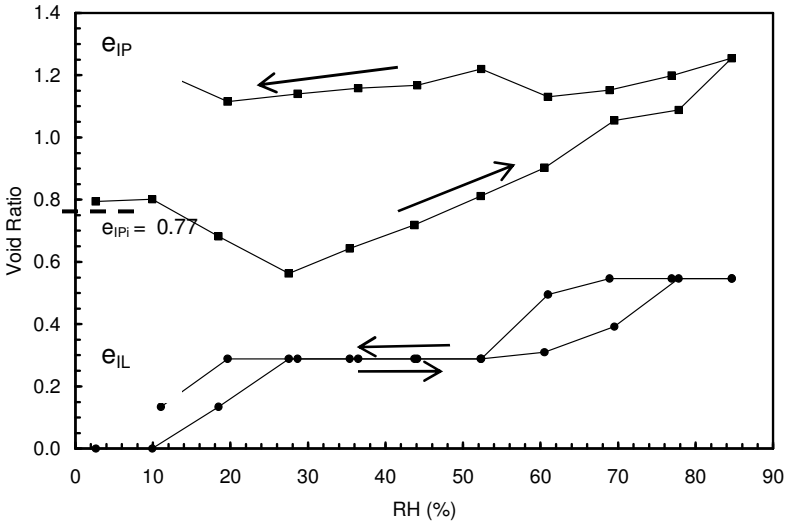

Figure 2.13. Evolution of interlayer, interparticle, and total void ratio for multi-step specimens (after Likos and Lu, 2006).

2.8. Barcelona Basic Model

Gens and Alonso (1992) presented a conceptual model describing the mechanical behavior of unsaturated expansive clays. This framework is based on the elasto-plastic

strain-hardening Barcelona Basic Model (BBM) work presented by Alonso et. al.(1987), which considers the behavior of unsaturated soils of low activity.

In the BBM, the concept of critical state for saturated soils is extended to unsaturated conditions. Following the theory of hardening plasticity, this framework considers a dependence of the yield surface on suction, which is portrayed in the p-q-s diagram (Figure 2.14), where p is either vertical or mean stress (depending on the test), q is the deviator stress , and s is suction. Considering the (p,s) space (Figure 2.15), irreversible volumetric strains occur if the stress path crosses the yield curve Loading-Collapse (LC); an elastic zone is assumed to the left of the LC curve. Volumetric strains are due to either an increase in the load (Loading strains) or a reduction of suction (Collapse strains). Thus, the hardening implied by the loading/collapse process is equivalent to that experienced by a saturated sample moving from A1 to A2; denser soils result in LC curves located further to the right. Note that the distance between the yield curves increases with suction because volumetric stiffness is larger at higher suction.

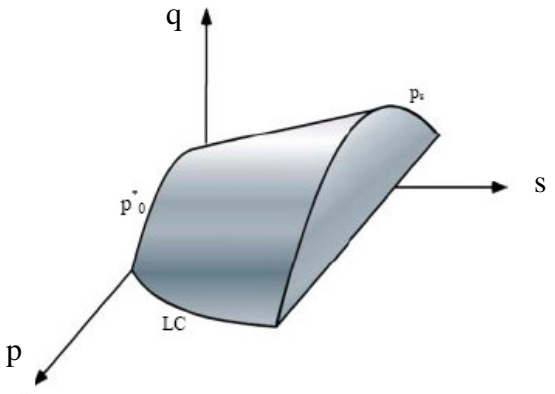

Figure 2.14. Three dimensional representation of the BBM yield surface (Gens & Alonso, 1992)

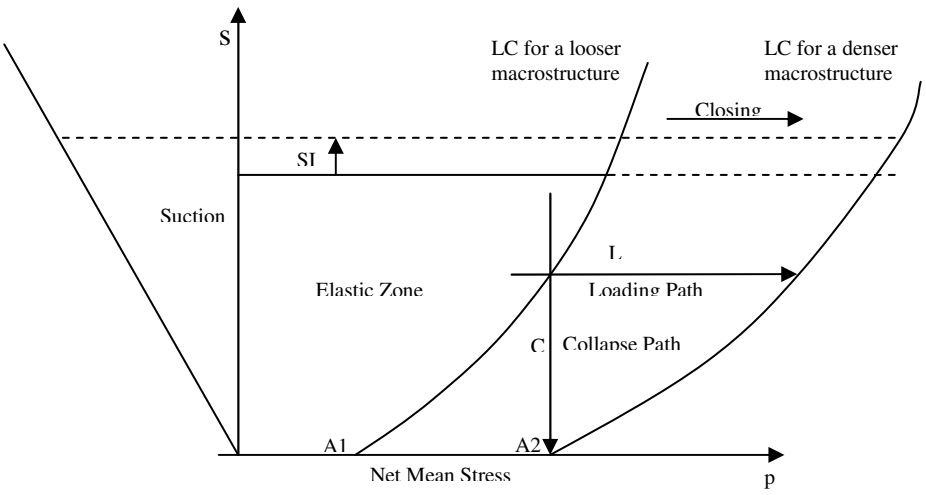

Figure 2.15. Loading-Collapse curve in p-s space (Gens & Alonso, 1992)

Another source of irreversible deformations is the increase of suction beyond the maximum past suction experienced by the soil; this is represented by the yield curve Suction Increment (SI), assumed to be parallel to the p-axis.

In the (p,q) space, the yield surface of a saturated soil can be the ellipse of the modified Cam-clay model (Figure 2.16). As suction increases, different ellipses are considered and the critical state line (CSL) varies resulting in an increase of strength.

The extended framework developed for unsaturated expansive soils (Gens & Alonso, 1992) incorporates phenomena occurring at particle level that cause large swelling strains. This means that both the interparticle and the interlayer void spaces are considered in addition to the macrostructural level that accounts for the larger scale structure of the soil. Strains on the microstructural level are controlled by physicochemical interactions at the particle level, are reversible, and are independent of macrostructural effects. Nevertheless, strains of the microstructure affect the strains in the macrostructure.

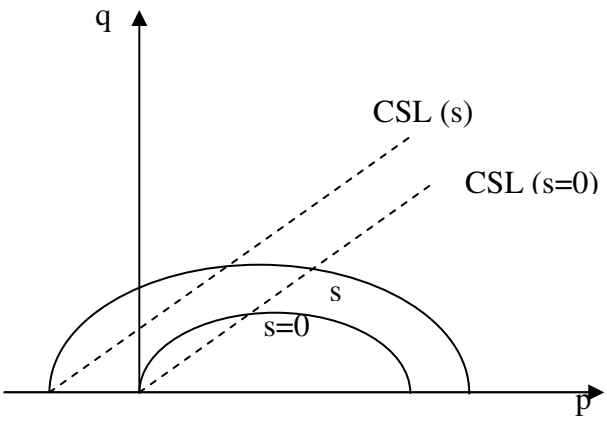

Figure 2.16. Yield surface and critical state line observed in p-q space (Gens & Alonso, 1992)

Gens and Alonso analyzed soil behavior at a microstructural level using the double-layer theory; however, other approaches may be implemented. In Figure 2.17, the neutral loading line NL separates stress paths leading to compression (increase of suction or pressure) from stress paths resulting in swelling (reduction of suction or pressure). Depending on the microstructural theory adopted, the inclination of this line may vary.

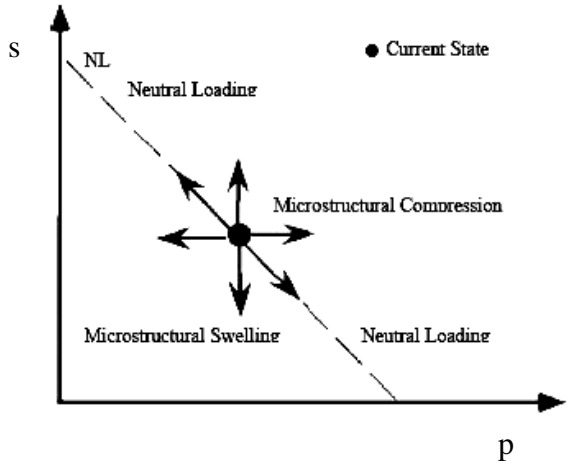

Figure 2.17. Microstructural behavior (Gens & Alonso, 1992)

The swelling rate becomes larger at low suction values or when lower pressure values are applied (Figure 2.18). Thus, larger swelling occurs for a reduction in suction

from higher values, or for decreasing stress from larger values. Microstructural swelling due to a suction reduction is smaller for larger applied stress.

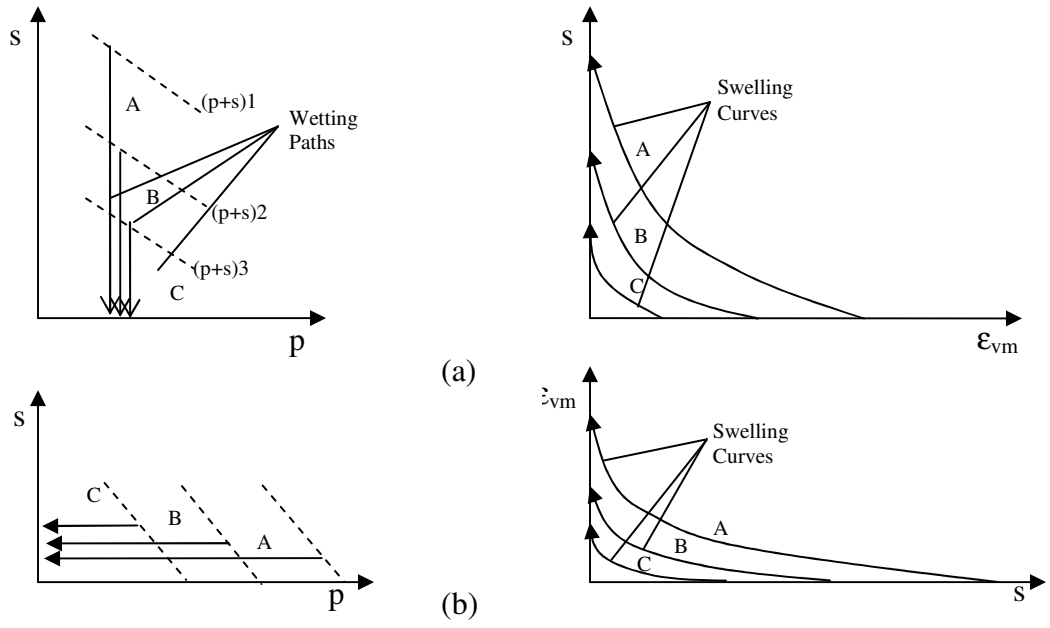

Figure 2.18. Stress paths for a) collapsing points at same stress from different initial suctions, b)unloading points at same suction from different initial stresses. (Gens & Alonso, 1992)

Coupling between both structural levels is demonstrated in Figure 2.19. The irreversible macrostructural swelling ε^{P}_{VM} caused by microstructural expansion ε_{vm} depends on the ratio between the applied stress to the apparent pre-consolidation stress of the soil at a given suction (p/p_o). Specimens with p/p_o close to 1 will have an open, potentially collapsible macrostructure. Conversely, decreasing values of this ratio imply denser packing and will result in larger macrostructural swelling upon saturation because the distance from the stress point to its LC yield curve is larger. When the specimen swells, the macrostructure softens up and the LC curve moves toward the right. If suction is reduced at a constant stress p, the microstructure undergoes reversible swelling as long as the stress path does not cross the initial neutral line NL_i (Figure 2.20). Plastic deformations are encountered when the stress path takes the yield locus to a position NL_f.

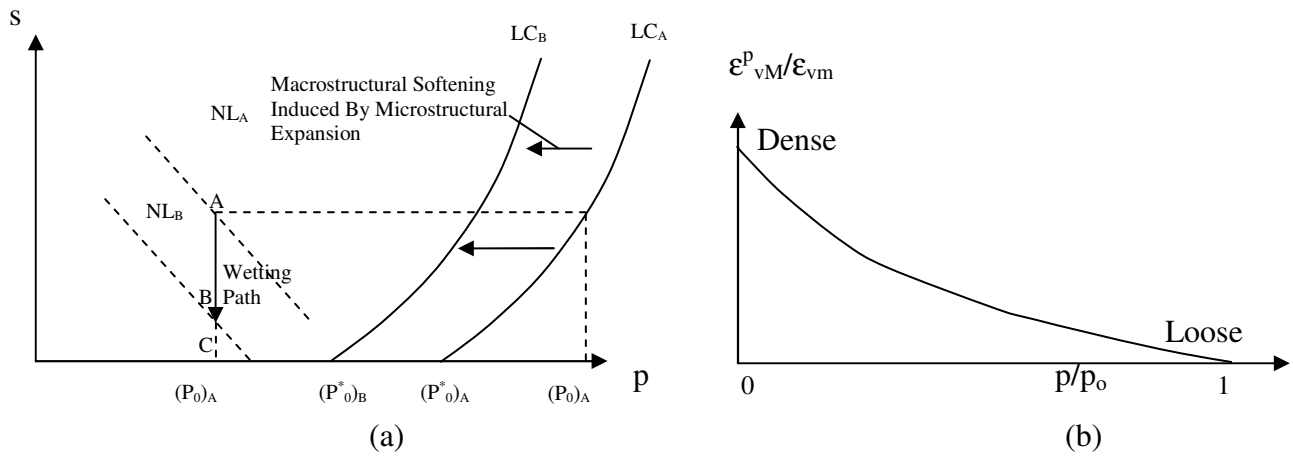

Figure 2.19. a) Coupling between microstructural deformation and macrostructural LC yield curve, b) Dependence of $\varepsilon^{p}_{vM}/\varepsilon_{vm}$ on the value of p/po (Gens & Alonso, 1992)

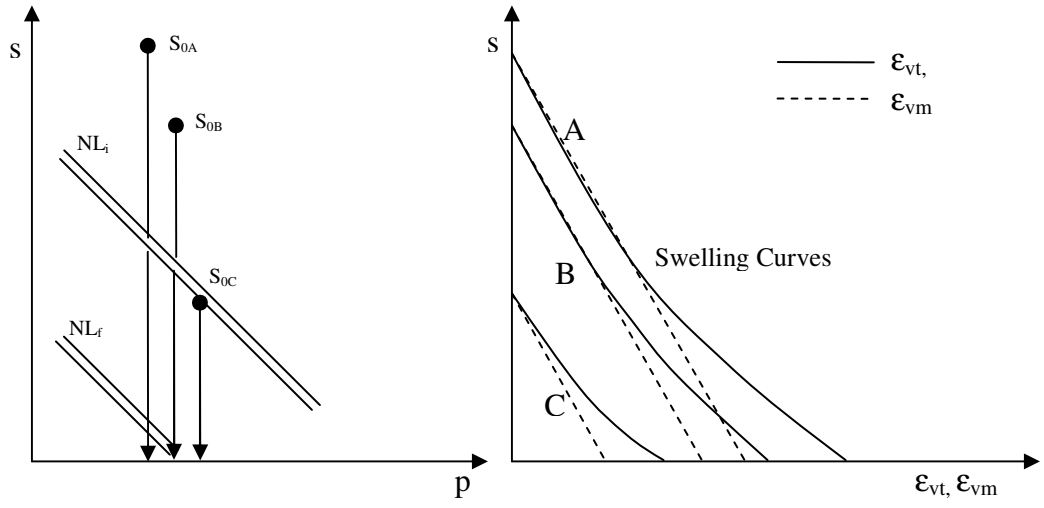

Figure 2.20. Microstructural and total deformations corresponding to collapse paths of elements with different initial suction values and neutral lines (Gens & Alonso, 1992)

Swelling pressure under constant strain boundary conditions is depicted in Figure 2.21. As suction is reduced, a pressure increment develops to maintain a constant volume. If the microstructure was the only factor for volume change, then the stress path

would follow the neutral line NL; however, the macrostructure is also deformed. At higher suctions, the soil structure reacts more rigidly against suction decrements; hence, changes in pressure are more likely to deform the soil. When the soil approaches saturation, the volume stress path follows the neutral line inclination down to zero suction (samples C and D). Swelling pressures for samples with same density but different initial suctions can be the same if the stress paths reach the LC surface (samples A and B).

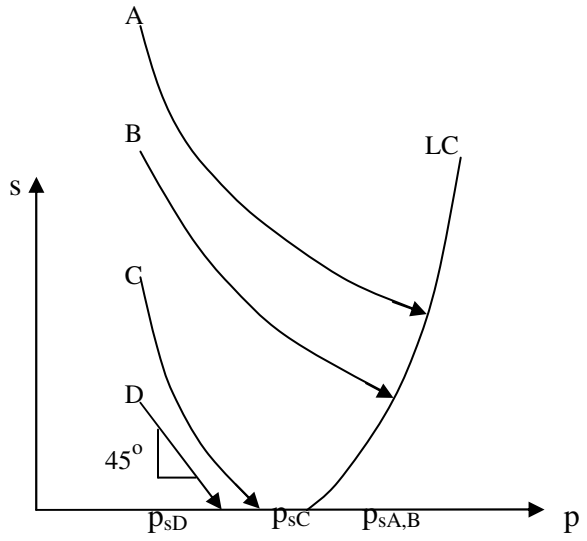

Figure 2.21. Swelling pressure under constant strain (Gens & Alonso, 1992)

CHAPTER III

METHODS AND MATERIALS

3.1. Introduction

The objective of this research is to gain a better understanding of how interlayer separation in the crystalline swelling regime in compacted expansive clay upscales to macroscopic volume change and swelling pressure behavior. The experimental portion of the work involved measurements of compacted clay volume change and swelling pressure under controlled boundary conditions and suction conditions. Factors considered in the scope and design of the experimental program include clay fabric (compaction condition), stress paths, water potential (relative humidity), clay mineralogy and cation exchange complex. This chapter describes the materials used for the experimental component of the research, the experimental apparatus, and procedures adopted for laboratory testing.

3.2. Materials

Three types of clay were selected for testing to evaluate the effects of mineralogy and cation exchange complex in crystalline swelling: Commercial Wyoming bentonite, a naturally occurring bentonite obtained from the Graneros Shale in Golden, Colorado, and a calcium-exchanged form of the Wyoming bentonite. The first two materials are the same as that used in previous studies described by Likos and Lu (2003, 2004, 2006).

The Wyoming bentonite is a powdered clay passing sieve #200 (75 μm). XRD patterns for oriented sample mounts obtained using CuKa radiation indicate predominance of smectite (assumed to be montmorillonite) with a small quartz

component and presence of zeolite (Figure 3.1.a). Cation exchange capacity (CEC) determined using the ammonium displacement method is 66meq/100g, with Na as the predominant cation. Liquid and plastic limits obtained following procedures in ASTM D4318 (ASTM, 2000) are 485% and 132% respectively, which also reflect the predominance of sodium in the exchange complex.

The second clay was obtained from a bentonite seam within an outcrop of the Graneros Shale located southwest of Golden, Colorado. XRD patterns indicate that the clay is mainly smectite with trace amounts of kaolinite and non-clay minerals (Figure 3.1.b). Traces were obtained on oriented evaporative sample mounts using CuK_{α} radiation. All samples were scanned from 2 to 35^{o} 2θ. Heat and ethylene glycol treatments were performed according to procedures described by Moore and Reynolds (1997). Cation exchange capacity for the Colorado clay determined using ammonium displacement was 82 meq/100g; predominant cations identified are Ca and Mg^{2+}. Liquid and plastic limits are 118% and 45% respectively; these values are lower than the sodium smectite clay, reflecting the predominance of divalent cations.

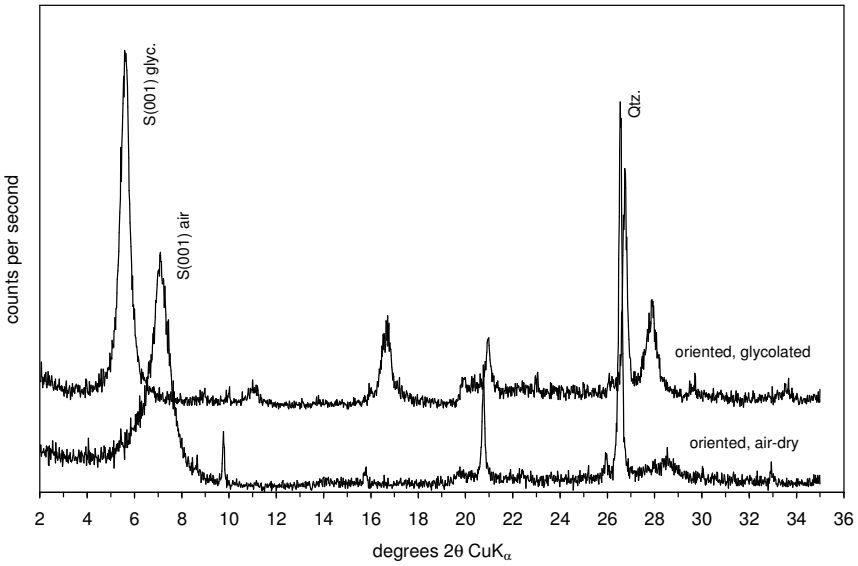

(a)

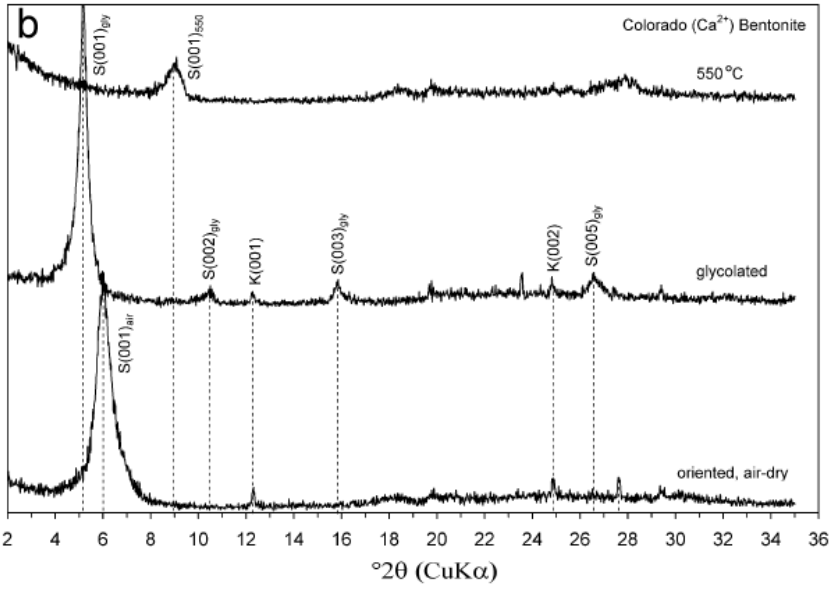

(b)

Figure 3.1. XRD patterns for oriented samples of (a) Sodium smectite, (b) Calcium smectite (after Likos & Lu, 2006)

The last type of clay utilized was prepared by exchanging cations in the Wyoming bentonite with calcium. In this way, a clay having similar aggregate structure to the sodium smectite clay, but with Ca^{+2} interlayer cations was created. The cation exchange

procedure was conducted following procedures described by Moore and Reynolds (1997) as follows: Wyoming bentonite clay was treated with 0.1M $CaCl_2$ solution so Na cations were replaced by Ca from the solution; the clay was washed 3 to 5 times with $CaCl_2$ centrifuging the clay suspension, wherefore the clay was washed with distilled water until chloride ions were removed. Excess chloride was detected using $AgNO_3$; a drop of $AgNO_3$ causes precipitation of AgCl.

Index properties (Atterberg limits) were not obtained for the Ca-exchanged clay due to the small amount of material available for testing. This clay will be referred as the Ca-exchanged smectite.

3.3. Specimen preparation

Swell tests were conducted under controlled humidity conditions and two different mechanical boundary conditions: free swelling and constant strain (zero volume change). The procedure outlined below to create compacted clay specimens was applied for samples tested under free swelling conditions. This procedure was slightly modified as described in section 3.4.2 for specimens tested under constant strain boundary conditions.

Prior to specimen preparation, the clay was first passed through sieve #200 (75 μm) and oven dried at 105^{o}C. Approximately 10 g of powdered clay were then poured into a cylindrical aluminum mold of 3.7cm diameter, an aluminum loading platen was placed on top and a compacted specimen or "cake" was obtained by statically loading it using a piston and 50 kN loading frame. The compacted height of the specimen varied according to the magnitude of load applied, but was generally around 0.5 cm (Figure 3.2). Different normal loads were applied depending on the desired density of the specimen.

The range of applied normal stresses varied from 490 kPa (71.1 psi) to 6374 kPa (924.5 psi). To minimize strain rate effects, loading was applied in small steps and the load was maintained constant until no more strain changes were observed. After desired density was achieved, the cakes were extruded from the mold by using the aluminum loading cap as a piston assembly. Compacting and extruding each cake took an average of 6 hours and resulted in cakes that could be handled without desintegration.

After extrusion, the cake was oven dried at 105 ^{o}C again for 24 hours, and the initial weight and height were measured. Instruments used included a balance and a micrometer assembly with 0.0001 g and 0.00025 cm (0.0001 in) (±0.05% axial strain) resolution, respectively (Figure 3.3).

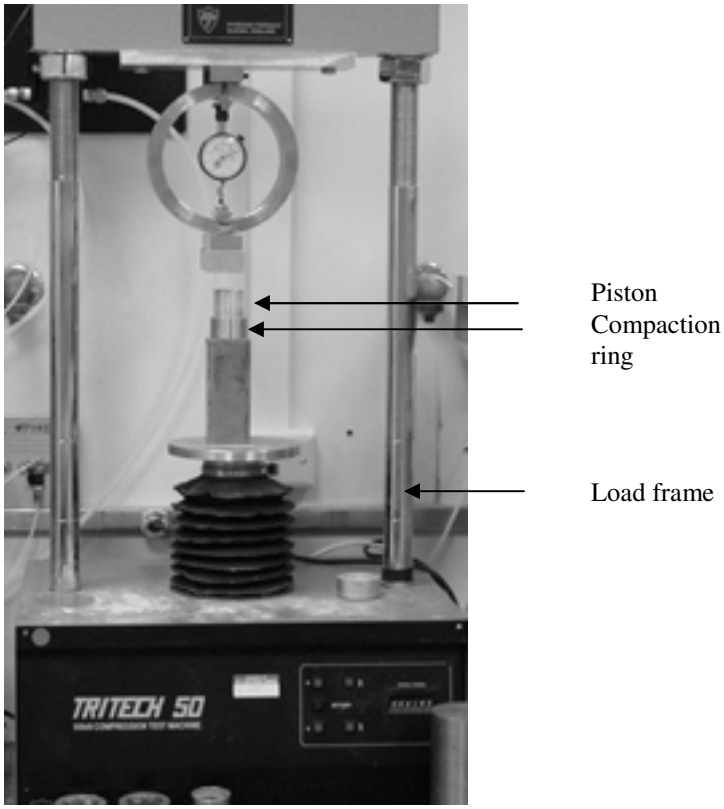

Figure 3.2. Experimental set up for initial compaction of specimens

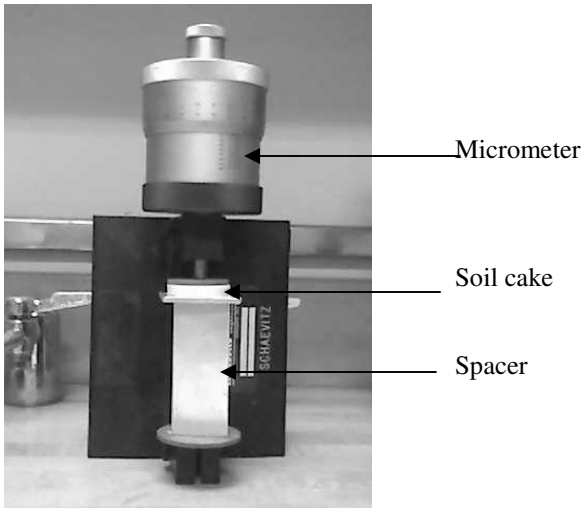

Figure 3.3. Micrometer assembly used for measuring axial deformation during free swell tests

3.4. Experimental set up

Control of the water potential was accomplished by controlling the relative humidity (RH) of the pore-water vapor and relating that measurement to total suction through Kelvin's equation (eqn 2.1). To generate total suction characteristic curves, the equilibrium water content of samples placed in the controlled-RH environmental chamber was measured as RH was increased or decreased. Control of RH in a closed chamber was accomplished in two different ways: using saturated salt solutions (Collis George, 1955; Nishimura and Fredlund, 2000, Lu and Likos, 2004)) and using computer-proportioned mix of wet and dry air flow (Likos and Lu, 2003). Two types of boundary conditions were applied to the cakes during adsorption and desorption: free swelling (zero normal stress) and constant strain.

3.4.1. Salt solutions for control of relative humidity

With this technique, RH is controlled in a sealed chamber by using saturated salt solutions; the specimens are placed on a ceramic disk spacer that allows vapor to go

through (Figure 3.4). Nine jars or desiccators were set up, the first one contained desiccant, and it was measured to maintain the jar at 5% RH; the remaining 8 desiccators contained one of the salt solutions in Table 3.1. Sorption isotherms and corresponding volume change response were obtained by placing the clay specimen successively in each desiccator and measuring equilibrium water content change and axial strain for each stage (Figure 3.5). The balance and micrometer assembly mentioned in Section 3.3 were used for taking these measurements. It was observed that water content and axial strain reached equilibrium conditions at about three days after a change in RH (Figure 3.6), so all cakes were placed in each controlled RH chamber for at least 3 days. Thus, a complete test involving a total of twenty steps (ten wetting, ten drying) required approximately 60 days to finish.

Table 3.1. Saturated salt solution properties for relative humidity control (from Young, 1967)

Salt Solution	Theoretical RH at 25°C	d(RH)/dT %/°C from 25°C
$NaOH \cdot H_2O$	7.0	0
$LiCl \cdot H_2O$	11.3	-0.01
$MgCl_2 \cdot 6H_2O$	32.7	-0.06
MgNO3	52.8	-0.29
$NaBr \cdot 2H_2O$	58.2	-0.28
NaCl	75.1	-0.02
KCl	84.2	-0.16
K_2SO_4	97.0	-0.05

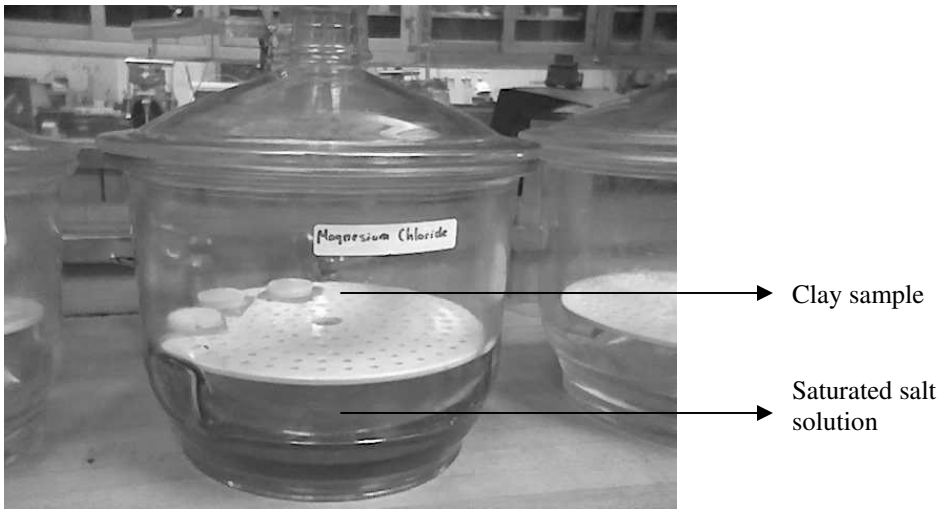

Figure 3.4. Experimental set up for measuring sorption isotherms and free swell volume change response using the saturated salt solution technique

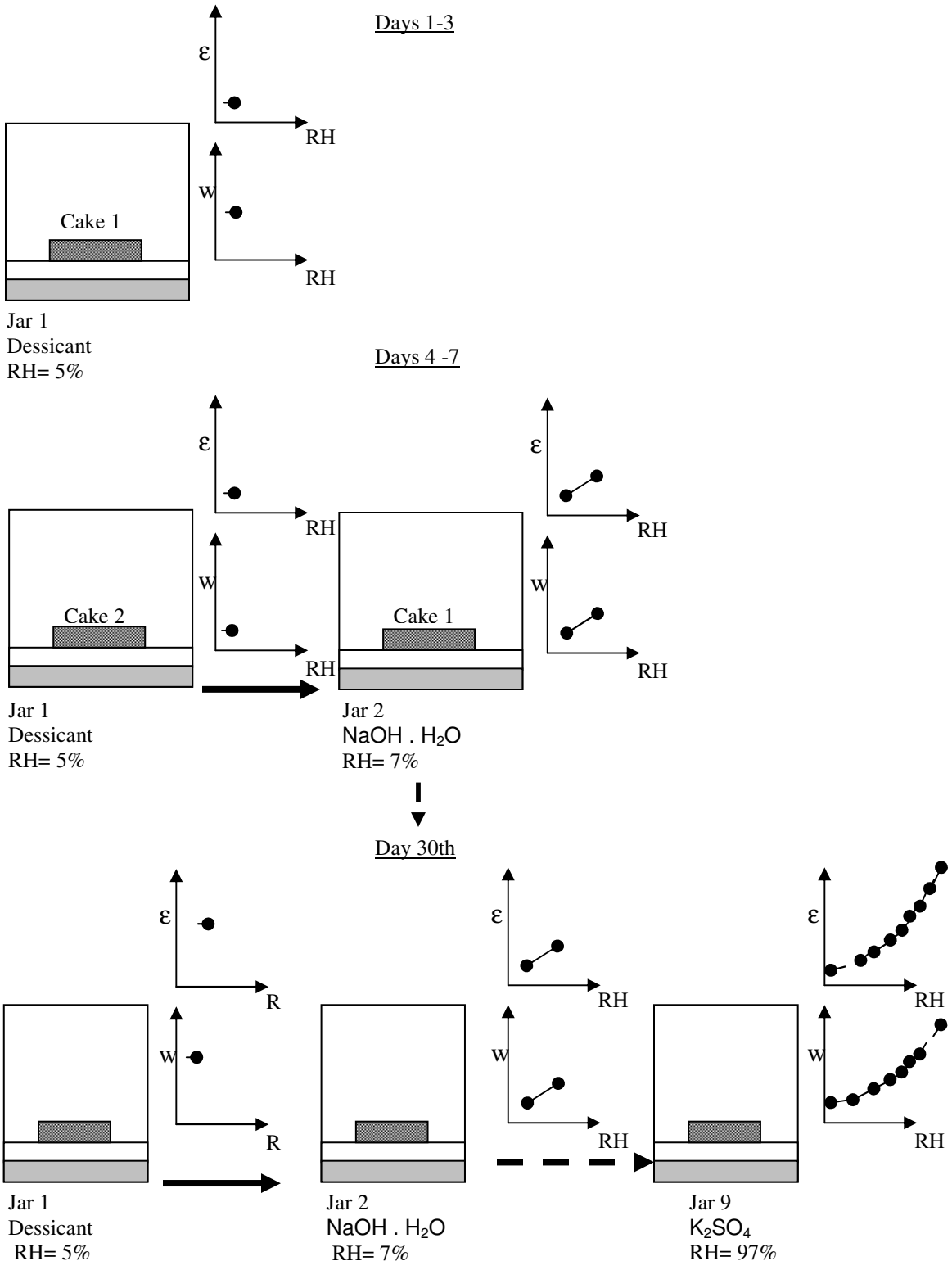

Figure 3.5. Schematic diagram of the procedure to obtain sorption isotherms and axial deformation functions using the saturated salt solution technique

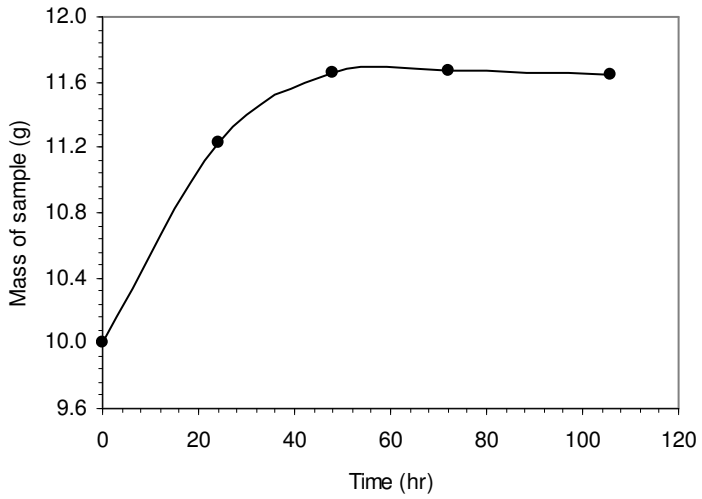

Figure 3.6. Typical transient data from free swell test

A first specimen (cake 1) was compacted, extruded, and oven dried for 24 hours. Initial mass and void ratio were obtained, and then it was placed in the jar with the lowest controlled RH (Jar 1). After three days, once the water content reached equilibrium, height and weight of the soil cake were measured in the minimum time possible, and the specimen was placed in Jar 2, corresponding to the next increment of RH. Three days later and after the new equilibrium height and weight were measured, specimen 1 was placed in Jar 3. At this point, a second specimen (cake 2) was placed in Jar 1 and the process started again. In this way, 10 soil cakes with different initial void ratios underwent wetting and drying paths.

Data obtained from this testing series was used to calculate gravimetric water content and final void ratio of a specimen at a given water potential under free swelling conditions. Radial strain was not measured; rather, it was assumed that volume change for free swelling conditions occurs isotropically and so, radial strain and axial strain are equivalent (Delage et. al, 1998).

3.4.2. Automated humidity control system

An automated system capable of controlling RH and boundary conditions of either constant stress or constant strain in a specimen was designed and mobilized. The technique to control the humidity is similar to the computer-proportioned wet and dry gas mixing technique described by Likos and Lu (2003).

As illustrated in Fugure 3.7, relative humidity in the environmental chamber is controlled by mixing dry (RH~0) and vapor saturated (RH~100%) air in a mixing chamber at a combined flow rate of 600 cm^3/min. The resulting "humid" air is then injected into the environmental chamber containing the soil specimen, where percentages of dry and wet air are adjusted by using mass-flow controllers depending on the RH desired. Dry and wet air streams are generated by passing the supply air through either a desiccant column or a gas-washing bottle filled with distilled water, respectively. Although the mass flow controllers have the capability of being computer controlled, the current system used the manual control option. A 0.5 mm in diameter vent in the specimen chamber was machined to avoid air pressure build up while not affecting the RH significantly. Relative humidity in the chamber was measured with a thin-film capacitance sensor of 0.1% RH precision and the data were logged directly into a computer through an NI-USB-6009 data acquisition board. The RH sensor was calibrated prior to testing using saturated salt solutions (Table 2.2) as standards.

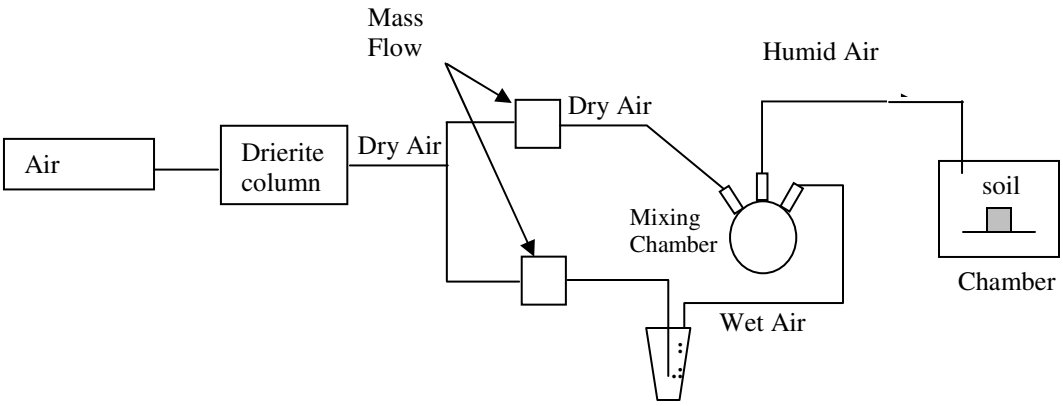

Figure 3.7. Schematic diagram of automated humidity control system

A LabVIEW 7.0 program for displaying, logging and plotting the RH data was modified from an existing template. The program has the flexibility to expand for n signals if needed (Figure 3.8). Calibration of the RH sensor was accomplished by using eight different saturated salt solutions; the conversion factor obtained was 1V=100%RH.

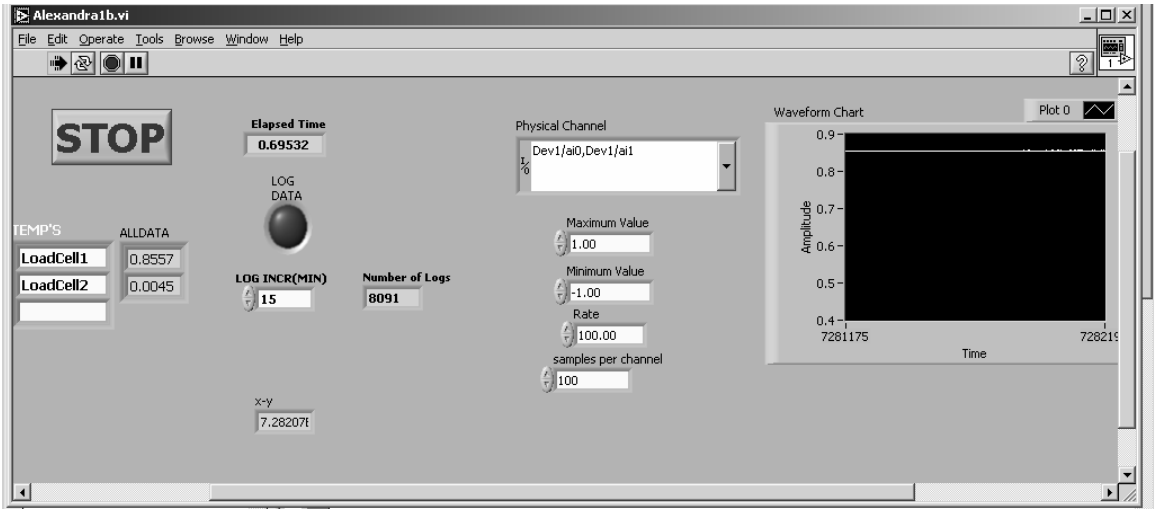

Figure 3.8. Screenshot of Labview data logging program

The main benefit of using the automated humidity control system (or humidity chamber) over the saturated salt solution jars is avoiding handling of the specimens after each increase in RH for measurements of axial strain or change in water content. Other advantages include real time data monitoring, automatic data recording, and recording

transient data prior to equilibrium. However; with this set up it is possible to test only one specimen at a time, while with the salt solution jars several specimens could be tested simultaneously at different RH values.

3.4.2.1. Humidity chamber: free swelling conditions

The set up for free swelling boundary conditions is illustrated in Figure 3.9. The specimen is placed directly on an electronic balance (Mettler-Toledo, Model SAG204) which has 210g range and 0.0001g resolution. Axial strain is measured using a linear voltage displacement transducer (LVDT) with 7.38 μm resolution. Gravimetric water content is obtained by placing the soil specimen directly on the balance. In this way, RH, water content, and axial strain are continuously monitored. For obtaining a sorption isotherm, typical RH increments are about 10%.

Prior to placing the specimen in the environmental chamber, all sensors were zeroed and the RH was set to about 0%. Initial mass and void ratio were measured, and then the soil cake was carefully placed in the chamber. The LabVIEW program was set to log data every 15 min. Data were monitored daily using a EXCEL spreadsheet, when equilibrium conditions were observed (increase in soil mass reached steady state), the next increment in RH was applied.

(a)

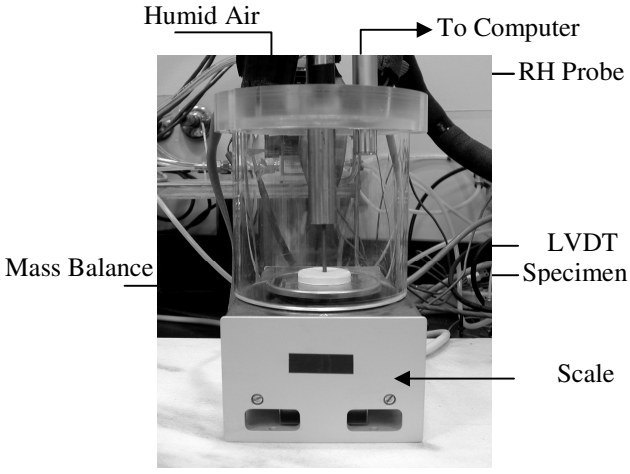

(b)

Figure 3.9. (a) Humidity chamber for free swelling conditions, (b) Detail of environmental chamber

3.4.2.2. Humidity chamber: constant strain/constant stress conditions

Figure 3.10 illustrates the general layout of the system developed for testing specimens under either constant strain or constant stress conditions at a given suction value. The environmental cell is equipped with an automated load actuator (GeoJac) capable of controlling and maintaining either normal stress or axial deformation (stress or strain controlled loading). A load cell of 2,000 lb range and 2 lb resolution is attached to the actuator and connected to the specimen through a stainless steel cone shaped spacer. The soil specimen is confined in an acrylic ring to prevent radial swelling, two aluminum spacers with small openings (~0.3 mm diameter) are placed on either side of the cake; the top spacer is connected to the stainless steel cone spacer while the bottom spacer is connected to a grooved aluminum piece. In this way, vapor can flow through the soil cake. The environmental cell is sealed with vacuum grease. Similar to the free swelling conditions, humid vapor is injected to the environmental cell, a thin air vent prevents pressure build up, and a sensor monitors the RH of the chamber continuously.

Variables that can be controlled with this system include RH, either stress or axial strain applied to the soil sample, and strain rate (if applicable). If the actuator (load frame) is used to control strain, then the corresponding swelling pressures measured by the load cell are monitored. Conversely, when normal stress is controlled, axial deformation is measured by the displacement of the actuator's piston.

The load actuator is controlled through the "Sigma-1-ICON" software provided by GeoTAC and originally designed to perform 1D consolidation tests. This software enables the user to either program loading schedules, or to control stress and strain applied to the soil manually. Figure 3.11 displays the manual control window for both

cases. Reading schedules are programmed as desired; in the current set up, data was taken every 15 minutes. All raw data are logged continuously to a text file.

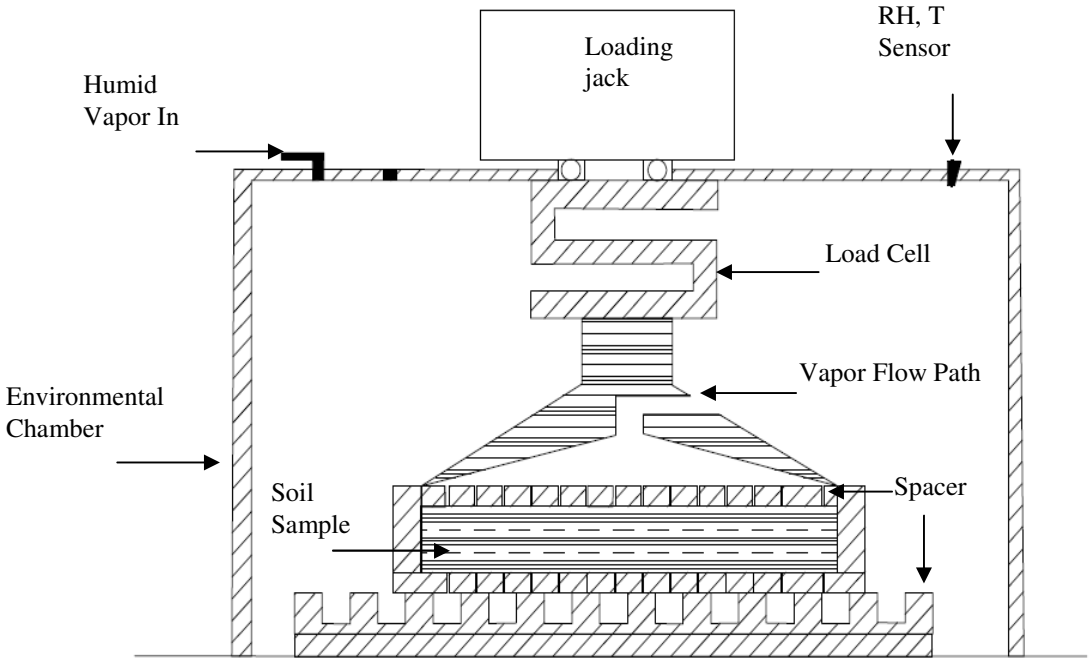

(a)

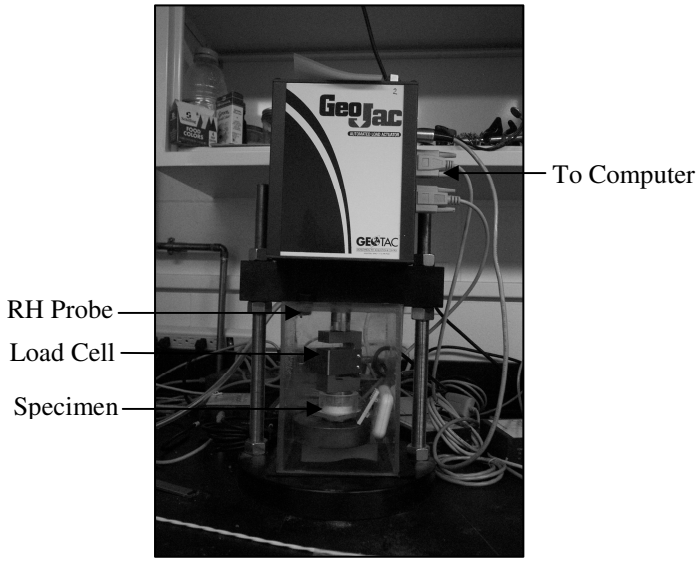

(b)

Figure 3.10 (a) Schematic diagram of cell for controlled stress or controlled strain loading, (b) Photograph of system

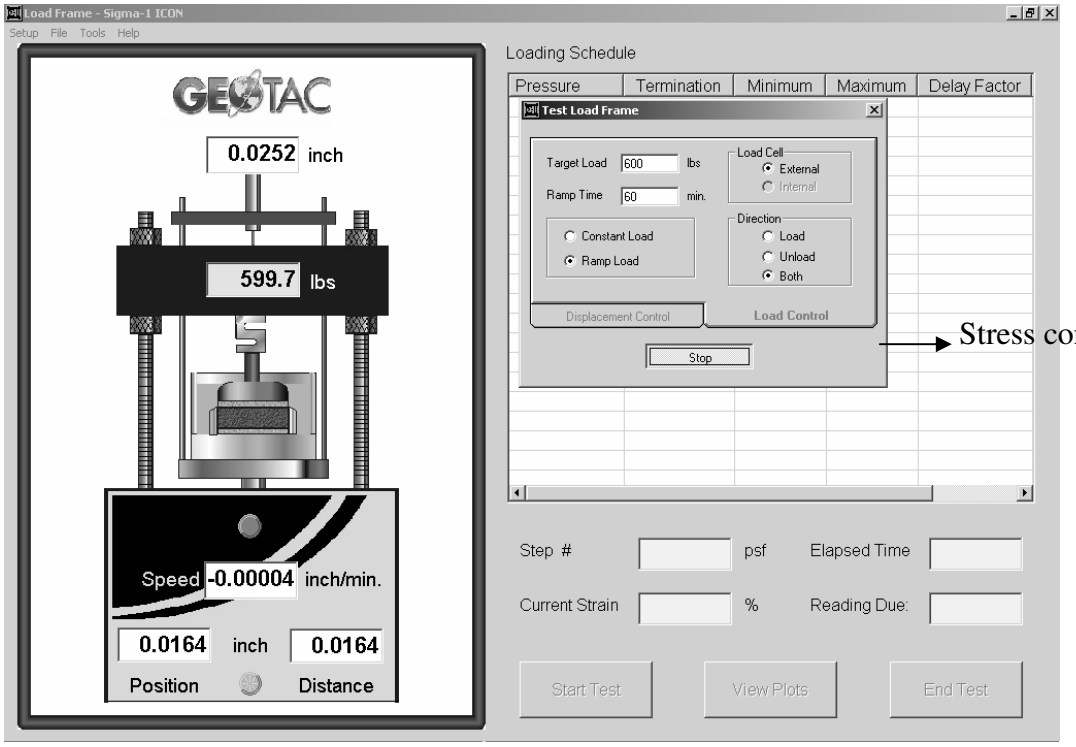

(a)

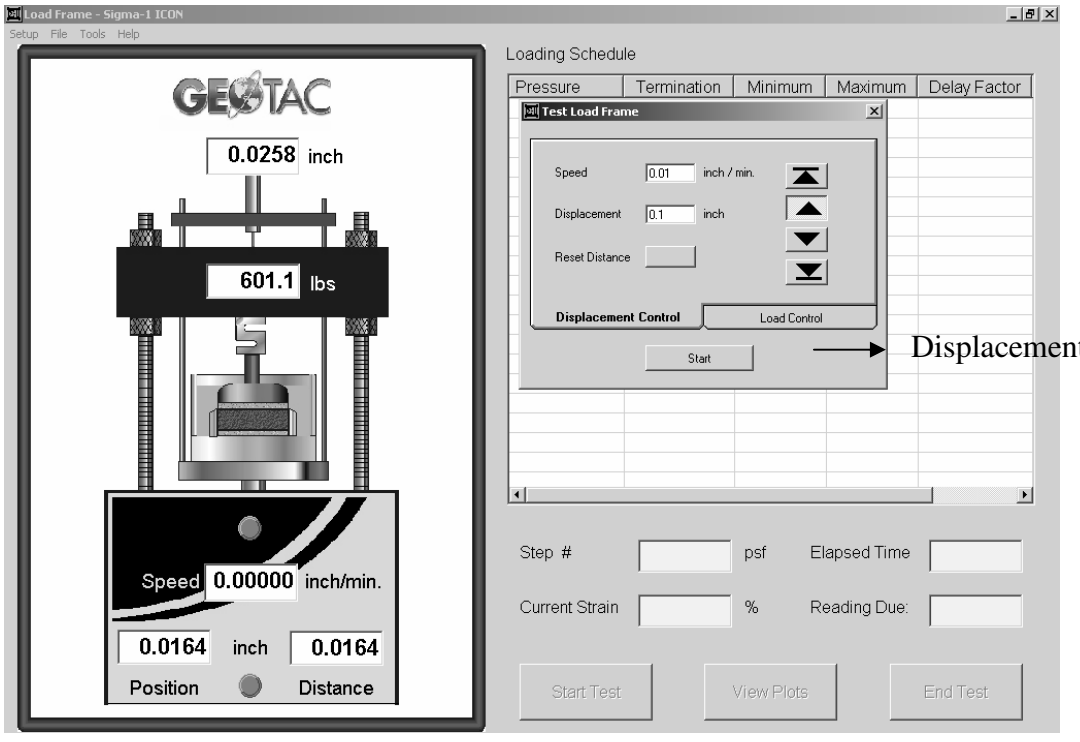

(b)

Figure 3.11. (a) Manual stress control window, (b) Manual strain control window.

Specimen preparation was modified slightly from the procedure described in Section 3.3. The specimen was compacted directly in the acrylic ring using the load actuator and was not subsequently extruded; RH close to zero was applied as soon as the specimen and equipment were placed properly and the environmental cell was closed. Compaction pressure required to obtain desired initial density was applied and maintained to the specimen for 24 hours. Later, the specimen was unloaded to 10 lb (41kPa) and maintained at that normal stress for another 24 hours. Lastly, the loading jack was programmed to maintain zero deformation, the first increment in RH was applied and the corresponding build up for swelling pressure was monitored for steady state conditions.

In order to determine the range of swelling pressures developed, the first three cakes tested were subjected to RH of 0% and 94% only. The remaining tests were performed in a stepwise fashion with RH increments of about 10%.

3.5. Experimental program

Figure 3.12 summarizes the experimental program of this research designed to study the variables affecting macroscopic swelling behavior due to interlayer swelling in the crystalline swelling regime. Three types of clay were tested under the same conditions to study the influence of interlayer cation. SEM images were obtained for the sodium and calcium smectite. Tests under free swelling conditions were performed for the three clays, each test included 10 RH increments. In the case of sodium and calcium smectite, 10 soil specimens with different initial densities were tested using the saturated salt solutions technique; this investigated the effects of clay fabric and compaction density on the bulk response. The Ca-ion-exchanged smectite was tested using the

humidity chamber set up. Swelling pressures were measured under constant strain boundary conditions for dense and loose specimens of Na and Ca smectite; ten increments of RH were used. In addition, dense, medium, and loose sodium smectite cakes were tested under constant strain boundary conditions with just one increment of RH from ~0% to 94%.

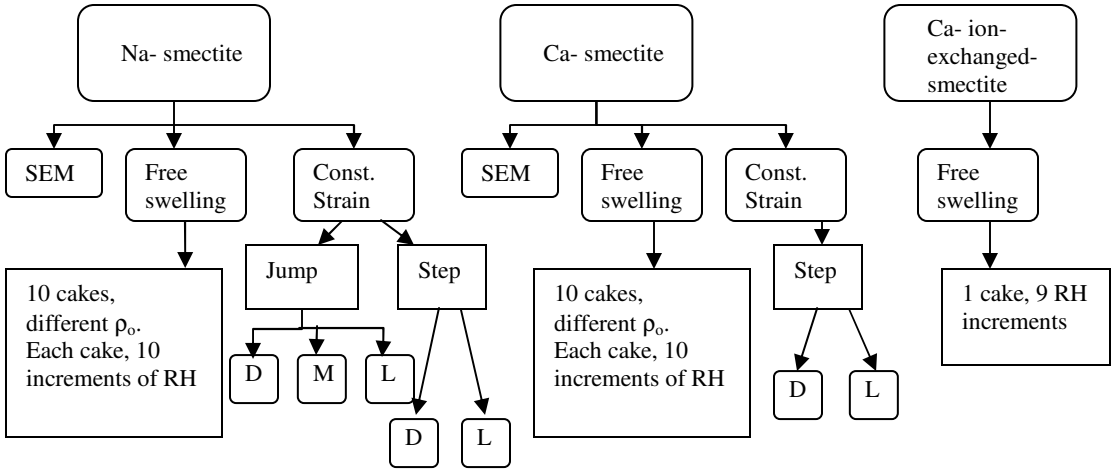

Figure 3.12. Flow diagram of experimental program. (D= dense, M=medium, L=loose compacted specimen)

CHAPTER IV

RESULTS

The experimental focus of this work is on measuring bulk volume changes, water content changes, and swelling pressures developed from crystalline interlayer swelling processes in smectite under controlled stress and suction boundary conditions. Three types of smectites were tested: sodium smectite, calcium smectite, and Ca-exchanged smectite. For each soil type, a suite of compacted specimens with different initial densities were prepared. Tests were performed under either free swelling or constant strain boundary conditions. A detailed description of the test set up, procedure, material properties and sample preparation was provided in chapter III.

4.1. Scanning electron imaging results

Scanning Electron Microscope (SEM) images were obtained for the sodium and calcium smectite specimens to provide qualitative observations of clay pore and particle fabric. Two smectite "cakes" with initial void ratio of 0.8, which underwent the wetting and drying paths were examined in a FEI Quanta 600 SEM; this machine is available in the Electron Microscopy Core facility of the University of Missouri-Columbia. The compacted specimens were split open along the axial axis and a portion of the specimen was mounted so that the freshly cut cross section of the cake was the imaged surface. The specimen was mounted on an SEM pin stub using silver paste, the sides of the sample were painted with silver paint, and about 10 to 20 nm of platinum were sputtered onto the surface.

Sodium smectite images are portrayed in Figure 4.1 at magnifications of 31X and 48X. Pores on a scale of 0.5 to 1 μm are observed, as well as larger pores on a scale of

5 μm or larger. Figure 4.2 displays an SEM image obtained for Ca-smectite; the multi-scale porosities appear less obvious, but thin aggregates of about 2 μm are evident.

The two levels of porosity observed in the SEM images are consistent with previous observations (Lloret et. al, 2003) and confirm the need to analyze expansive clays by considering multi-scale level porosities.

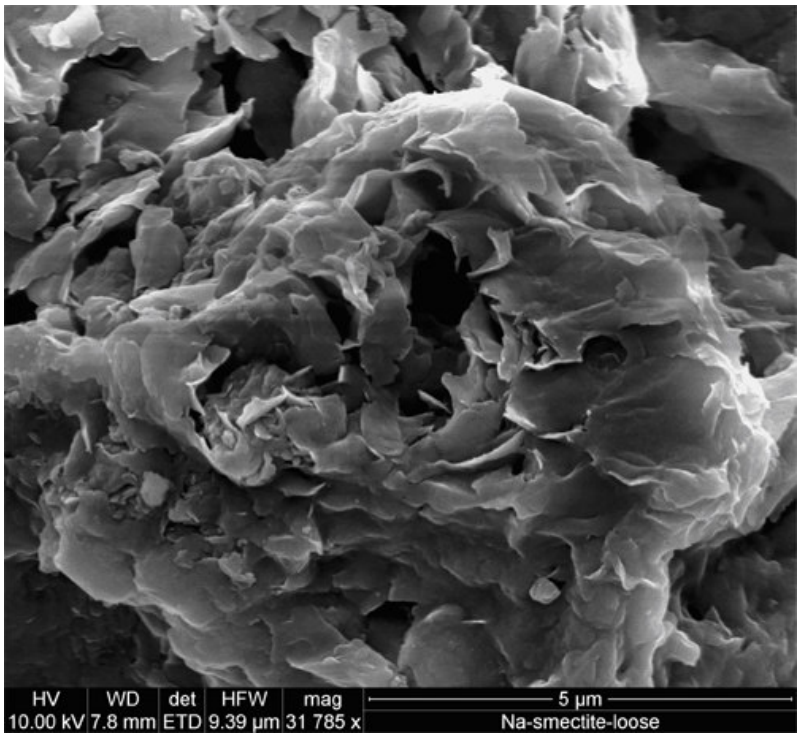

(a)

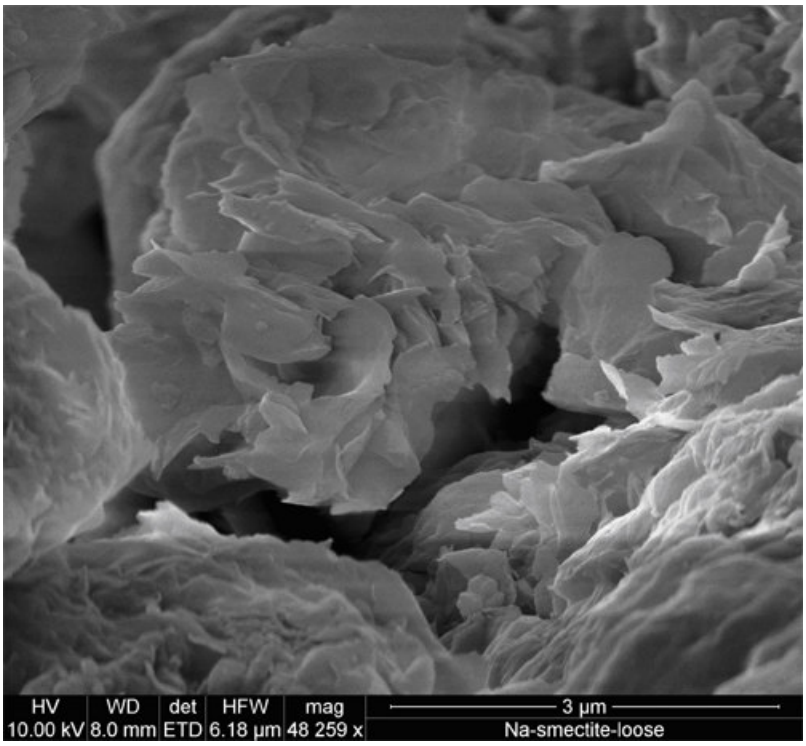

(b)

Figure 4.1. SEM image for Na-smectite

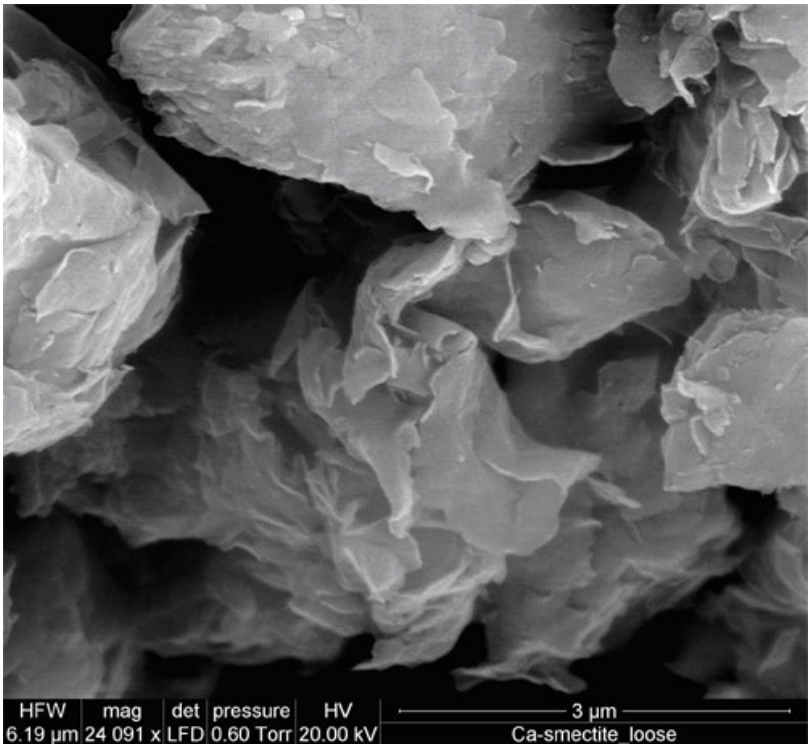

(a)

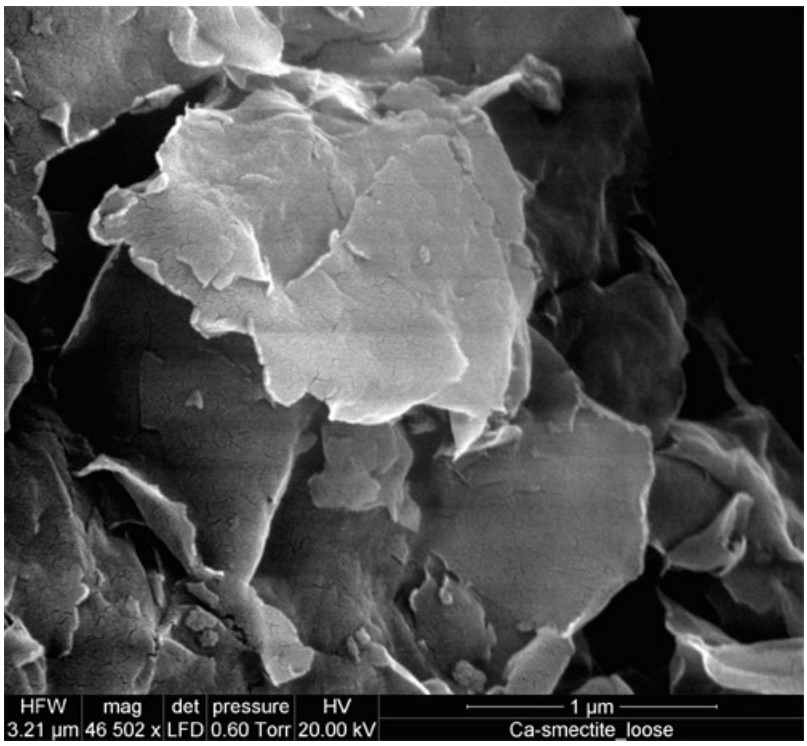

(b)

Figure 4.2. SEM image for Ca-smectite

4.2. Void ratio and compaction pressure

Sodium and calcium smectite specimens were statically compacted to different densities by varying the magnitude of applied compaction pressure. An example of the transient data of applied normal stress and void ratio is provided in Figure 4.3. The process of loading and unloading the sample in this case took about one day; the loading schedule was controlled with an automatic load actuator used for testing under constant strain conditions.

The void ratio measured after the specimen was extruded is shown as a function of the applied compaction pressure in Figure 4.4a. Pressures ranging from 500 to 6400 kPa correspond to void ratios of 1.34 to 0.68 and densities of 1.2 Mg/m^3 to 1.8 Mg/m^3. Figure 4.4b displays a comparison between the new data obtained in this research (plotted with hollow symbols) and previous documented data by Likos & Lu, 2006 (plotted with filled symbols) for both sodium and calcium smectite. The agreement is good, which indicates that the applied normal stress vs. initial density relation is repeatable.

As explained in Chapter III, specimens tested for constant strain conditions were not extruded out of the compaction mold. Data of applied normal stress vs. void ratio during loading and unloading were obtained. Typical curves for sodium and calcium smectite are shown in Figure 4.5. The rebound slope for Ca-smectite is steeper than the one for Na-smectite; also a steeper slope on the rebound curve for lower applied normal stress values.

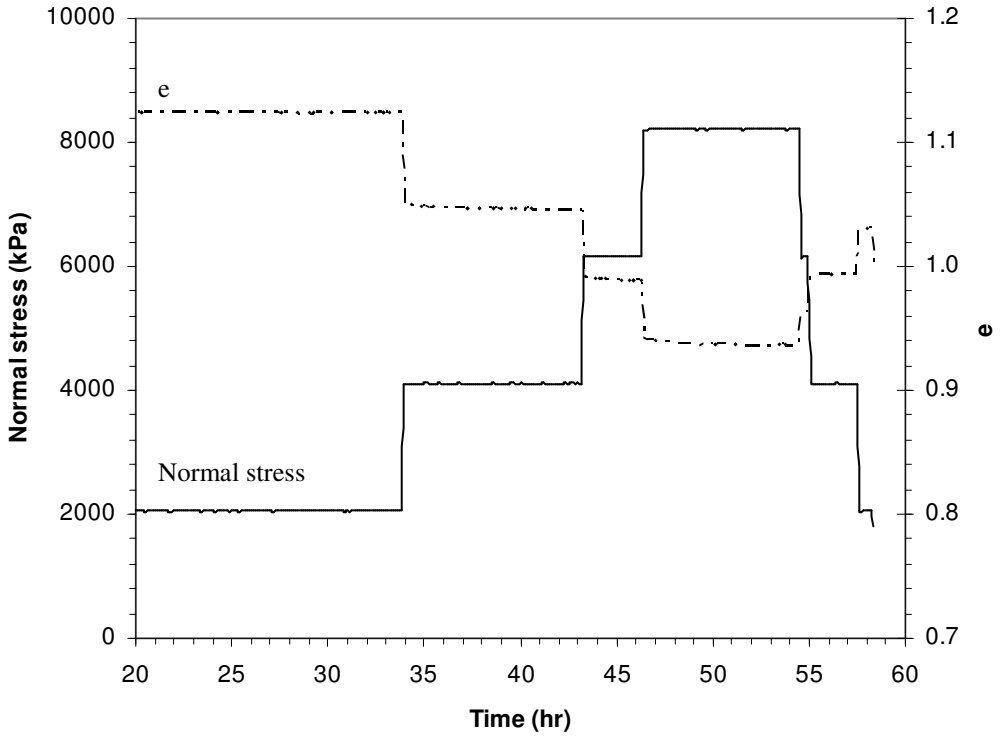

Figure 4.3. Transient volume change response during compaction of Na-smectite.

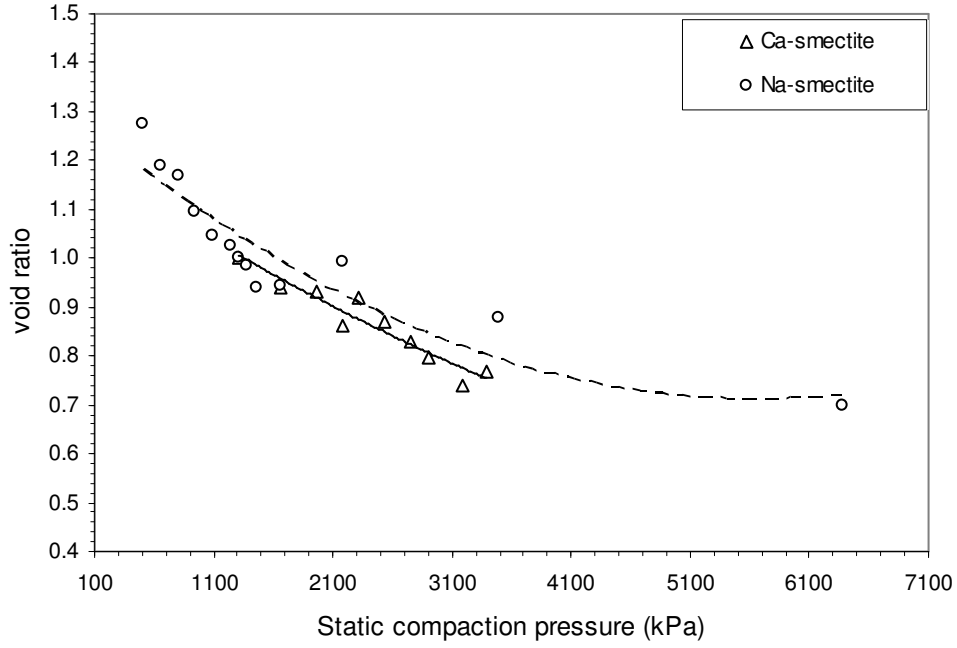

(a)

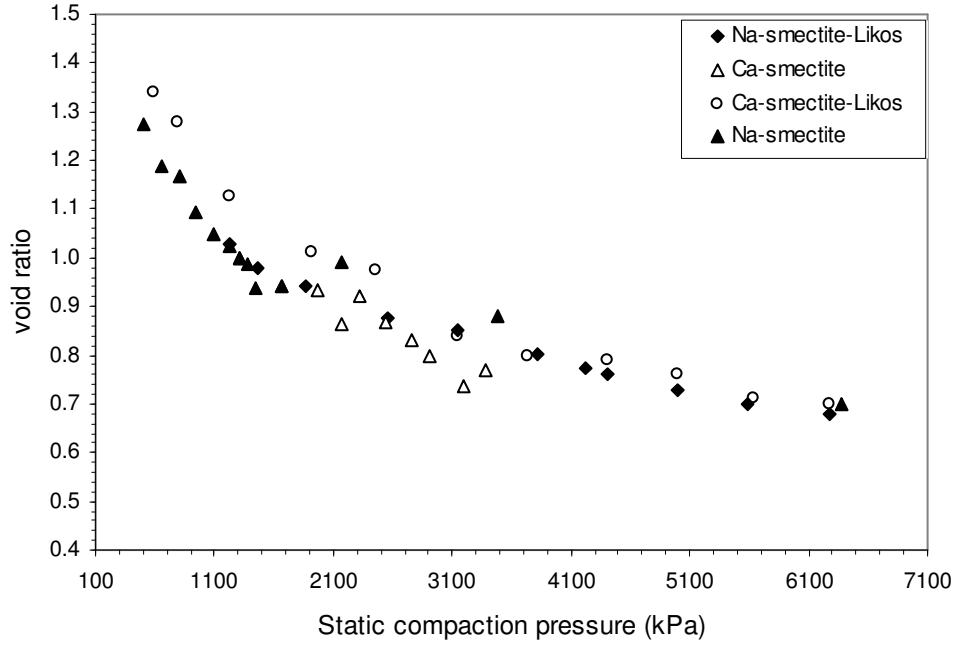

(b)

Figure 4.4. Void ratio as a function of static compaction pressure a) in this research, b) comparison with Likos & Lu data.

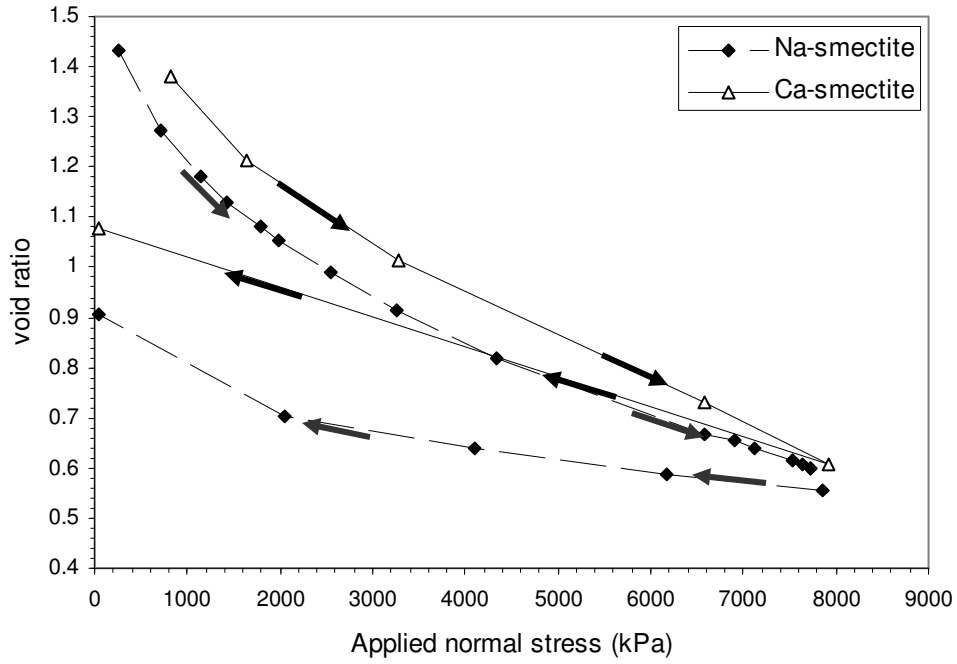

Figure 4.5. Typical loading and unloading curves for Na and Ca-smectite.

4.3. Free swelling behavior

Water vapor sorption isotherms and bulk volume change were obtained for the Na, Ca, and Ca ion exchanged smectite specimens from the free-swelling boundary conditions, multi-step testing series. Results for the Na and Ca smectites were obtained using the saturated salt solution jars set up and a suite of 10 specimens compacted at different initial densities. Data for the Ca^{+2} ion exchange smectite specimen were obtained using the humidity chamber system with boundary conditions of free swelling.

The duration time for the saturated salt solution tests was about 3 months for both wetting and drying; on the other hand, 1800 hours (~2.5 months) were necessary to complete the wetting process for the test performed using the automated humidity system.

4.3.1. Sorption isotherms

Typical isotherms for loose (e=1.3), medium (e=1.1), and dense (e=0.88) compacted sodium smectite samples are portrayed in Figure 4.6. The wetting-drying path ranges from 5% to 97% and back to 7% RH. Gravimetric water content at the maximum RH is around 24%. The effect of initial density of the specimens is negligible on the sorption isotherms. Loose, medium, and dense specimens follow almost identical wetting paths; a small difference is observed in the drying portion for the medium compacted sample. Results exhibit hysteretic behavior.

The wavy behavior with a defined double step observed previously for Na-smectite (Rouquerol, 1999) is not as evident in these results, probably due to larger RH intervals in the data. However, an analysis of change in axial deformation as a function of RH for these data (Chapter V) confirms the presence of two steeper portions in the axial deformation at RH 10 to 30% and 60 to 90%.

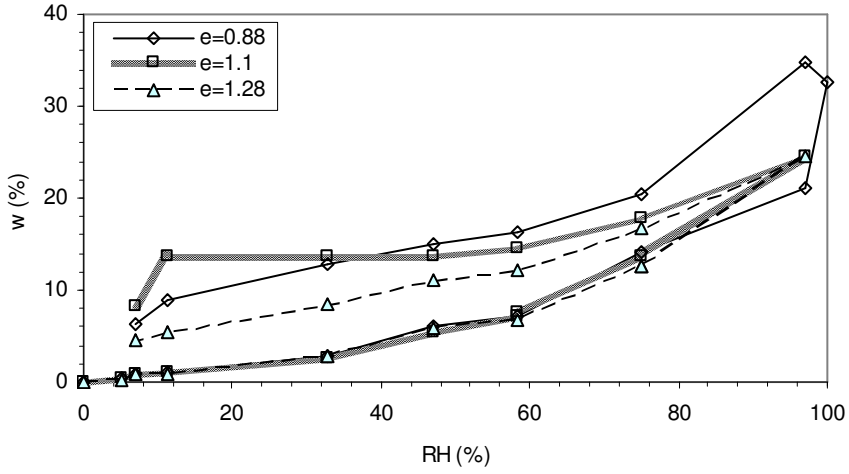

Figure 4.6. Sorption isotherms for Na-smectite: dense, medium, and loose cakes

Sorption isotherms for ten compacted calcium smectite specimens were also obtained using the saturated salt solution jars set up. Typical behavior for loose, medium,

and dense specimens are presented in Figure 4.7. Similar to the Na-smectite results, sorption isotherms seem independent of the initial density of the specimen. A steeper portion in the curve is observed at RH ranging from 10% to 40%.

Gravimetric water content corresponding to 85%RH is about 20%, which agrees with previous observations (Likos & Lu, 2006). For the next increment in RH (97%), the corresponding water content is close to 30%. Hysteresis in Ca-smectite is smaller than for Na-smectite.

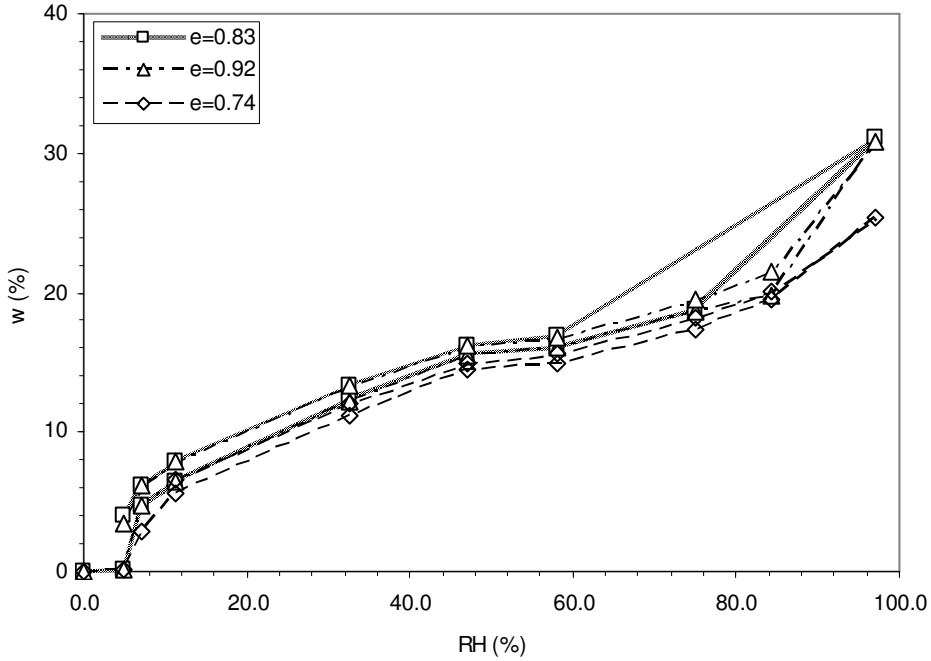

Figure 4.7. Sorption isotherm for Ca-smectite: dense, medium, and loose cakes

In the third test, a specimen of Ca-exchanged smectite with e=0.88 was tested under free swelling conditions using the automated humidity system set up. Relative humidity was increased in stepwise increments of around 10% from 0% to 80%. An example of the transient data obtained for this test is presented in Figure 4.8. The data were logged every 15 min, the mass recorded includes an offset due to the mass of the

LVDT and a base plate where the specimen was placed. Noise in the balance and in the RH sensor increased when the air conditioning system in the laboratory was active. Steady state values of RH and mass recorded from the transient data were obtained by taking an average value of the variable when the pattern of both RH and mass functions indicated no more change.

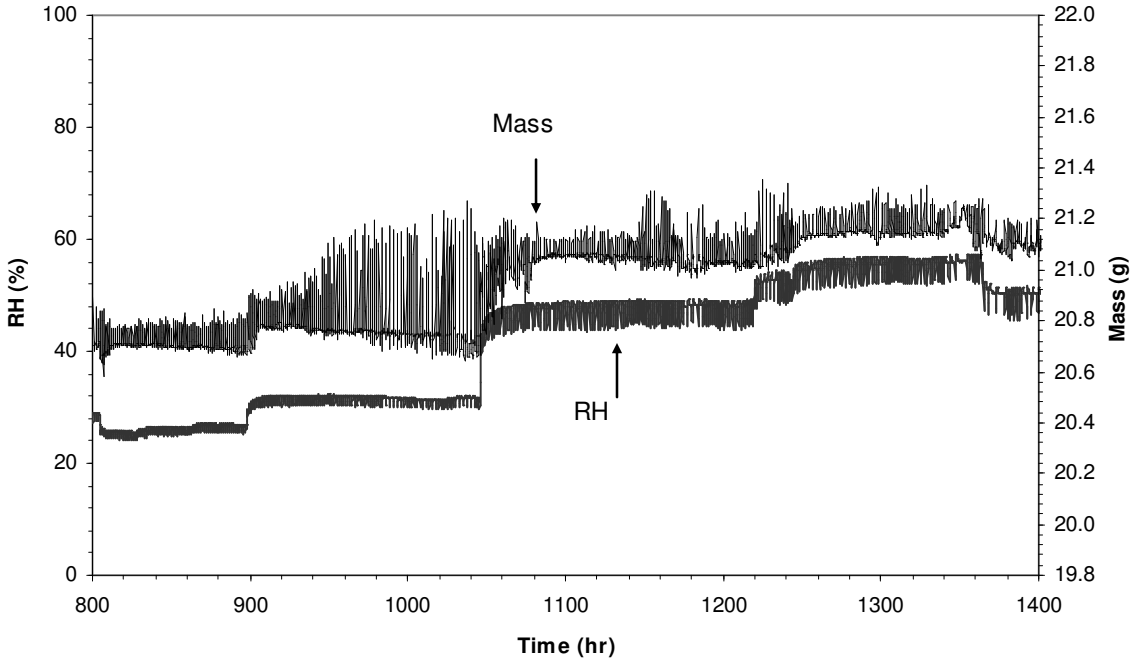

Figure 4.8. Mass and RH transient data for Ca-exchange smectite, e=0.88

Figure 4.9 compares the sorption isotherms of the three clays used in this research for specimens with similar initial void ratio (e=0.83 to e=0.88). Isotherms for Ca-exchanged and Ca-smectite are very similar. In both clays, a steep increase in water content is observed at RH of about 55%. As illustrated here, it was also noted that gravimetric water content throughout the test is higher for the clays with Ca^{+2} interlayer

cations than for clays of the Na form. At RH=80%, the water content of the specimen was measured to be 20%.

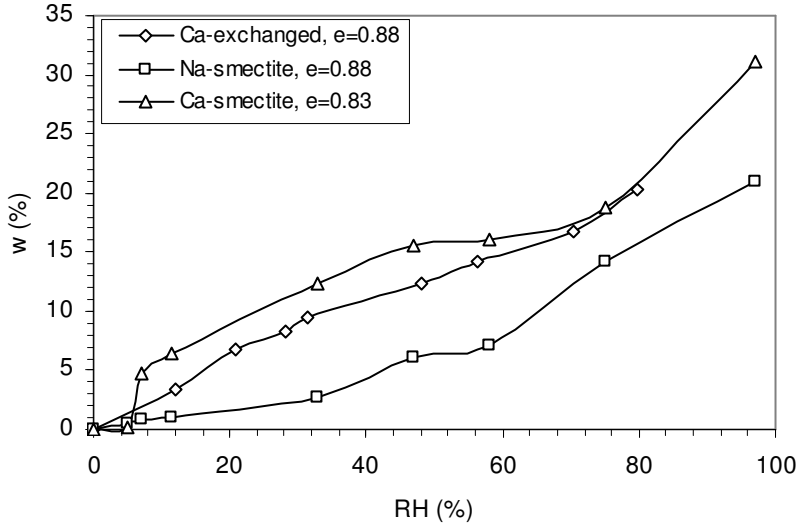

Figure 4.9. Comparison of sorption isotherms for three clays

4.3.2. Bulk volume change

Axial strain at equilibrium was measured after each change in RH during the wetting and drying cycles. As explained in the previous chapter, calculation of the final void ratios was based on the assumption that axial and radial strains are equivalent.

Typical curves for dense (e=0.9), medium (e=1.1), and loose (e=1.3) compacted sodium smectite specimens are displayed in Figure 4.10. Unlike the sorption isotherms, bulk volume change is very sensitive to the initial density of the soil sample; a larger increase in bulk volume was observed for the denser specimens. The maximum axial strain values for soil samples with void ratios of 0.9, 1.1, and 1.3 are 25%, 17%, and 13% respectively. Thus, for an increase in void ratio of 0.4, the corresponding axial strain increased by 92% its original value.

The wavy behavior corresponding to the hydration layer transitions was not so evident for the first hydration layer (RH=10%-30%), but a steeper portion in the curve was observed at RH of 60% to 80%, which correspond to the second layer hydration. In general, the effect of initial void ratio in axial strain for lower RH values was significantly lower than that of RH equal or larger than 60%. Hysteresis was evident in the three cases, with axial strain being greater during the drying cycle than for the same RH during wetting; thus, plastic volume changes occur.

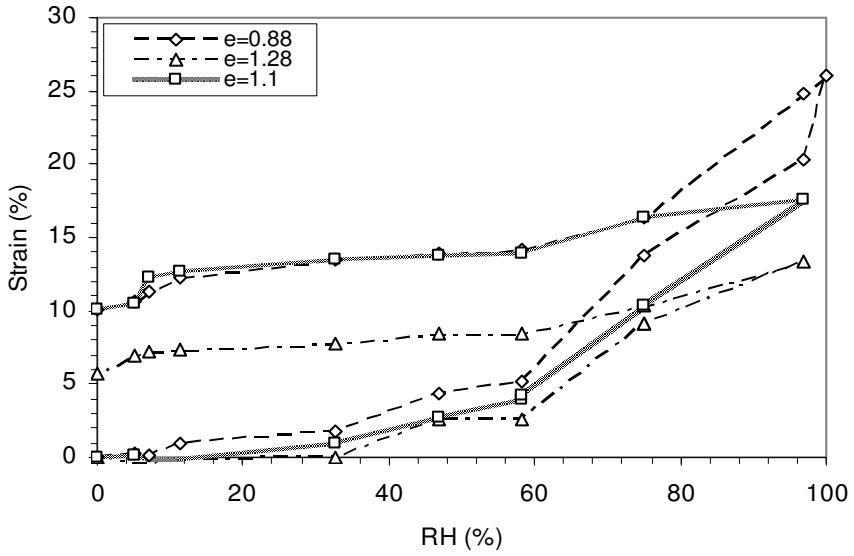

Figure 4.10. Bulk volume change for Na-smectite: dense, medium, and loose specimens

A similar analysis was performed for volume change in Ca-smectite specimens. Typical curves for a dense, medium, and loosely compacted soil cakes are depicted in Figure 4.11. The maximum axial strain values for soil samples with void ratios of 0.74, 0.83, and 0.92 are 48%, 42%, and 27% respectively. Thus, the effect of initial density on total volume change is larger than for Na-smectite.

The sorption isotherm behavior was also reflected in the axial strain response for Ca-smectite. Significant volume increase is observed at RH ranging from 5% to 40%,

but in general, the total volume of the specimen increased throughout the whole RH range. Hysteresis was more significant for the Na-smectite than for the Ca-smectite at the same RH values and initial void ratios. Within the same clay, denser specimens present larger unrecovered volume.

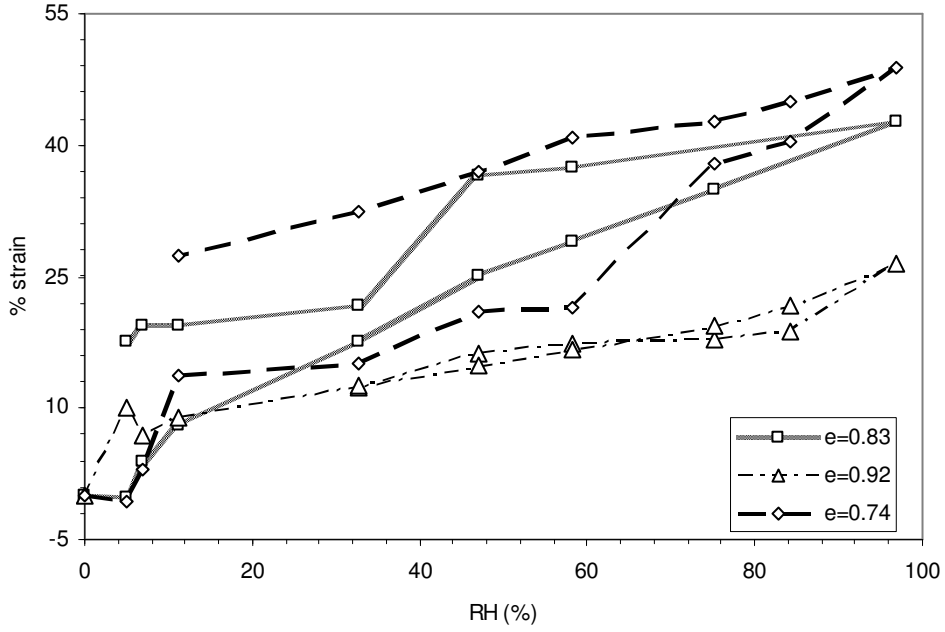

Figure 4.11. Bulk volume change for Ca-smectite: dense, medium, and loose specimens

Total volume change as a function of RH was also obtained for the Ca-exchanged smectite specimen. An example of transient data of the axial deformation and RH values is provided in Figure 4.12; each increment in RH was reflected by an increase in axial strain. Figure 4.13 compares the bulk volume change response of the three clays for specimens compacted to the similar initial void ratio (e=0.83 to e=0.88). Axial strain values at RH of 80% are 8%, 15%, and 37% for the Ca-exchanged, sodium, and calcium smectite respectively. Similar to the Ca-smectite, the shape of the volume change curve for the Ca-exchanged smectite reflects larger volume increase at RH ranging from 5% to

40%, and a smaller but steady increase for larger RH values. In terms of magnitude, the Ca-exchanged smectite had the lowest axial strain of the three clays. Thus, from Figures 4.9 and 4.13, it is observed that the exchange cation affects sorption response but it does not affect the volume change response.

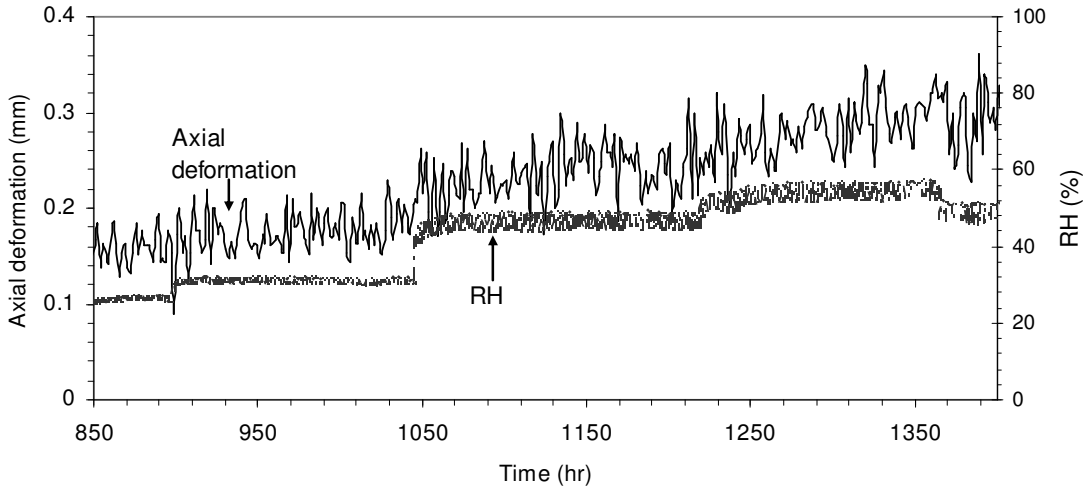

Figure 4.12. Deformation and RH transient data for Ca-exchange smectite

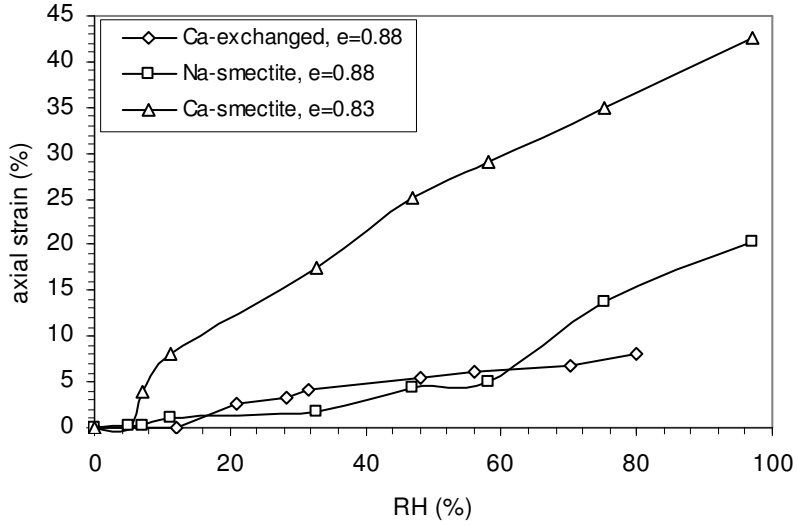

Figure 4.13. Comparison of bulk volume change for three clays

4.4 Swelling pressure under constant strain conditions

Swelling pressure resulting from the increase of RH while the soil cake was maintained at constant strain boundary conditions was obtained using the automated humidity control system. Three preliminary tests for sodium smectite specimens compacted at initial void ratios of 0.77, 0.8, and 0.84 were performed to obtain the range of expected swelling pressures; in this way, the range and accuracy of the load cell used in the set up were determined. The samples were extruded and later placed back in the confining ring; RH was then increased directly from 0% to 90%. An example of the transient data obtained for the e=0.77 soil cake is portrayed in Figure 4.14. Swelling pressure increased steadily up to 315 kPa during the first 500 hours; it reached steady state 300 hours later at 374 kPa. Data was accidentally lost for the time interval of t= 355 hr to 440 hr due to a malfunction of the program. A leak in the chamber was detected at times t= 220 hr and t= 480 hr; the set up was fixed to ensure no future leaks would occur. Since the objective of this test was to evaluate the range of expected swelling pressures and the effectiveness of the set up, the test was carried out to termination despite the drawbacks during the process. Results for specimens with void ratios of 0.8 and 0.84 indicated swelling pressures of 367 kPa and 304 kPa respectively. It took an average of 800 hours (~33 days) for the swelling pressure to reach steady state. The general observation is that larger swelling pressures are developed for denser specimens, which is consistent with the results in section 4.3 where the largest strain was measured for the specimen with lowest initial void ratio.

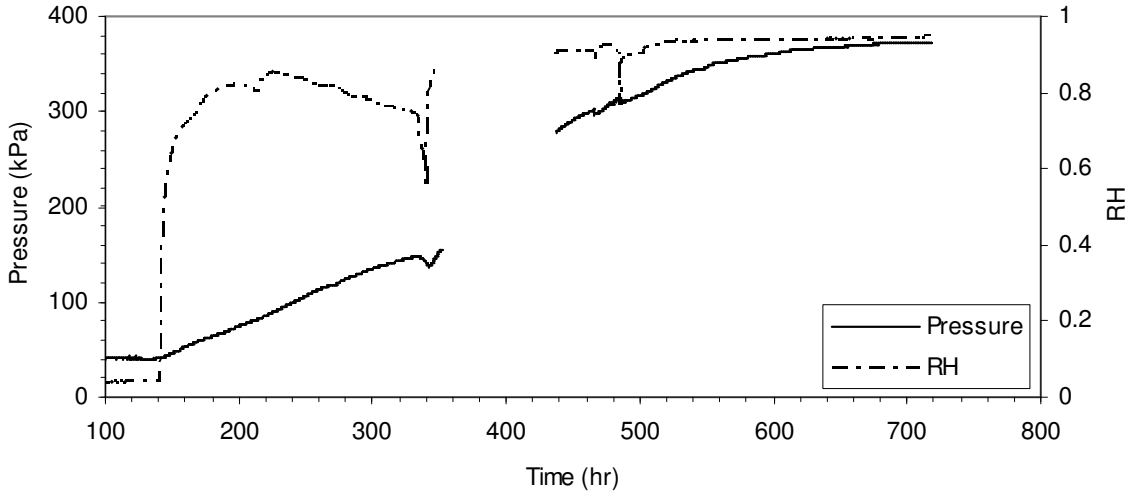

Figure 4.14. Transient response for Na-smectite, e=0.77

A second set of tests consisted of measuring the equilibrium swelling pressure of sodium and calcium smectite at incremental RH values; dense and loosely compacted soil cakes of each clay were tested. Examples of the transient data for the dense specimens of sodium and calcium smectite are shown in Figures 4.15 and 4.16. Results for the Na-smectite samples display a fast increase in swelling pressure right after RH was increased, followed by a small sudden pressure release and a consecutive slow build up in the next 500 hours. Results for the Ca-smectite samples indicate that swelling pressure actually decreased for RH greater than 50% (suction smaller than 100 kPa). It took 3,800 hours (5.2 months) for the Na-smectite and 5,000 hours (6.9 months) for the Ca-smectite to complete the test using 8 RH increments.

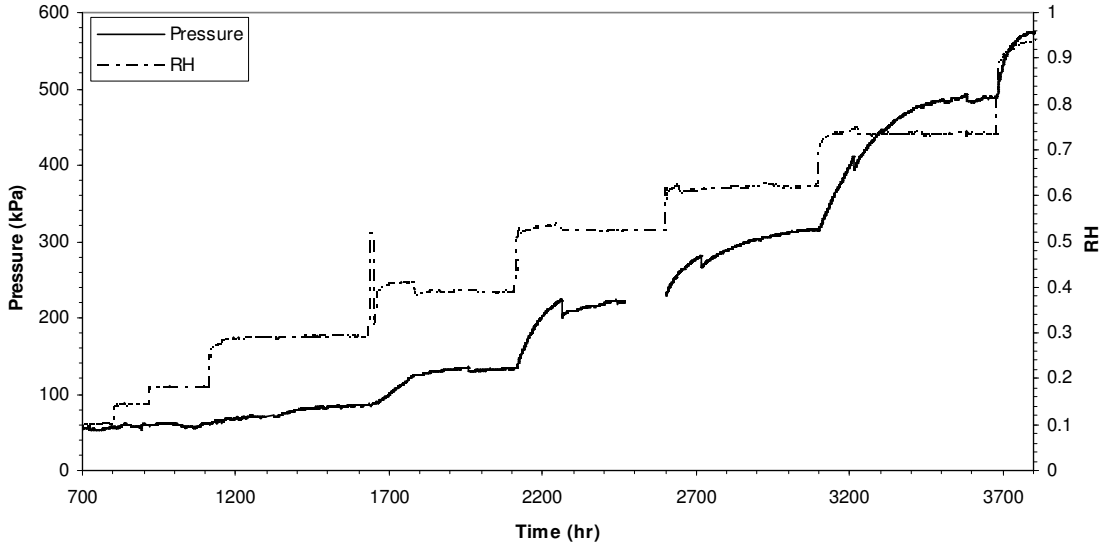

Figure 4.15. Transient response for Na-smectite, stepwise RH increments

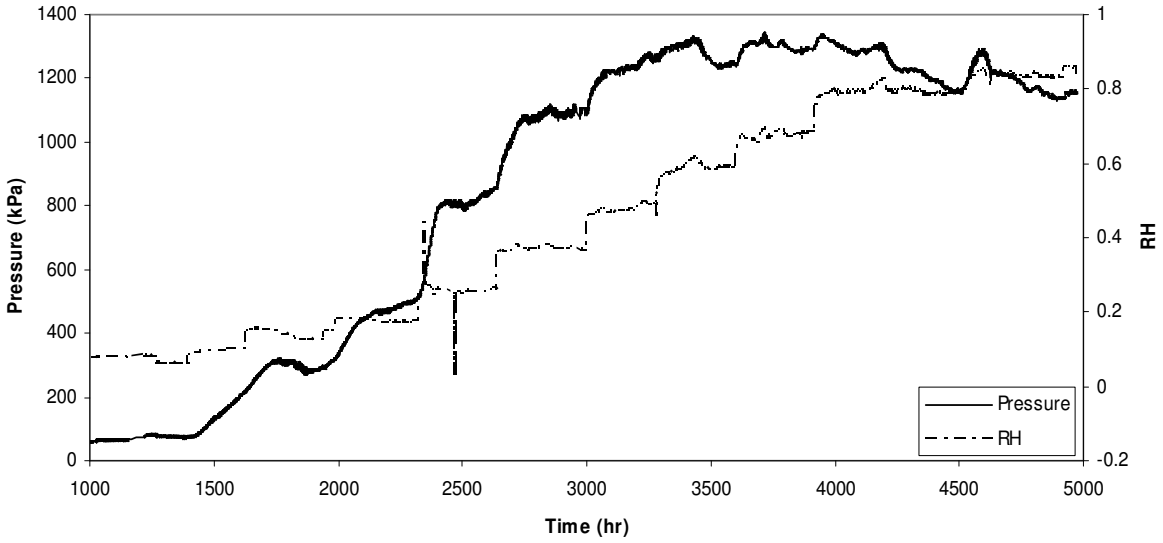

Figure 4.16. Transient response for Ca-smectite, stepwise RH increments

Equilibrium swelling pressure measured at a given suction value was obtained for the loose and dense specimens of the sodium and calcium smectite (Figure 4.17). Results indicate that the sodium smectite develops similar swelling pressures for suction values greater than 87 MPa (RH <52%) regardless of the initial packing density; it is only for

lower suction values that the denser specimen develops larger pressures. At RH of 95% (suction of 7 MPa), dense and loose Na-smectite cakes show corresponding swelling pressures of 573 kPa and 317 kPa respectively.

Ca-smectite specimens are more sensitive to the initial void ratio. A difference of up to 714 kPa was measured between loose and dense cakes at 100 MPa of suction. Swelling pressures decreased in both cases for suctions lower than 100 MPa. The maximum pressure values for the dense and loose specimens are 1294 kPa and 538 kPa respectively.

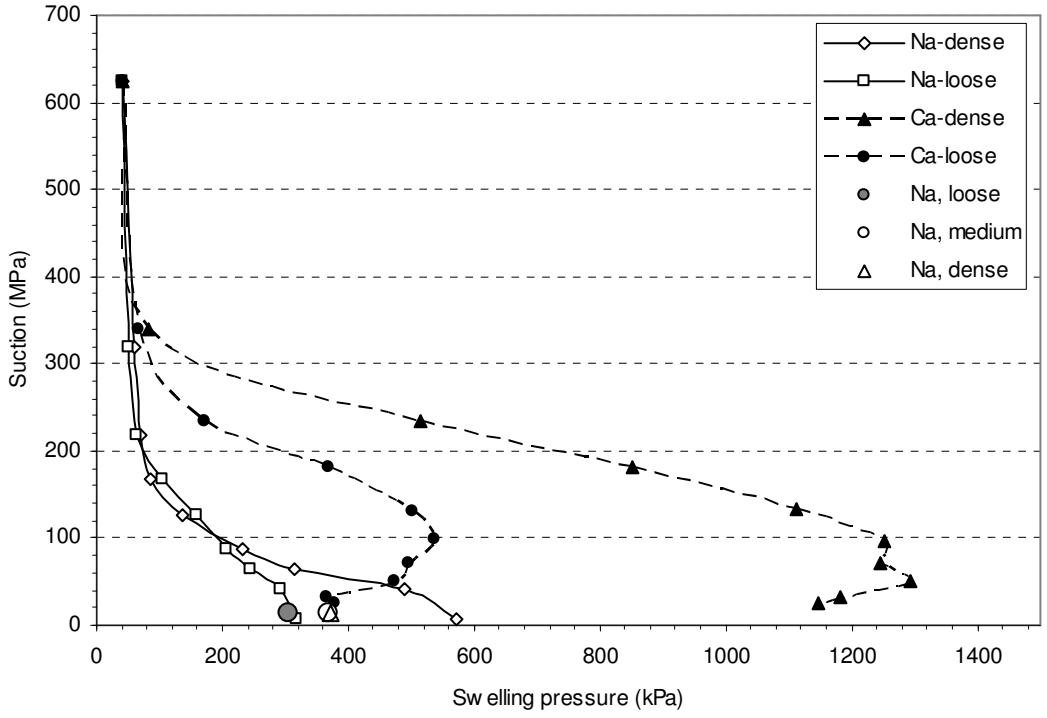

Figure 4.17. Swelling pressure response for decreasing suction (increasing RH) for Na and Ca-smectite.

4.5. Summary of experimental observations

The following are the general observations obtained from the experimental results:

1) Two levels of porosity were identified in the SEM images. The images reflect previous studies with MIP (Lloret et. al, 2003), confirming the existence of multi-scale level porosities in expansive clays. Sodium smectite quasicrystals formed a rose-like structure; calcium smectite quasicrystals were more randomly oriented.
2) Relation between initial void ratio and compaction pressure follows an exponential pattern; the data proved to be fairly repeatable.
3) The wavy behavior expected for Na-smectite sorption isotherms is not readily apparent; however, it is supported by previous observations and consistent with analysis in Chapter V.
4) Sorption isotherms for Ca- smectite exhibit a steeper portion in the curve for RH of 10% to 40%; in general, water content increases with RH throughout the test.
5) Effect of initial density in specimens is negligible in the sorption isotherms.
6) During the crystalline swelling regime, the Ca-smectite was observed to absorb more water than the Na-smectite at a given RH value.
7) Sorption isotherms for the Ca-exchanged and Ca-smectite clays are similar to each other both in shape and in magnitude.
8) The wavy behavior of sorption isotherms is reflected both in the axial strain response for free swell tests and in the swelling pressures measured for constant strain tests.
9) The Ca-exchanged smectite is the clay with lowest axial strain out of the three clays used.
10) The exchange cation affects sorption response but it does not affect the volume change response.

11) Initial density has a significant effect on the bulk volume change and swelling pressures measured, especially for RH values greater than 60%.

12) Swelling pressures for the Ca-smectite specimens undergoing wetting decrease for suctions lower than 100 MPa.

CHAPTER V

ANALYSIS OF RESULTS

Review of the literature (Chapter II) reveals a number of distinctive features in expansive soil behavior: 1) all clays swell to some extent; key factors governing the amount of swelling include mineralogy, exchange cation identity, initial density, and initial water content; 2) macroscale swelling strains depend on confining stress; and 3) stress paths and suction paths (e.g., wetting and drying paths) have strong effects on bulk clay response, with reversible and irreversible components of strain occurring along these paths.

Results from the current experimental program are qualitatively analyzed in this chapter in the context of these generalities, as well as quantitatively in the context of three specific models or conceptual frameworks. These include the Likos and Lu (2006) porosity evolution model, the Gens and Alonso (1990) Basic Barcelona Model (BBM), and a new microstructural model developed by considering the hydration behavior of an idealized pore element representative of expansive soil fabric. The Likos and Lu (2006) model was initially described in Section 2.9 and is considered here in Section 5.3. The BBM was initially described in Section 2.10 and is considered here in Section 5.4. The new clay fabric model is introduced and considered in the context of the experimental results in Section 5.1. All three models share the common thread of treating interactions among the multiple levels of porosity in compacted expansive soil systems as a governing factor for capturing the effectiveness of how micro or particle-scale volume change translates to macro or bulk-scale volume change and swelling pressure.

5.1 Interpretation of general observations

Section 4.5 summarized a series of experimental observations made from the results of the laboratory testing program. The following sections provide interpretation and analysis of these observations.

5.1.1. Sorption isotherms

Water vapor sorption isotherms for the sodium, calcium, and calcium-ion-exchanged smectites were presented in Figures 4.6, 4.7, and 4.9, respectively. It was noted that the isotherms exhibit wavy behavior, which was interpreted to indicate the successive adsorption of molecular water layers in the interlayer space as associated with crystalline swelling.

The effect of initial density in sodium and calcium smectite specimens is negligible on the sorption isotherms. Loose, medium, and dense specimens follow almost identical sorption paths. This may be explained by considering that regardless of the initial compaction level, the number of discrete water layers intercalated between the clay minerals depends mainly on the adsorption energy of water on the cations and clay mineral surface. Interlayer sorption is a phenomenon occurring on the sub-particle scale, and therefore, is insensitive to the fabric or geometry of the larger scale pores influenced by compaction. In Figure 4.6, the difference in the drying portion of the moderately compacted Na-smectite sample (e = 1.1) is probably due to mass loss while transferring the specimen from jars of 47%RH to 32.7%RH.

Gravimetric water contents at 97% RH values are larger than previous reported measurements (Figures 4.6, 4.7) (Karaborni *et al.*, 1996, Likos & Lu, 2006). This may be due to osmotic swelling occurring at RH values greater than 90%.

In general, Ca-smectite was observed to absorb more water at a given RH value, which reflects higher forces of initial hydration. This is consistent with the probability that a Ca-smectite has more mineral layers in each quasi-crystal (Tessier, 1990).

5.1.2. Bulk volume change and swelling pressure behavior

5.1.2.1 Sodium Smectite

Relationships between bulk volume change (axial strain) and RH along hydration and dehydration paths for dense, medium, and loose Na-smectite specimens in the crystalline swelling regime and under free-swell boundary conditions were presented in Figure 4.10. Relationships between bulk swelling pressure and RH under zero-volume-change boundary conditions were presented in Figures 4.14, 4.15, and 4.17.

The wavy behavior of sorption isotherms observed in previous studies (Figure 2.12) is not as evident in the data obtained. However, a closer analysis of bulk volume change and swell pressure response of the compacted clay specimens reflect the wavy behavior noted in the sorption isotherms. To illustrate this point, derivative forms of the volume and pressure change behavior for the three clays (Na-smectite, Ca-smectite, and Ca-exchanged smectite) are presented in Figures 5.1-5.3.

Figure 5.1a depicts volume change response for the Na-smectite compacted to three initial densities (e = 0.9, 1.1, and 1.3). Figure 5.11b shows swelling pressure response for the Na-smectite prepared to two initial compaction conditions: dense, where e = 0.75, and loose, where e = 0.9. The axial strain response (Figure 5.1a) exhibits two peaks that are interpreted to correspond to the 0-to-1 and 1-to-2 hydration layer states, respectively. These occur nominally at 10% to 30% RH and at 60% to 80% RH. Denser

specimens result in larger axial deformation because they have less inter-particle pore space, so crystalline interlayer swelling can translate more effectively into bulk volume change. Two peaks are also observed in the swell pressure response (Figure 5.1b), which are consistent with the locations of the peaks (similar RH ranges) noted in the free swell volume change response. The loose Na-smectite exhibits a humped peak at RH of approximately 37% (first layer hydration); a lower regime of relatively constant pressure may also be observed at RH of about 70%, which corresponds to the second layer hydration. Conversely, for the dense specimen, the second peak at RH of 74%, corresponding to the one-to-two layer hydration transition is sharper. These observations may be interpreted as follows.

As illustrated conceptually on Figures 5.2-5.3., the fabric of specimens compacted at lower densities is expected to have larger inter-particle void space. During the zero-to-one layer hydration transition, the interlayer swelling is partially absorbed into the inter-particle void space, while the remaining portion translates as macroscopic swelling pressure. It was observed in each RH increment of the transient data (Figure 4.15) that a small sudden pressure drop occurred right after swelling pressure had reached a peak value; this pressure release may be due to a collapse and re-arrangement in the fabric. During the subsequent one-to-two layer transition, some of the interlayer swelling may be still be absorbed into the now re-arranged inter-particle voids, resulting in a lower $\Delta P/\Delta RH$ peak (Figure 5.2).

On the other hand, the initial fabric in the denser specimen has smaller inter-particle void space; transient data show lower swelling pressure release which indicates minimum collapse and re-arrangement of the fabric. During the first hydration layer

some of the swelling is absorbed into the interparticle void space, but with less space available, a significant increase in swelling pressure was measured for RH corresponding to the second hydration layer state (Figure 5.3).

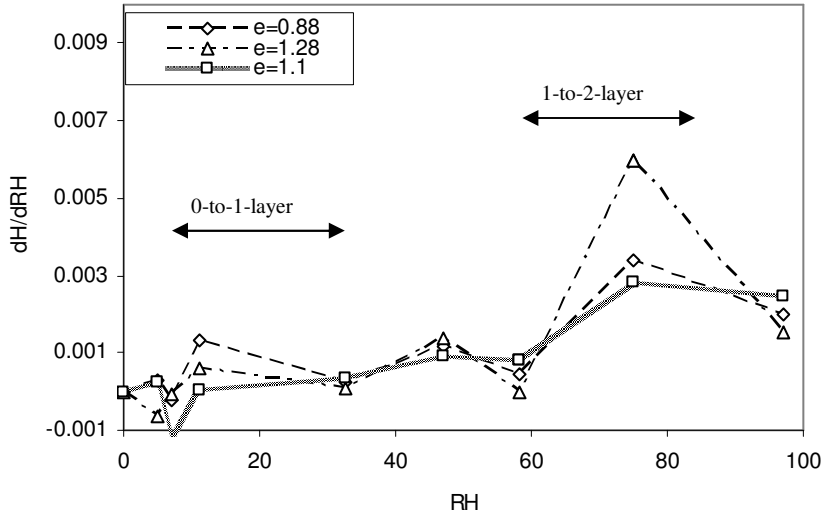

(a)

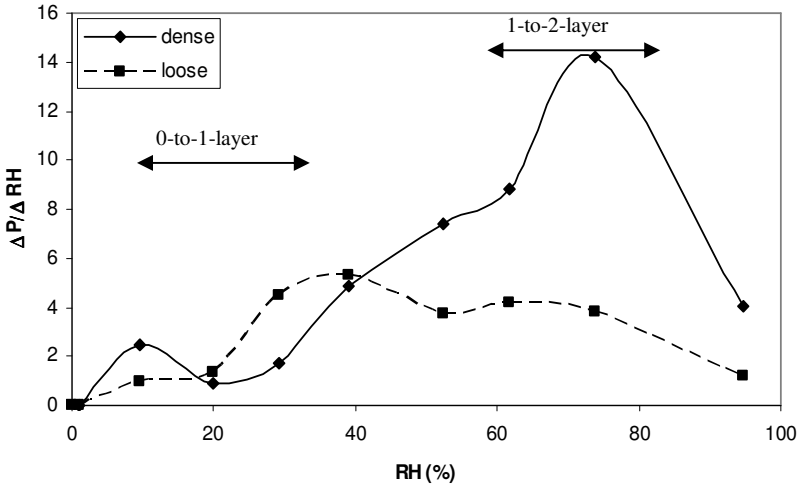

(b)

Figure 5.1. Derivative of (a) axial strain, (b) swelling pressure as a function of RH for Na-smectite

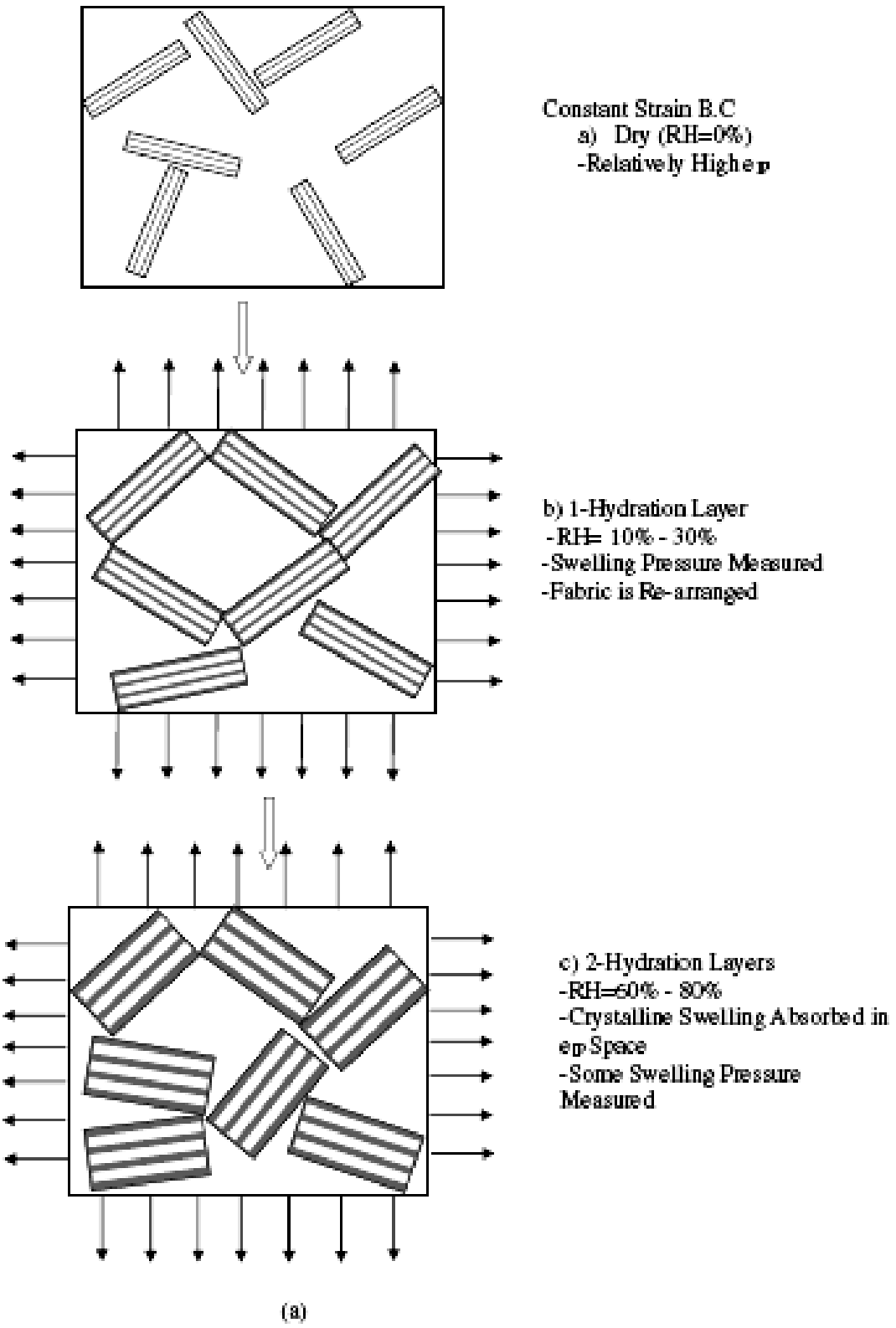

Figure 5.2. Schematic diagram of Na-smectite swelling pressure process for a loose specimen

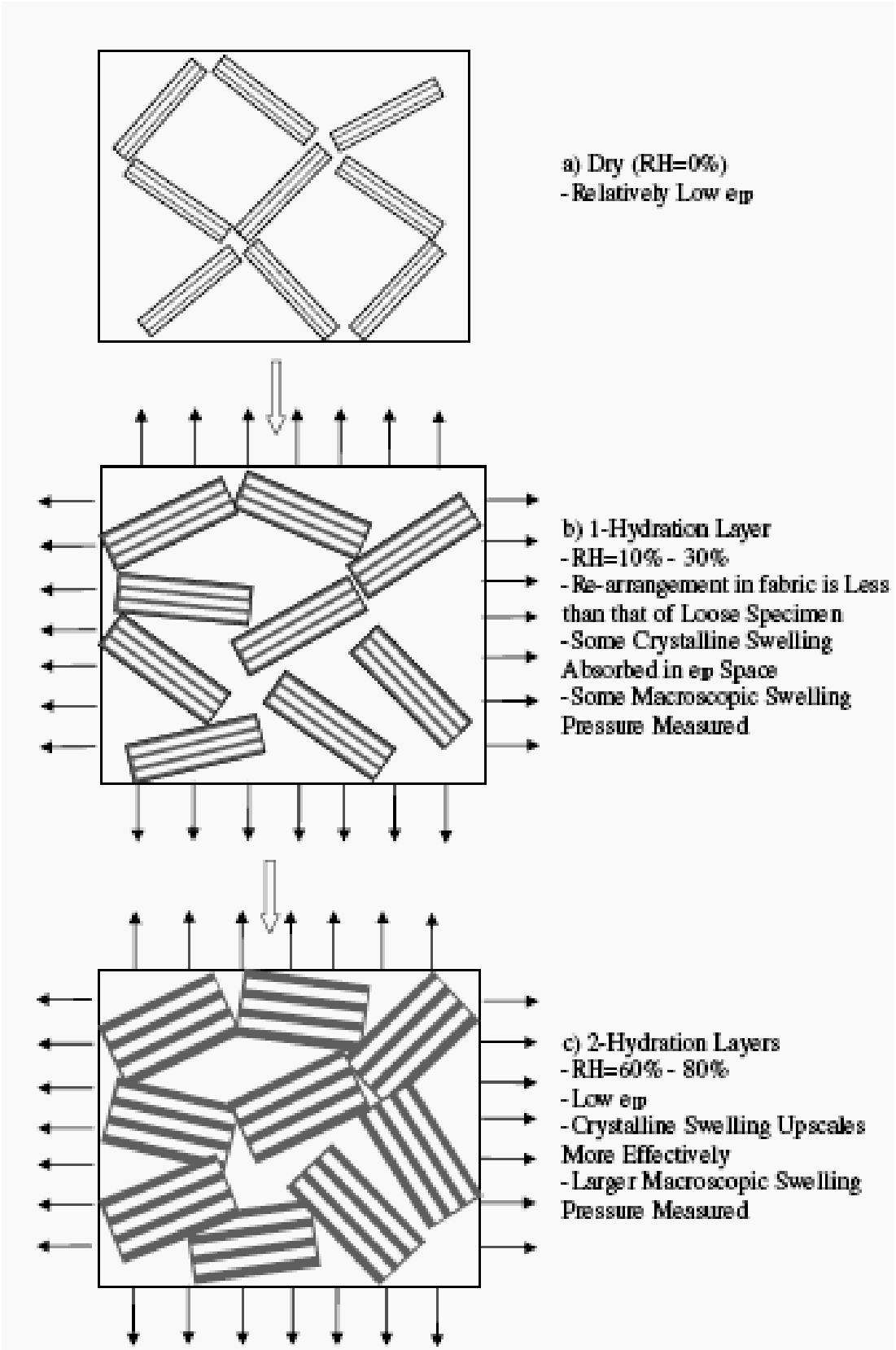

Figure 5.3. Schematic diagram of Na-smectite swelling pressure process for a dense specimen

5.1.2.2 Calcium smectite

A similar analysis of axial strain and pressure response may be performed for the Ca-smectite results. The derivative volume change response and the derivative swell pressure response are shown in Figure 5.4. Volume change results are reported for specimens initially compacted to e = 0.74, 0.83, and 0.92. Swell pressure results are reported for e = 0.78 (dense), and e = 1.14 (loose).

Relatively sharp peaks are observed for both the volume change (Figure 5.4.a) and swell pressure results (Figure 5.4.b) over a range of RH from about 5% to 30%, which corresponds to the 1-to-2-layer transition. Similar to the Na-smectite results, denser specimens exhibit a larger increase in bulk volume change and swelling pressure during this range in RH. The magnitude of both the volume change and swelling pressure is larger for this clay than for that of Na-smectite. This can be explained by realizing that the number of mineral layers in the quasicrystal is larger for Ca-smectite, reaching up to 400 face to face oriented layers compared to the ~20 layers for Na-smectite (Tessier, 1990, Quirk, 1971). It must be noted that in general, the total volume of the specimen increased throughout the whole RH range (Figure 4.11), which indicates additional swelling in the larger-scale interparticle pore space.

Change in pressure with respect to RH ($\Delta P/\Delta RH$) is negative for RH greater than 50%, which reflects the decrease in swelling pressure observed in Figure 4.17. This pressure drop is explained in section 5.4.5 in context of the Barcelona Basic Model.

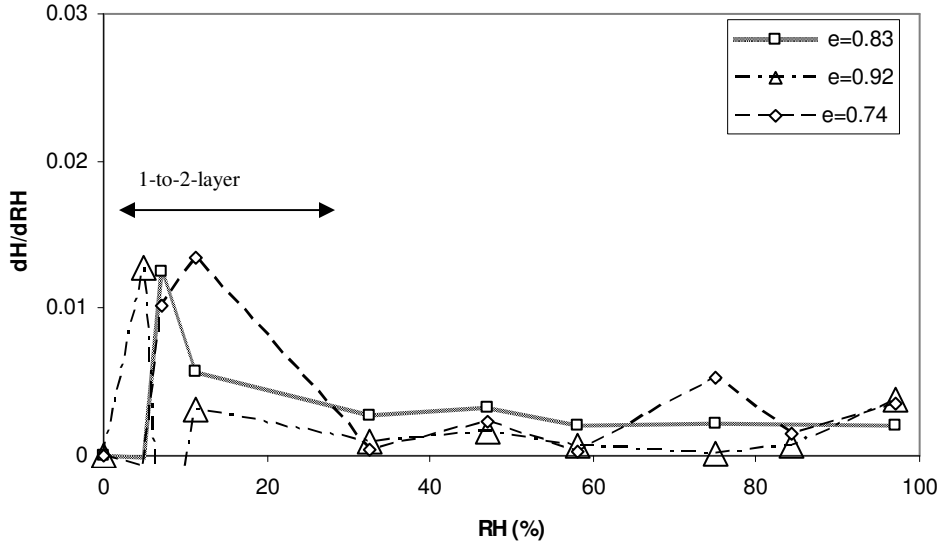

(a)

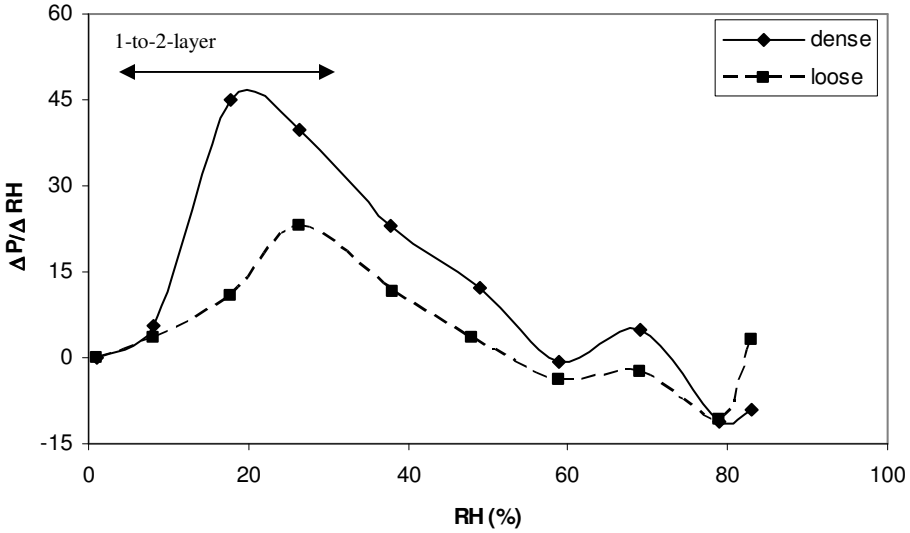

(b)

Figure 5.4. Derivative of (a) axial strain, (b) swelling pressure as a function of RH for Ca-smectite

5.1.2.3 Calcium-exchanged smectite

Ca-ion exchanged smectite has the lowest axial strain for the three clays (Figure 4.13). This can be explained by two phenomena that combine to lead to less crystalline

swelling than for either of the other two clays. Since the fabric has similar aggregate structure to that of Na-smectite, the number of mineral layers per quasicrystal may be lower than for Calcium smectite, thus, there are less layers to hydrate. Also, Ca-smectites have already hydrated one layer at very low RH values; so the increase of RH leads to only one additional hydration layer (1-to-2-hydration layer).

Figure 5.5 shows volume change response for a single specimen of Ca-exchanged smectite compacted to initial void ratio of e = 0.88. Two peaks are observed in the range of RH=10% to 40%; however, since the scale in the y-axis is small, it is possible that the datum point at RH=28% is "wrong". Ignoring this datum point, only one peak that is consistent with the 1-to-2 layer transition for Ca-smectite would be observed (see dotted line).

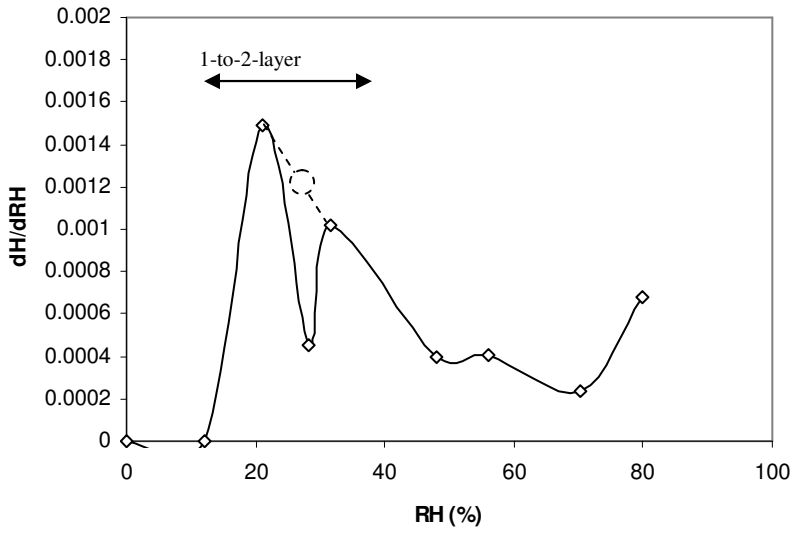

Figure 5.5. Derivative of axial strain as a function of RH for Ca-exchanged-smectite

5.1.3. Effect of compaction density

As explained in Chapter III, clay fabric is a very important factor considered when investigating how crystalline swelling upscales to macroscopic behavior; therefore,

initial density of the specimen is a key variable in this analysis. Chapter II reviewed previous works documenting that cylindrical specimens compacted at a lower density undergo less total axial strain when following a wetting path (Figure 2.8). Figures 4.4-4.5 provide the relation obtained between initial void ratio and applied compaction pressure for the sodium and calcium smectite. The range of normal stress applied during compaction ranges from 500 kPa to 6,500 kPa, with corresponding void ratios from 1.35 to 0.73. Figures 4.6 and 4.7 display axial deformation as a function of RH for sodium and calcium smectite samples compacted to three different initial densities; a clear influence of initial density in the volume change behavior was observed. Likewise, swelling pressure was measured for "dense" and "loose" sodium and calcium smectite soil cakes to investigate the effect of compaction density (Figure 4.17).

5.1.3.1 Effect on bulk volume change

The effect of initial void ratio (e_i) on volume change response under free swell boundary conditions may be evaluated for different RH values. Figure 5.6 is a plot of equilibrium axial strain measured at RH of 32.7%, 58%, and 97% for three Na-smectite samples compacted to three different initial densities. Initial density is defined in terms of initial void ratio, and ranges from values 0.88 to 1.1, to 1.3, thus representing dense, moderately dense, and loose compaction conditions respectively.

At RH of 32.7% and 58%, the free swell volume change of the three specimens is similar, or independent of initial void ratio. In both cases, there is a slight decrease in volume change with increasing initial void ratio. However, the difference in measured axial strain for the three specimens at RH of 32.7% is less than 1.8%. The difference in measured axial strain for the three specimens at RH of 58% is less than 2.6%. At RH of

97%, however, there is significant dependency between measured axial strain and initial void ratio. The trend of decreasing volume change with increasing void ratio, noted to a lesser extent in the response at lower RH, is much more evident. The difference in measured axial strain for the specimens with initial void ratios of 0.88 and 1.28 is 7%.

The difference in measured axial strain is smaller for RH of 32.7% and 58%, both of which are included in the one-layer hydration state. A larger difference was observed at RH=97%, which represents the two-layer hydration state (and maybe the transition to osmotic swelling). Therefore, these results indicate that the two layer transition is more effectively upscaled to bulk response. This may be explained because during the first layer transition, most of the crystalline swelling was absorbed into the inter-particle void space, which may not be the case for transition to the second hydration layer.

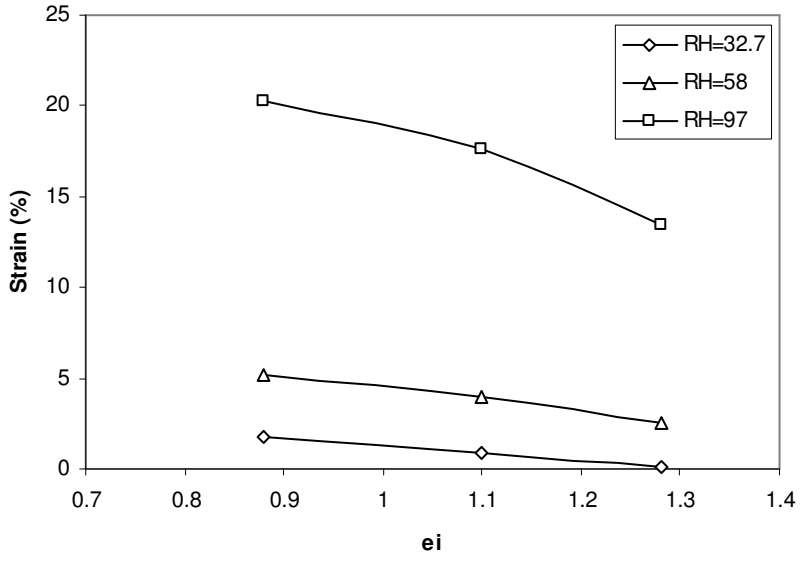

Figure 5.6. Axial strain as a function of e_i for different RH in Na-smectite

Figure 5.7 is a plot of equilibrium axial strain measured at RH of 11%, 75%, and 97% for nine Ca-smectite samples compacted to initial void ratios ranging from 0.73 to

1.0. Comparison with Figure 5.6 indicates that the bulk volume change response for Ca-smectite is more sensitive to initial void ratio than that of Na-smectite. A difference of 5% is observed at RH of 11.3%, increasing subsequently to 15% and 19% for RH of 75% and 97%, respectively. Similar to the Na-smectite results, the general trend for both Na and Ca smectite indicates that lesser axial deformations occur for specimens with lower initial densities, and that the effect of initial compaction is larger for higher hydration layer states (larger RH values).

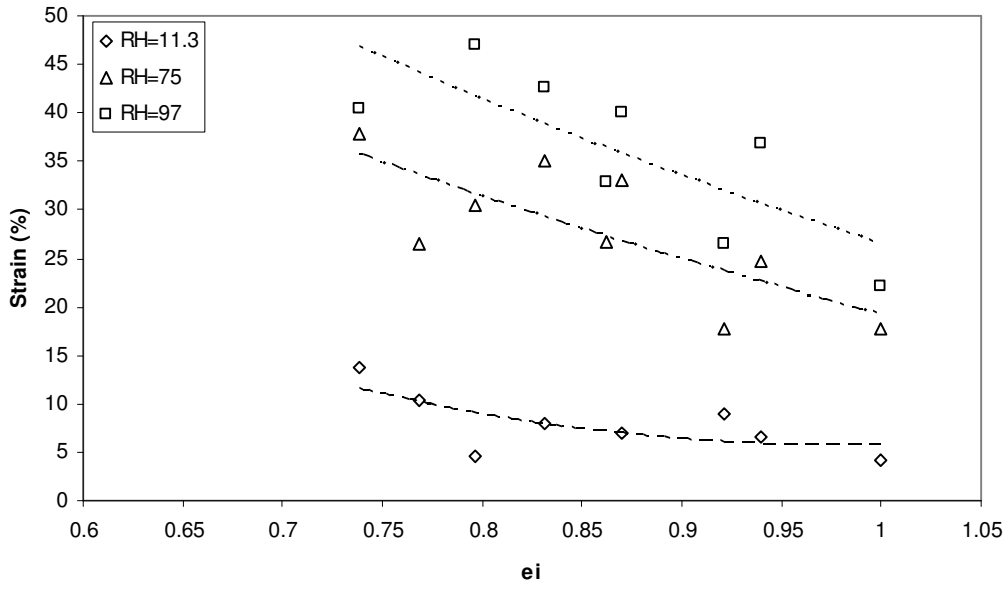

Figure 5.7. Axial strain as a function of e_i for different RH in Ca-smectite

The effect of initial void ratio was also investigated in the bulk volume change response of Ca-smectite specimens subject to a wetting and subsequent drying path. In Figure 5.8, the difference between the axial strain during drying and the axial strain during wetting at the same RH is plotted as a function of RH for samples with initial void ratios of 0.74, 0.83, and 0.92. This difference is expressed as a percent, and designated "percent hysteresis." The more densely compacted specimens exhibit more hysteresis,

especially at the end of the drying path (low RH values). This behavior was expected because the increase of interparticle void space for denser specimens is larger and during the drying path the clay fabric stays open (interparticle void ratio stays constant) while only the interlayer void space decreases.

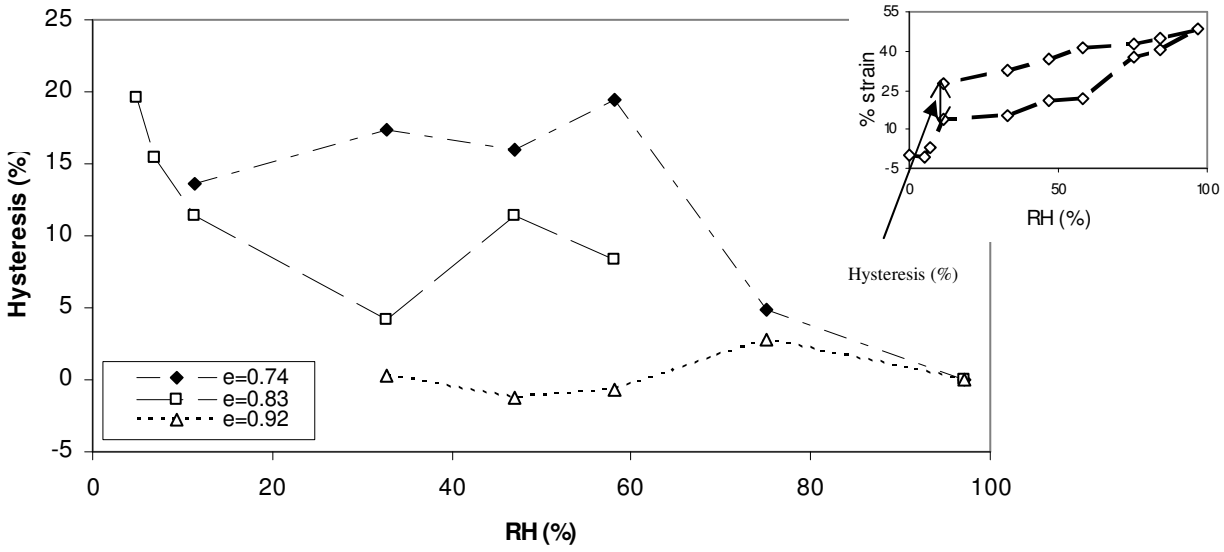

Figure 5.8. Hysteresis as a function of RH for specimens with different initial void ratio

5.1.3.2 Effect on bulk swelling pressure

Similar observations are noted in the bulk swelling pressure response for specimens compacted to relatively dense and loose initial conditions and hydrated under zero-volume-change boundary conditions. Figure 5.9 shows bulk swelling pressure response for loosely compacted (e = 0.76) and densely compacted (e = 0.9) sodium smectite specimens ramped continuously from RH of 1% to 94%. The curves plotted with hollow symbols are the swelling pressures measured for loose and dense Na-smectite samples; the curve plotted with solid circles is the difference in swelling pressure measured between the "dense" and "loose" samples. This difference is

negligible for RH lower than 50%, but becomes very significant for RH ranging from 60% to 80%, increasing up to 260 kPa for RH=95%. Thus, during the first interlayer hydration, most of the increase in the interlayer void space is absorbed by the interparticle void space for both dense and loose specimens. It is only during the second hydration layer state that crystalline swelling translates more effectively to macroscopic behavior for denser specimens.

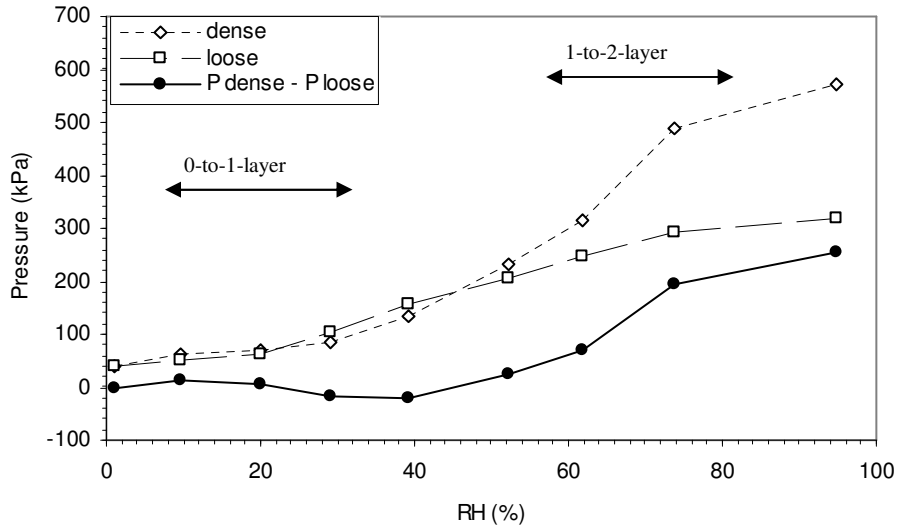

Figure 5.9. Difference in swelling pressure for dense and loose Na-smectite

Figure 5.10 illustrates the bulk swelling pressure for calcium smectite specimens compacted at initial void ratios of 0.78 (dense) and 1.14 (loose). Curves plotted with hollow symbols represent the measured swelling pressure for the specimen while the curve plotted with solid circles represents the difference in swelling pressure between both specimens. The difference $P_{dense} - P_{loose}$ is significant even at lower RH values, increasing rapidly with RH until about 50%. At this point, swelling pressure decreases with an increase in RH. The difference in pressure between dense and loose samples stays constant at around 800kPa. As described previously, the capability of translating

crystalline swelling to macroscopic behavior at earlier RH values for Ca-smectite is probably due to the high number of mineral layers composing each quasicrystal and the fact that the 0-to-1-hydration layer state occurs at very low RH.

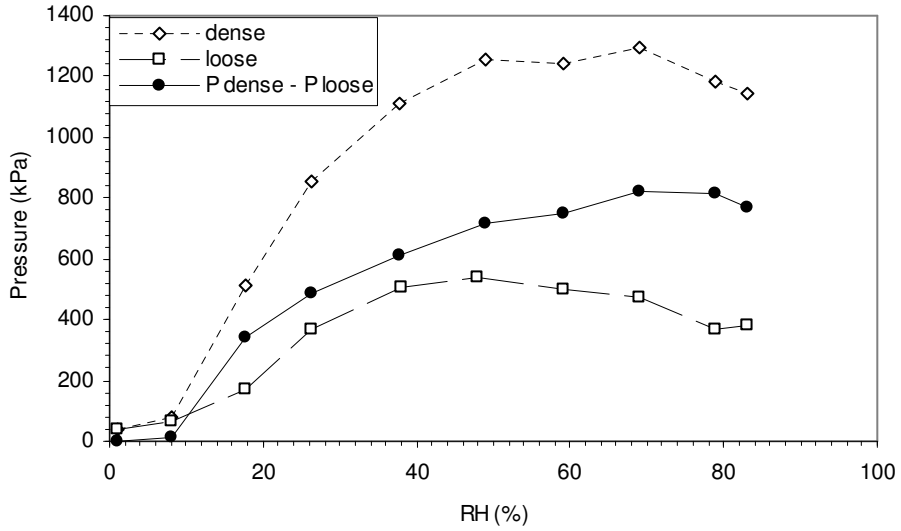

Figure 5.10. Difference in swelling pressure for dense and loose Ca-smectite

5.2 Fabric model for upscaling interlayer volume change

This section describes a new microstructural fabric model that was developed to examine the bulk volume change of compacted expansive clay specimens in the crystalline swelling regime. The basic premise of the model is that the discrete changes in interlayer spacing associated with the successive sorption or desorption of molecular water layers may be upscaled to changes in bulk volume by considering the change in geometry of a basic parallelepiped fabric unit. Particle fabric was modeled using a lamellar structure comprising tactoids with interlayer and interparticle void space. Bulk volume change resulting from mineral interlayer hydration is predicted as a function of RH. The general behavior of the model is evaluated using the results obtained from the free swelling tests for sodium, calcium, and calcium-exchanged smectite (Section 4.3.2.)

5.2.1. Idealized fabric geometry

Section 2.5 described previous works suggesting that expansive clay minerals are generally in the form of colloidal-size tactoids with a lamellar nature (e.g., Quirk, 1986; Tessier, 1990). Tuller & Or (2003) proposed an idealized clay fabric element in the form of four tactoids forming a parallelepiped micropore (Figure 5.11). This basic parallelepiped unit is adopted as the basis of the microstructural volume change model developed in this research.

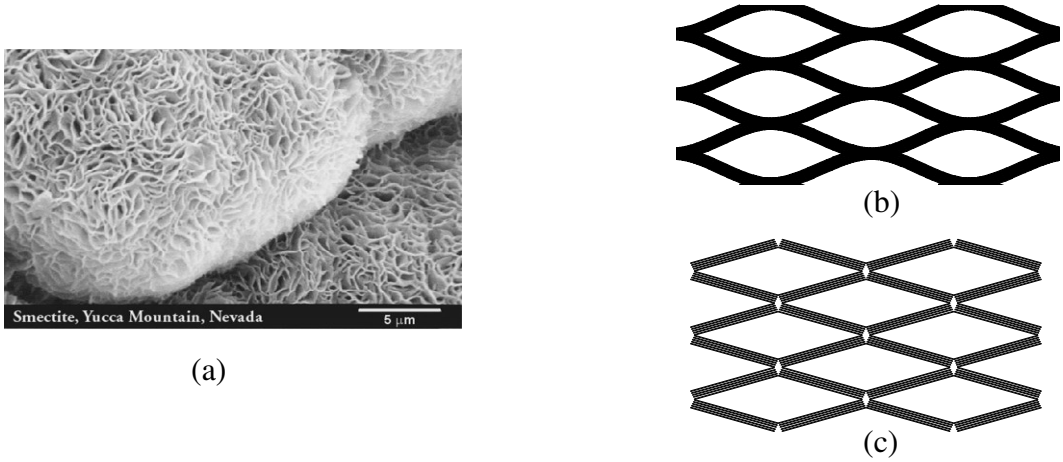

Figure 5.11. Development of idealized clay fabric representation based on unit elements. (a) SEM smectite (Clay Minerals Society), approximated clay fabric structure; (b) Idealized clay fabric representation (after Tuller & Or, 2003)

Figure 5.12 shows a closer view of the basic parallelepiped unit. Changes in micropore size may be parameterized by changes in the angle α that quantifies the internal acute angle of the parallelepiped. The vertical dimension of the unit cell (Lx) is a function of RH or water potential (μ), and is defined as:

$$Lx(\mu) = 2(x(\mu) + \Delta x(\mu)) = 2L\sin(\alpha) + 2W\cos(\alpha) \quad (5.1)$$

Where W(μ) is the tactoid width (Figure 5.12):

$$W(\mu) = n \cdot t + (n-1) \cdot h(\mu) \quad (5.2)$$

The horizontal dimension of the unit cell(Ly) is also a function of RH or μ:

$$Ly = 2 \cdot (y(\mu) + \Delta y(\mu) = 2L\cos(\alpha) + 2 \cdot W \cdot \sin(\alpha) \tag{5.3}$$

and the void ratio of the unit cell is quantified as its volume of voids over its corresponding volume of solids:

$$e = \frac{Lx(\mu) \cdot Ly(\mu) - 4n \cdot t \cdot L}{4 \cdot n \cdot t \cdot L} \tag{5.4}$$

Substituting equations (5.1-5.3) into (5.4), a relation between void ratio, the angle alpha, and clay mineral characteristics (crystallite length L, n, t, and W) is obtained:

$$e = \frac{(L^2 + W^2)\sin(2\alpha) + 2LW}{2ntL} - 1 \tag{5.5a}$$

Which may be rearranged to solve for alpha:

$$\alpha = \frac{1}{2}\sin^{-1}\left(\frac{(e+1)2ntL - 2LW}{L^2 + W^2}\right) \tag{5.5b}$$

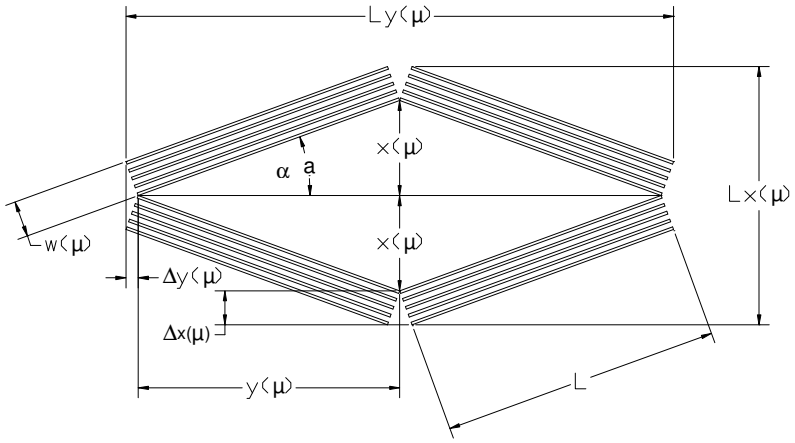

Figure 5.12. Idealized unit element for clay fabric representation.

As defined above, void ratio depends on the parameter alpha, the basal spacing as a function of RH, and the clay mineral type (which governs n, L, and t). If a specimen is initially compacted to a given void ratio, the bulk volume change due to an increase in RH can be upscaled if the parameter alpha is well defined.

5.2.2. General model behavior

The parallelepiped model considers both interlayer and interparticle void space. The former is defined by the void space between the individual clay layers. The latter is defined by the void space formed among the stacked clay crystallites. Bulk volume change for a specimen resulting from an increase in RH results from the combined effects of a change in the tactoid volume (interlayer void ratio) and a change in the parallelepiped geometry (interparticle void ratio). Crystalline swelling due to interlayer hydration occurs in a discrete or "step-wise" fashion, where transitions in basal spacing occur relatively abruptly as subsequent water layers are adsorbed into the interlayer space. The corresponding change in parallelepiped geometry may be investigated by quantifying the magnitude of angle α.

The general behavior of α was investigated by considering the free swelling test results summarized in Chapter 4, specifically, the bulk volume change data as a function of RH (Section 4.3.2). Note that general observations from these data indicate that specimens compacted to lower initial densities undergo less axial strain. Equation (5.5b) was used in conjunction with this experimental data set to obtain initial α values corresponding to the initial packing void ratios (Figure 5.13). Lamellae thickness value used for the analysis is 9.7 Å; length of the tactoid (L) for Na-smectite ranges from 1000Å to 3000Å (Tessier, 1990), L for Ca-smectite ranges from 1000Å to 1500Å. The total number of mineral layers comprising the quasicrystal is on the order of 20 for the Na-smectite and 400 for the Ca-smectite. As indicated on Figure 5.13, initial corresponding alpha values are higher for loosely compacted samples, with values ranging from 8.4^{o} to 14.5^{o} for Na-smectite and from 15^{o} to 23^{o} for Ca-smectite. The large

values of alpha reflect the relatively open macrostructure associated with loosely compacted samples, while the small values of alpha reflect the closed macrostructure (smaller interparticle void volume) associated with dense compaction. Initial alpha values for Ca-smectite were higher than those for Na-smectite, probably because the length L of the platelet is smaller for Ca-smectite.

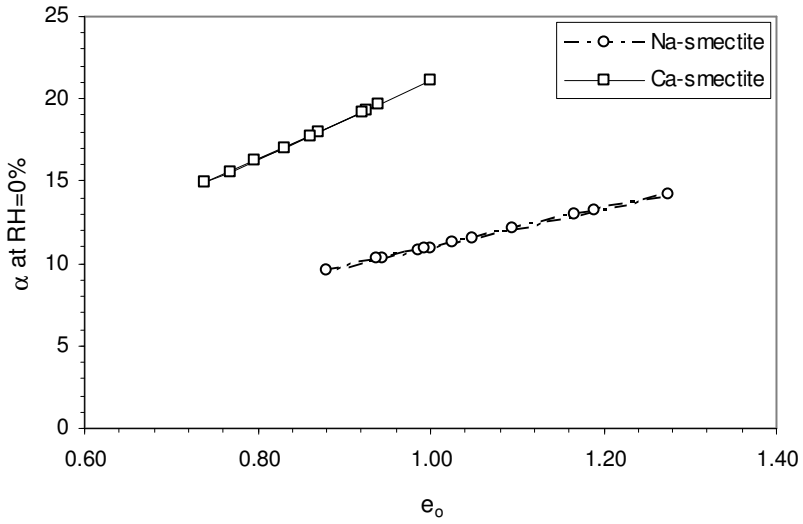

Figure 5.13. Alpha values as a function of compaction void ratio

Figures 5.14 and 5.15 show α and the change in α, respectively, for typical loose, medium, and dense dry Na-smectite for each of the RH increments. In general, α values remain relatively constant until RH is greater than 33%, whereupon the angle decreases by 1.6° to 2.9°. This reduction coincides approximately with the zero-layer to one-layer hydrate state transition. Physically, this may be interpreted to indicate that the increase in basal spacing associated with the zero-to-one layer transition is absorbed by the interparticle void space (i.e., α decreases to accommodate the interlayer swelling process). Correspondingly, macroscopic swelling is only significant for RH values

greater than about 33%. It is also observed that loosely packed specimens have lower α values, which supports the more general observations that specimens of initially lower density (i.e., loosely compacted) exhibit smaller macroscopic changes in volume than those of initially higher density (i.e., heavily compacted). During the next RH increment (near 47%), the change in α ranges from -1.5^{o} for loosely compacted samples (e=1.28) to 0^{o} for e=0.77. These values increase only by 1^{o} when RH is equal to 58.2%. A significant increase in α is observed when RH reaches 75.1%. This is likely to correspond to a transition in the interlayer hydration state from one-layer to two-layers. The corresponding total bulk volume change is significant because both the interlayer and interparticle space increase in volume. At this point, the change in α is significantly higher for denser specimens, which leads to a larger amount of bulk swelling. These results support the previous observation by indicating that the particle-scale volume changes in the lower density specimens are more completely adsorbed by the larger voids associated with the interparticle void space. The net effect is a smaller bulk volume change. Finally, a dramatic increase in α is observed at 97% RH. This response may correspond to the onset of osmotic swelling associated with longer-range electrical double layer effects or continued adsorption of water in the interparticle voids under capillary sorption mechanisms. Results from water vapor sorption experiments, for example, show that many clays typically adsorb a significant amount of water for RH greater than about 95% (Figure 5.16), which may be interpreted to mark a transition from sorption dominated by properties of the mineral surfaces (or interlayers) to sorption dominated by properties of the larger-scale pores and pore geometry.

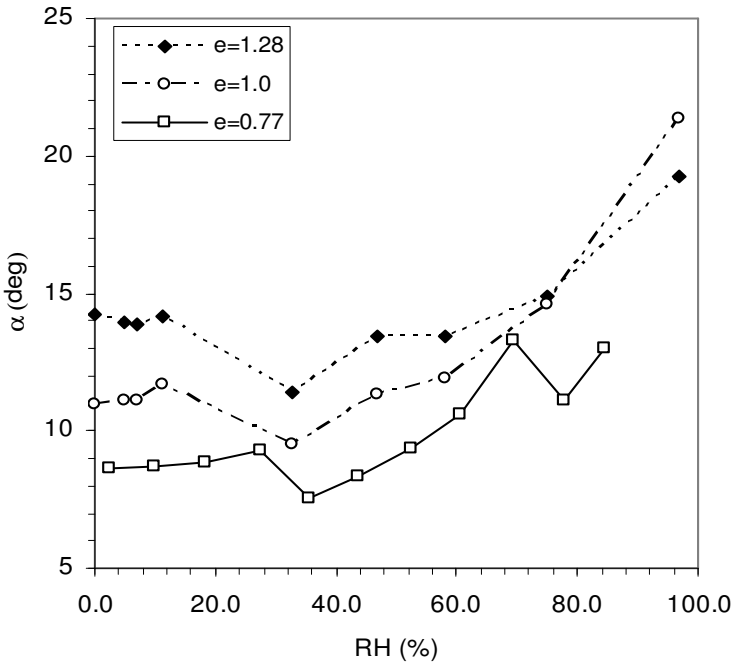

Figure 5.14. Alpha values as a function of RH for Na-smectite

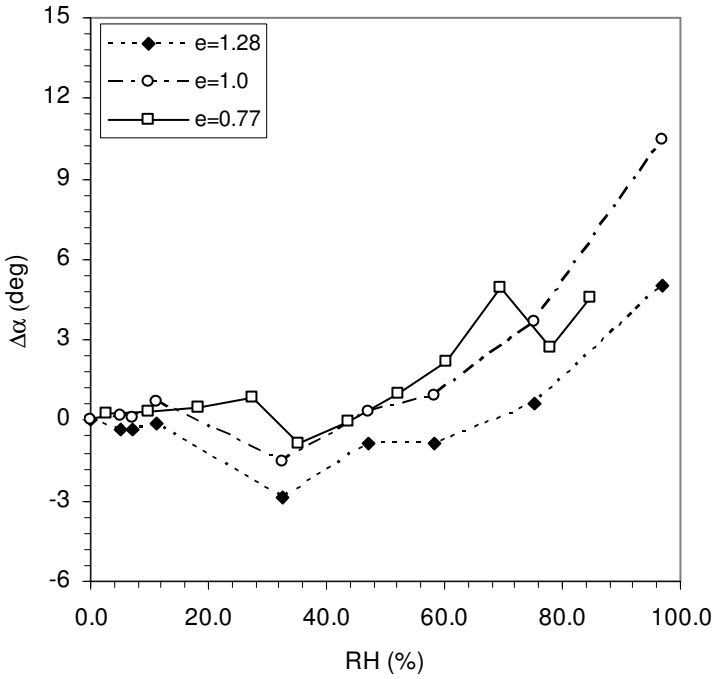

Figure 5.15. Change in alpha as a function of RH for Na-smectite.

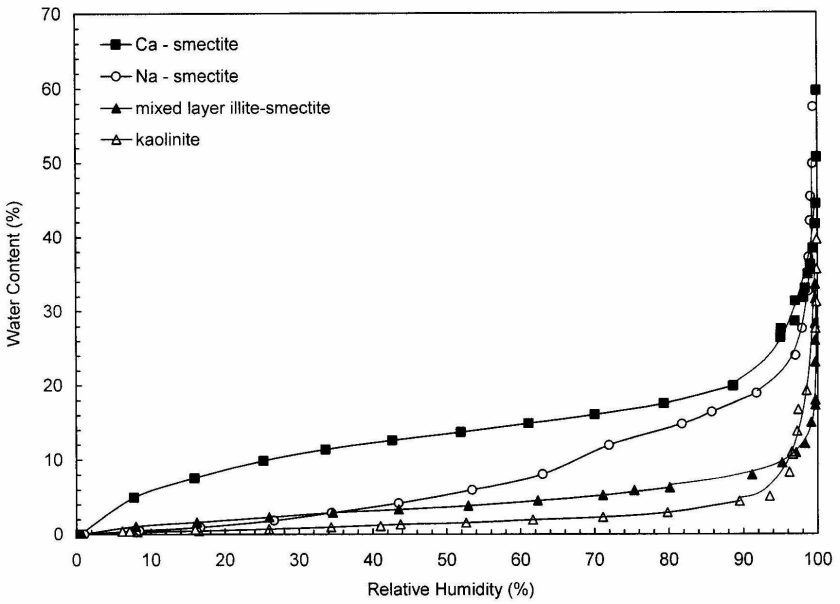

Figure 5.16. Gravimetric water content as a function of RH for different clays (Likos, 2004)

Alpha and the change in alpha for typical loose, medium, and dense dry Ca-smectite as a function of RH are portrayed in Figures 5.17 and 5.18. Alpha values displayed in these figures correspond to RH equal or greater than 5%, after the first hydration layer for Ca-smectite already occurred, thus, the lower values in alpha. The loosely compacted cake exhibits a reduction of 4^{o} in alpha at RH of 35%, which coincides with the 1-to-2 hydration layer state. This implies that the increase in basal spacing associated with the layer transition is absorbed by the interparticle void space (i.e., α decreases to accommodate the interlayer swelling process). Correspondingly, macroscopic swelling is not very significant. On the other hand, medium and dense compacted samples had a positive change in angle at the same RH. This indicates an increase in volume in both the interlayer and interparticle space. The change in alpha for RH greater than 40% is negligible for the loose and medium specimens, but significant

for the dense sample. Likewise, alpha stays fairly constant during drying for loose and medium samples, but decreases about 5^{o} for the dense specimen.

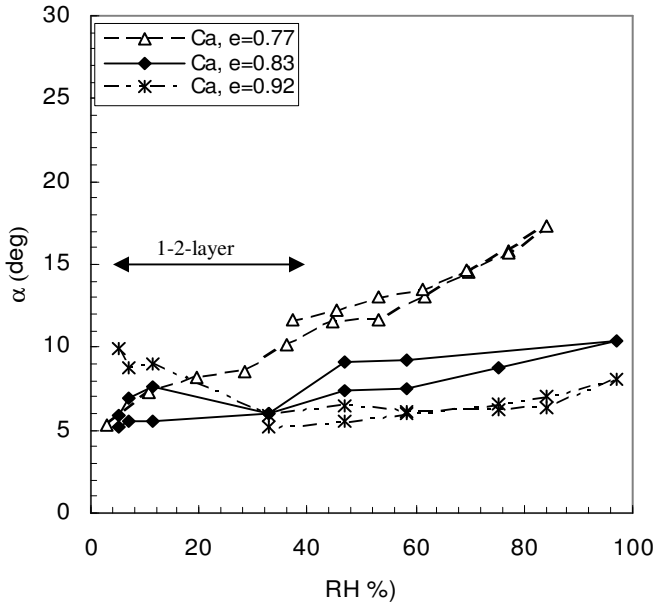

Figure 5.17. Alpha values as a function of RH for Ca-smectite

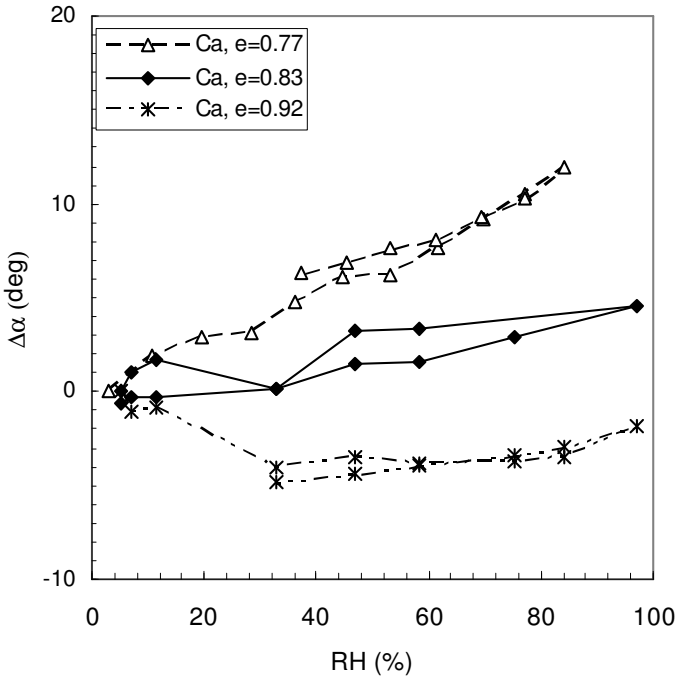

Figure 5.18. Change in alpha as a function of RH for Ca-smectite

The Ca-exchanged smectite free swell test was also analyzed in the context of this model (Figure 5.19, 5.20). For a specimen with void ratio of 0.8 (medium to densely compacted), alpha values ranged from 6^o to 8^o corresponding to RH of 12% to 82%. A steeper portion was observed at RH 35%-45% coinciding with the 1-to-2 hydration layer state for Ca-smectite.

By comparing the behavior of the three clays for samples at similar packing void ratios, it is observed that Ca-smectite has the largest change in alpha (most "open" structure) under identical conditions (Figure 5.19, 5.20). This can be explained by considering that Ca-smectite is composed by shorter tactoids (L of 1000 – 1500Å) and more mineral layers per quasicrystal (400 vs. 20). Also, the change in the alpha angle for the Na-smectite and the Ca-exchanged smectite are very similar in terms of magnitude, but the functional relationships with RH have different characteristics or "shape." Both clays have similar aggregate structure (~20 mineral layers per quasicrystal, L~2000 Å) but the hydration layers occur at different RH intervals, which may explain the similitude in general $\Delta\alpha$ magnitude but the difference in steeper portions of the curves.

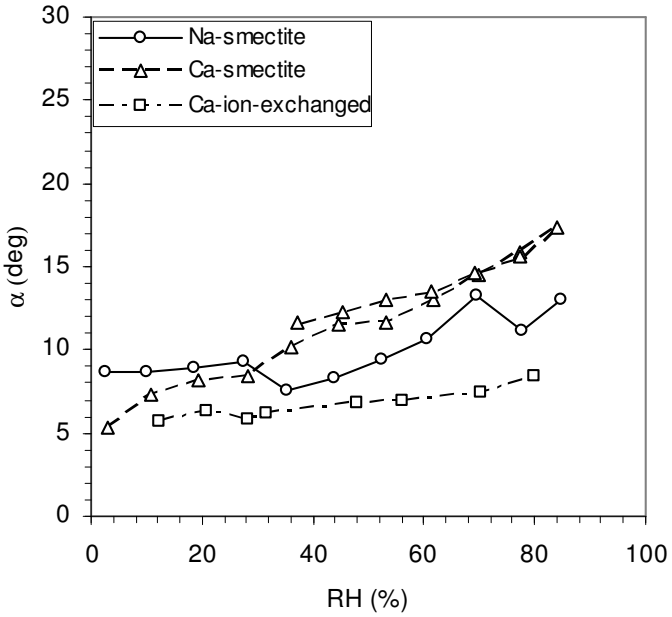

Figure 5.19. Comparison of alpha functions for Na and Ca smectite

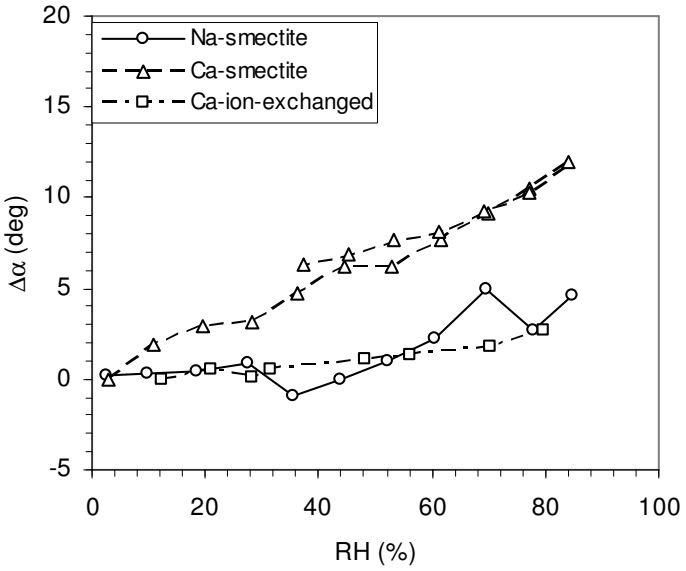

Figure 5.20. Comparison of change in alpha for Na and Ca smectite

5.3. Porosity evolution

Up-scaling interlayer swelling to bulk volume change and swelling pressures may also be examined by tracking the evolution of the multiple porosity scales during cycles of hydration and dehydration. Transitions in interlayer hydration states that occur as RH increases or decreases cause a corresponding increase or decrease in the interlayer void ratio, which may be computed directly if the change in interlayer spacing (basal spacing) is known. This volume change may then translate into macroscale volume change or swelling pressure as dependent on the sample boundary conditions. The efficiency with which particle scale volume changes are upscaled strongly depends on relative changes in the volume of pore space defined among individual clay aggregates, particles or quasicrystals, and interlayers.

This section examines the current experimental results in the context of the Likos and Lu (2006) porosity evolution model developed to track the changes in interlayer and interparticle porosity during interlayer hydration and dehydration. As illustrated previously in Section 2.3, the increase (or decrease) in volume of a given quasicrystal due to crystalline swelling is a function of the hydration state of the interlayers and the number of mineral layers in the quasicrystal. Initial inter-particle void ratio will vary depending on the compaction pressure applied during sample preparation. The effectiveness of up-scaling interlayer volume changes to macroscopic behavior depends on the relative volume of interlayer and inter-particle voids, the size of the quasicrystal, and the size and distribution of the inter-particle voids. For lower inter-particle to interlayer volume ratio (dense specimens), crystalline swelling will translate to change in

total volume or pressure more effectively. Conversely, interlayer swelling is more completely absorbed internally by the inter-particle voids in loose specimens.

Likos & Lu (2006) defined total void ratio as the sum of inter-particle (e_{IP}) and inter-layer (e_{IL}) void ratio, with e_{IL} being the ratio of interlayer space 2δ and plate thickness τ.

$$e_T = e_{IP} + e_{IL} \quad (5.6)$$

$$e_{IL} = 2\delta/\tau \quad (5.7)$$

Thus, the change in total void ratio under free swelling conditions can be calculated as:

$$\Delta e_T = \Delta e_{IP} + \Delta 2\delta/\tau \quad (5.8)$$

For fully confined specimens (constant strain conditions):

$$\Delta e_T = \Delta e_{IP} + \Delta e_{IL} = 0 \quad (5.9)$$

Thus, an increase in interlayer volume will correspond to an equal decrease in inter-particle volume. Quantitative changes in interlayer void ratio can be estimated from basal spacing measurements as a function of RH (e.g. as reported by Chipera et. al. (1997).

Relative changes of interlayer and interparticle volume play a key factor on the translation of crystalline swelling to macroscopic behavior. Interlayer separation at a given RH for Na and Ca smectite has been documented previously (Chipera et. al, 1997). Using these data, interpolated values for desired RH (Table 5.1) and equation 5.7, interlayer void ratio was calculated for Na and Ca smectite tests. Interparticle void ratio then is calculated as the difference between the total void ratio and interlayer void ratio.

Table 5.1. Interlayer separation as a function of RH for Na and Ca smectite.

Na-smectite			Ca-smectite		
RH	2d (A)	eIL	RH	2d (A)	eIL
0.0	0.0	0.0	0.0	0.0	0.0
5.0	0.0	0.0	5.0	3.2	0.3
7.0	0.0	0.0	7.0	3.2	0.3
11.3	0.2	0.0	11.3	3.4	0.3
32.7	2.8	0.3	32.7	5.3	0.5
47.0	2.8	0.3	47.0	5.4	0.6
58.2	2.9	0.3	58.2	5.8	0.6
75.1	4.8	0.5	75.1	5.8	0.6
84.2	5.3	0.5	84.2	5.8	0.6
97.0	5.3	0.5	97.0	5.8	0.6
84.2	5.3	0.5	84.2	5.8	0.6
75.1	5.3	0.5	75.1	5.8	0.6
58.2	4.2	0.4	58.2	5.8	0.6
47.0	2.8	0.3	47.0	5.8	0.6
32.7	2.8	0.3	32.7	5.8	0.6
11.3	1.3	0.1			
7.0		0.0			
5.0		0.0			

Typical interlayer and interparticle void ratios for dense, medium, and loose Na-smectite samples that underwent wetting under free swelling conditions are plotted in Figure 5.21. The solid rhomboids represent the interlayer void ratio with its two distinct "jumps" (at RH 5%-30% and 60% to 80%) that correspond to hydration of a new layer. Interparticle void ratio for the three specimens decreased during the 0-to-1 hydration layer state even though the total volume increased slightly as a combination of both interlayer and interparticle void spaces. At this point, the denser sample has the lowest e_{IP}. As RH increases, e_{IL} remains constant but total bulk volume increases slightly, probably due to water adsorption in the interparticle void space. During RH corresponding to the 1-to-2 hydration layer state, (60% to 80%) interlayer void space

increases once again. This time, the interparticle void ratio also increases in the three cases, with the dense specimen having the highest e_{IP} and the most gain in bulk volume.

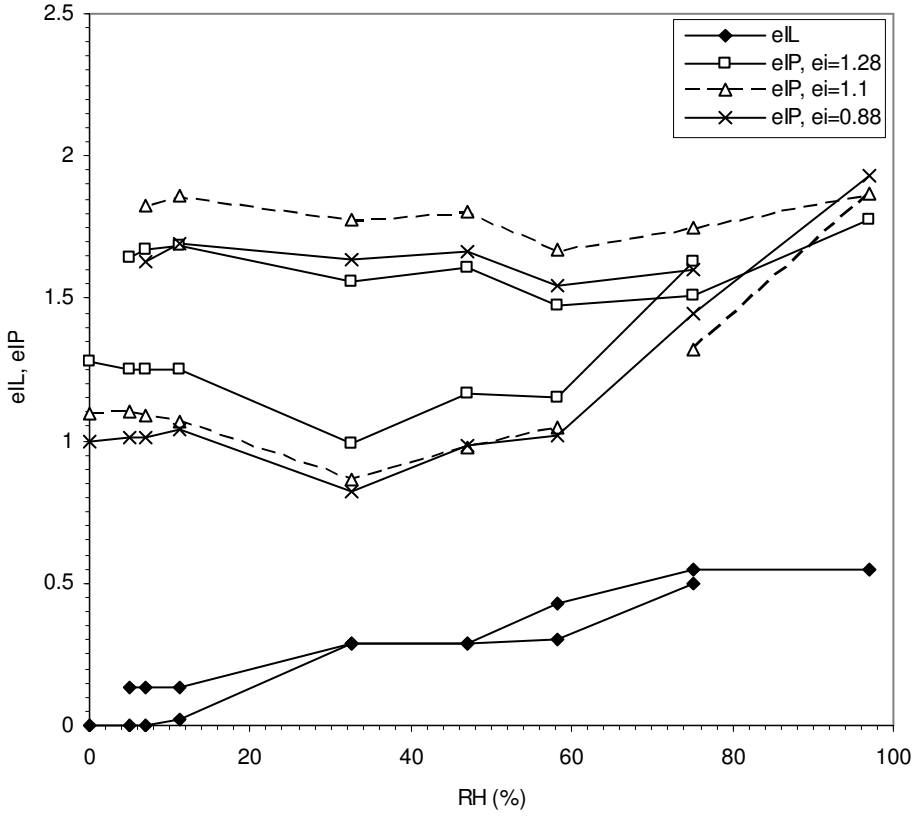

Figure 5.21. Interlayer and interparticle void ratio for Na-smectite, free swelling.

A similar analysis was performed for dense, medium, and loose Ca-smectite cakes tested under free swelling conditions (Figure 5.22). Interlayer void ratio exhibits one steep portion corresponding to the 1-to-2 layer hydration (RH= 2% - 30%), with a decrease in interparticle void ratio as a consequence. Specimen with lowest e_{IP} at this point is the dense one. As RH increases, e_{IL} remains constant but e_{IP} increases steadily leading to a constant increase in total void ratio. The dense soil cake has the largest e_{IP} and e total at the end of the wetting path.

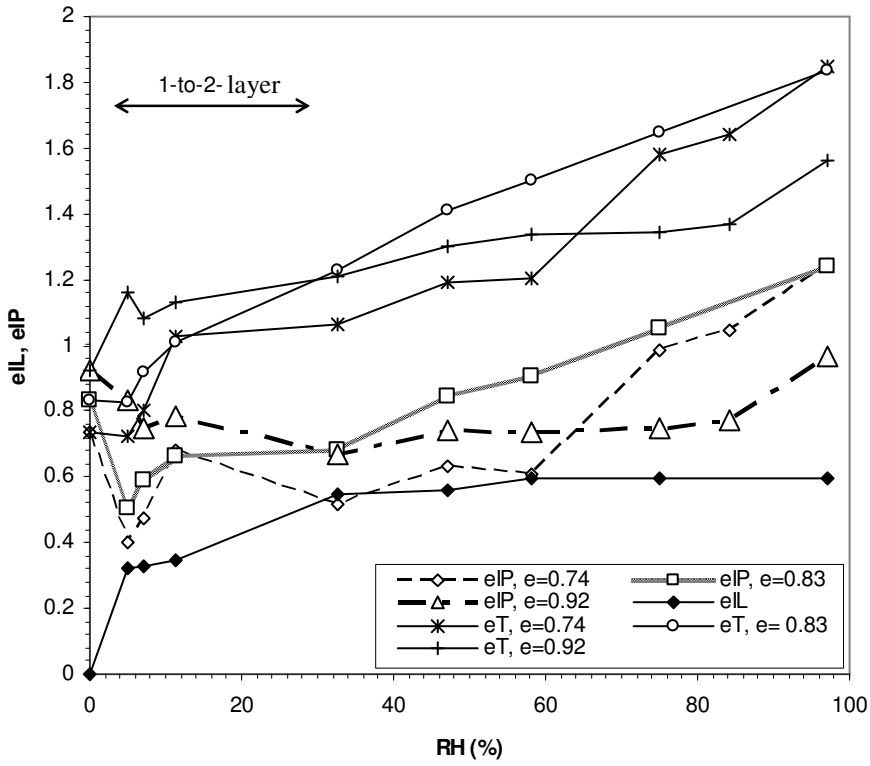

Figure 5.22. Interlayer and interparticle void ratio for Ca-smectite, free swelling.

Finally, interlayer and interparticle void spaces were analyzed for the Ca-exchanged smectite tested under free swelling conditions (Figure 5.23). Interlayer void space was the same as for Ca-smectite, since it is controlled by the interlayer cation. The interparticle void space absorbed interlayer swelling internally during the 1-to-2 hydration layer transition (RH= 2% - 30%), but did not increase too much afterwards. Thus, the total change in void ratio was by far less than for the other two clay types.

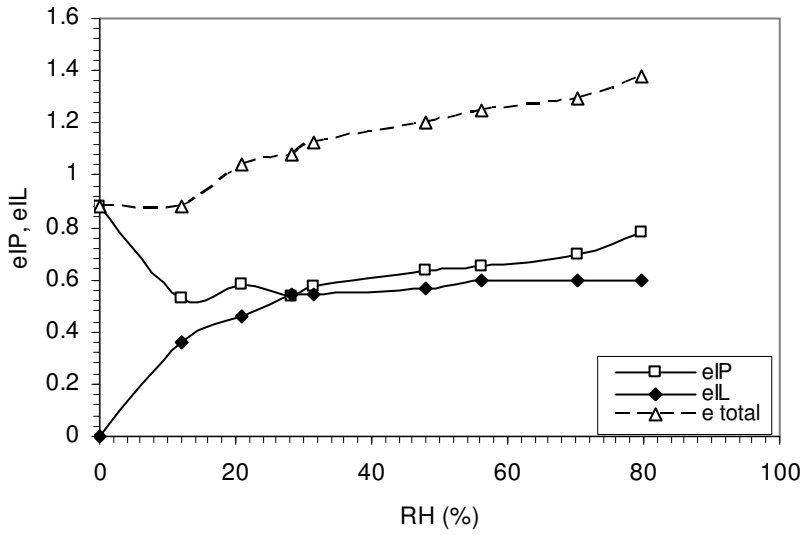

Figure 5.23. Interlayer and interparticle void ratio for Ca-exchanged smectite, free swelling.

When constant strain conditions were applied (total void ratio remains constant), the change in interlayer void ratio is the same in magnitude and opposite in sign to the change in interparticle void ratio. Dense and loose specimens for Na and Ca smectite were analyzed (Figures 5.24, 5.25); the main observation is that significant increase in swelling pressure occurred when e_{IL} increased and e_{IP} decreased. In all cases, after the second hydration layer e_{IP} is smaller than e_{IL}.

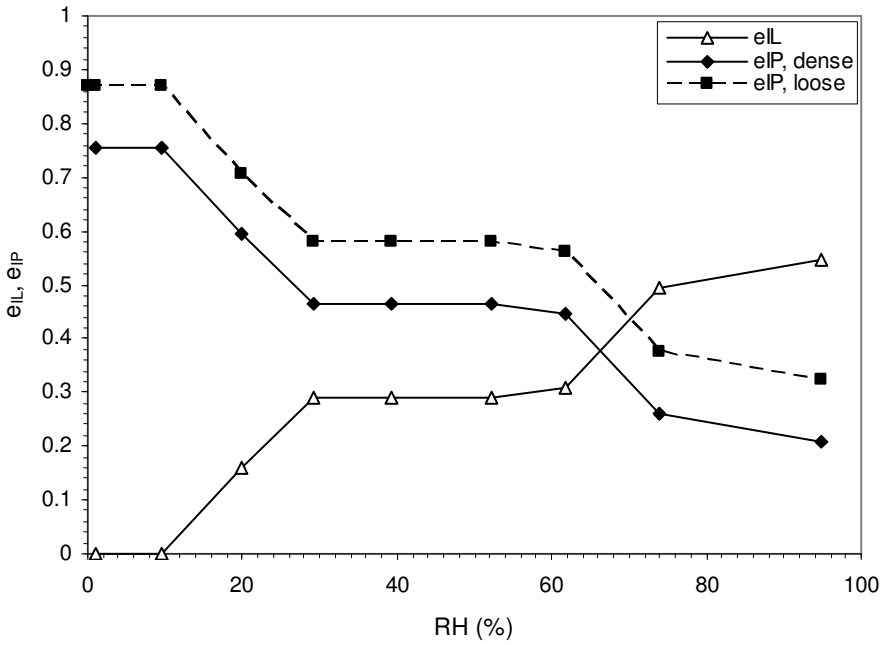

.

(a)

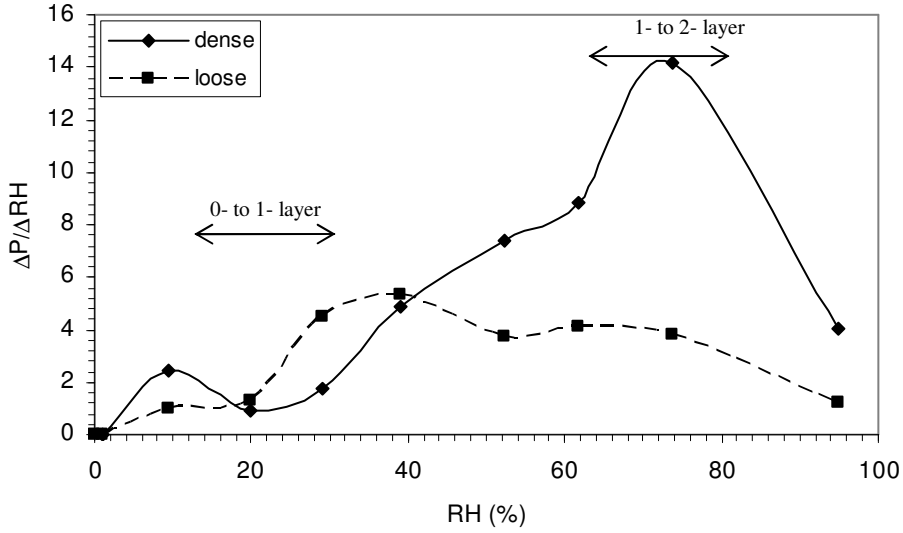

(b)

Figure 5.24. a) Interlayer and inter-particle void ratios as a function of RH; b) Change in pressure vs. RH for Na-smectite

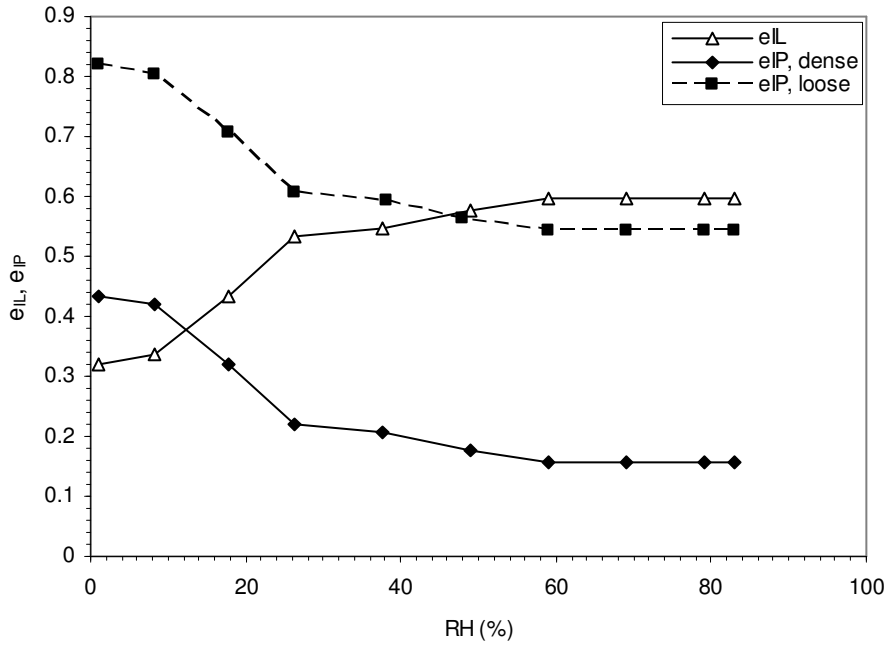

(a)

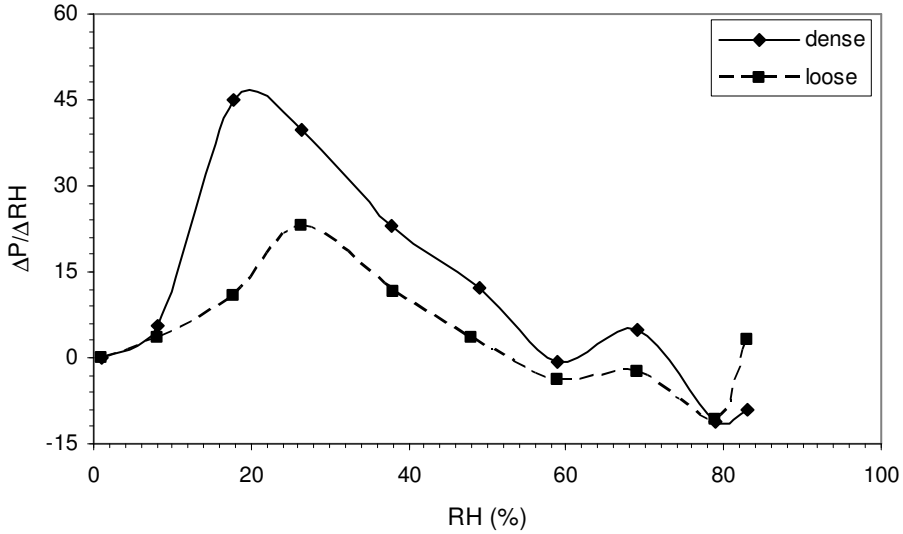

(b)

Figure 5.25. a) Interlayer and inter-particle void ratios as a function of RH for Ca-smectite; b) Change in pressure vs. RH for Ca-smectite

5.4. Barcelona Basic Model

Results may also be interpreted in light of the Barcelona Basic Model (BBM) to gain better understanding of the relationship between the microstructural and macrostructural behavior of expansive soils during crystalline swelling. This analysis helps define the effects that particle-level phenomena have on the general behavior of the soil taking into account the yield envelope and stress paths.

A comprehensive summary of the BBM is explained in the literature review portion of this thesis (Section 2.10). Some of the postulates of this framework used in this analysis are:

1) Interaction between two different scales (microstructure and macrostructure) and stress paths must be taken into account when analyzing the behavior of expansive soils.
2) Microstructural volumetric strains (ε_{vm}) are assumed to be reversible; they are controlled by physicochemical reactions. Microstructural behavior is independent of the macrostructure, but the reverse is not true.
3) Considering the macrostructure, a loading-collapse (LC) yield curve representing the locus of yield points is defined in the stress-suction space (p,s). Denser soil specimens will have a LC yield surface located further to the right.
4) The relationship between microstructural and macrostructural strains (ε_{vm} and ε^{P}_{vM}) depends on the ratio of the applied net stress (p) to the apparent preconsolidation stress at the current value of suction (p_o). A value of p/ p_o equal to 1 means a very open macrostructure; in this limiting case, $\varepsilon_{vM}/\varepsilon_{vm}$ is zero.

5) In general the microstructural level will have more influence for dense specimens, while the macrostructural level plays more of a role for soils with more open structures.

5.4.1. Macrostructural behavior

As explained before, the loading-collapse (LC) curve in the normal stress-suction (p-s) space represents yield points that if a stress path crosses them, irreversible volumetric strains will occur. The LC pattern indicates that at lower applied normal stress, a larger change in suction is required to reach the initial yield surface (Figure 5.26).

Only one point of the LC curve for each specimen tested was obtained; when the soil cake was compressed during specimen preparation, the normal stress applied for specimen compaction gives one point on the LC curve. Suction value for this point is unknown; oven dried powder was used to prepare the soil cakes, but some hydration from the environment must occur during specimen preparation leading to very high suctions in the sample. Normal stresses applied ranged from 500 kPa to 6500 kPa. Denser soil samples have a LC surface located further to the right (higher stresses applied at the same suction).

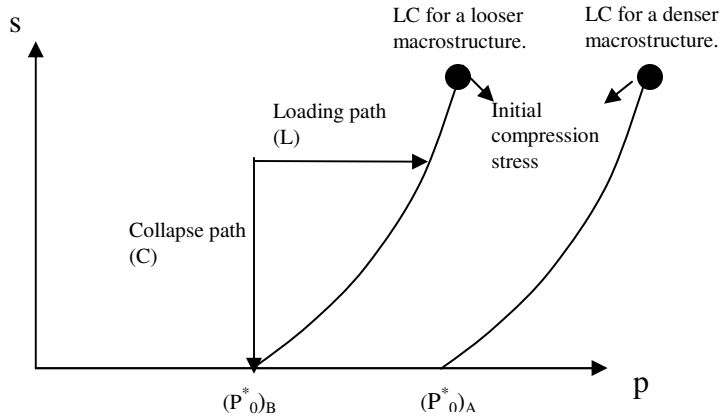

Figure 5.26. LC yield surface for loose and dense macrostructures.

5.4.2. Microstructural behavior

For the crystalline swelling regime, the controlling phenomenon for microstructural volume change of expansive clay minerals is interlayer hydration; thus, microstructural strains are a function of suction. Microstructural deformations are considered reversible and independent of the macrostructure. In the (p,s) space (Figure 5.27), the stress trajectories OA and OB are considered neutral loading paths (where no volumetric strains occur). Reductions in suction or pressure cause microstructural expansion, whereas compression will occur with the increase of suction or pressure. At higher suction values, the neutral line (NL) follows a stepwise pattern corresponding to the 0-to-1 and 1-to-2-hydration layer states. A linear pattern is expected once osmotic swelling starts, which occurs at suction values lower than about 22 MPa (RH>85%).

The NL portion corresponding to crystalline swelling can probably be defined by analyzing the work and associated swelling pressures required for removing the fourth, third, second, and first water layers of the smectite. In 1963, van Olphen used sorption isotherms to calculate these pressures for calcium montmorillonite, which are 20 MPa, 127 MPa, 258 MPa, and 600 MPa for the fourth through first hydration states

respectively. Since none of the testing was carried out at such pressures, it is assumed that in this research the position of the specimen in the microstructural NL is solely dependent on the suction applied. Depending on the number of hydrated layers, microstructural swelling due to a suction reduction is larger for reduction from higher suction values.

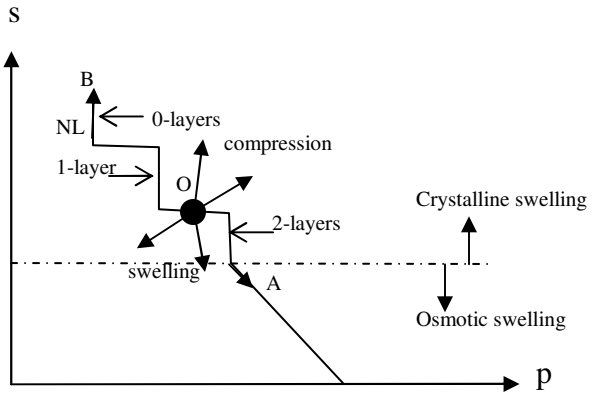

Figure 5.27. Microstructural behavior. NL line separating compression from swelling regions.

5.4.3. Coupling of micro and macrostructure

Volume change in the micro-structure (inter-layer void space) is independent of the macrostructure; however, the reverse is not true. For example, in Figure 5.28 a specimen starting at the conditions defined by point A undergoes wetting at a constant stress and reaches point B. Reduction in suction will result in micro-structural swelling, which in turn will increase the macro-structural void ratio (inter-particle), causing the LC to move to the left (specimen softens). This softening due to a more open structure was evident during all the free swelling tests; once the specimens underwent wetting from RH=0 to RH=97%, handling the specimens without breaking them became a challenge.

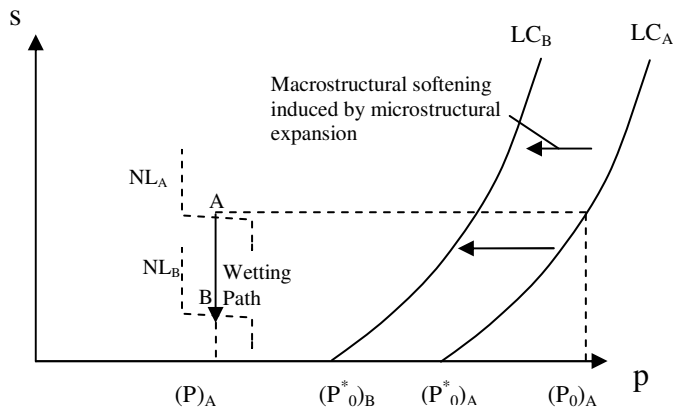

Figure 5.28. Interdependence between microstructure and macrostructure.

Macrostructural strains induced by microstructural swelling are greater for samples with larger distance to the corresponding LC yield curve.

5.4.4. Bulk volume change

The stress path imposed on the samples during the free swelling tests is shown in Figure 5.29. Two specimens are considered: specimen A and B. The first one is initially compacted at a higher normal stress. The positions of the loading collapse curves are indicated as LC_A and LC_B. Both samples were tested under zero constant stress while suction was reduced from 405 MPa to 4 MPa. In both cases, the specimens crossed the NL initially located at NL_i. Swelling deformation response for sodium and calcium smectite is depicted in Figure 5.30. The curve with filled rhomboids represents the microstructural strain (interlayer strain); the hollow triangles and rhomboids represent the macrostructural strain for loose and dense samples respectively. Interlayer strain was calculated as follows:

$$\varepsilon = \frac{\Delta H}{H} = \frac{n\left[(\tau + 2\delta)_f - (\tau + 2\delta)_i\right]}{n \cdot (\tau + 2\delta)_i} = \frac{2\delta_f - 2\delta_i}{\tau + 2\delta_i} \tag{5.10}$$

Where n is the number of mineral layers per quasicrystal, τ is the plate thickness, and 2δ is the interlayer space. Considering that $2\delta_i$ is zero for oven dried clays, interlayer strain in percentage is defined as:

$$\varepsilon = \frac{2\delta_f}{\tau} \cdot 100\% \tag{5.11}$$

Unlike the swelling deformation response outlined by Gens and Alonso (1992), the microstructural strains were actually larger than the total strains. This is explained by realizing that not 100% of the interlayer strain is translated to bulk volume change, but a large portion of it is absorbed internally into the inter-particle void space. The rate of macrostructural swelling increases significantly at lower suctions. In both cases (Na and Ca smectite) larger plastic strains were observed for specimen A (dense), which is a result of it having larger distance in terms of p between the initial stress state and the yield state p_o.

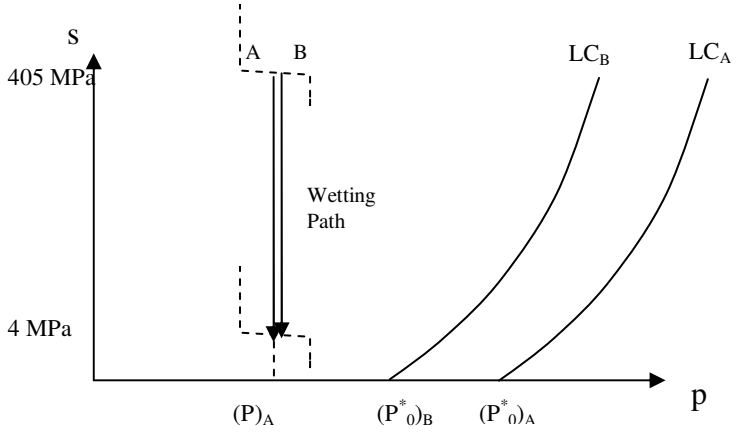

Figure 5.29. Effect of the relative position of the LC yield curve on the magnitude of swelling.

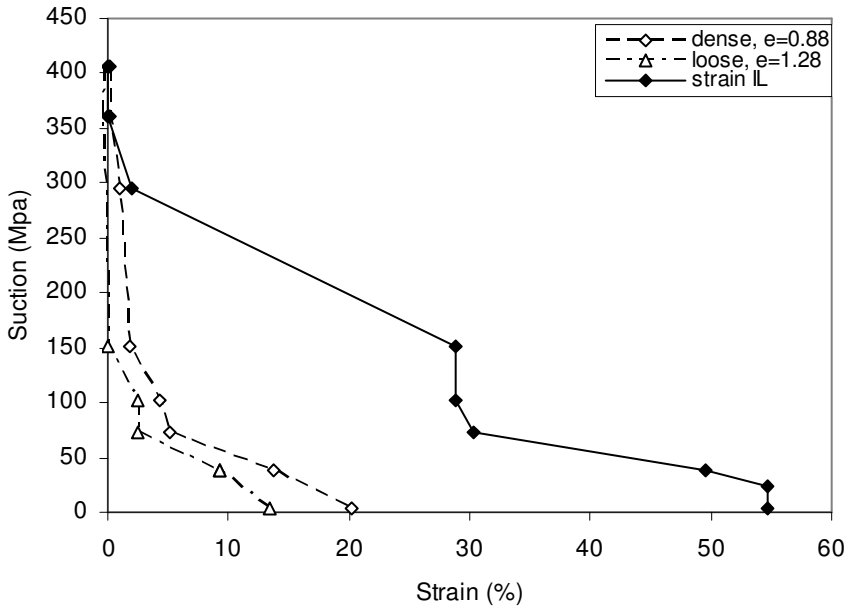

(a)

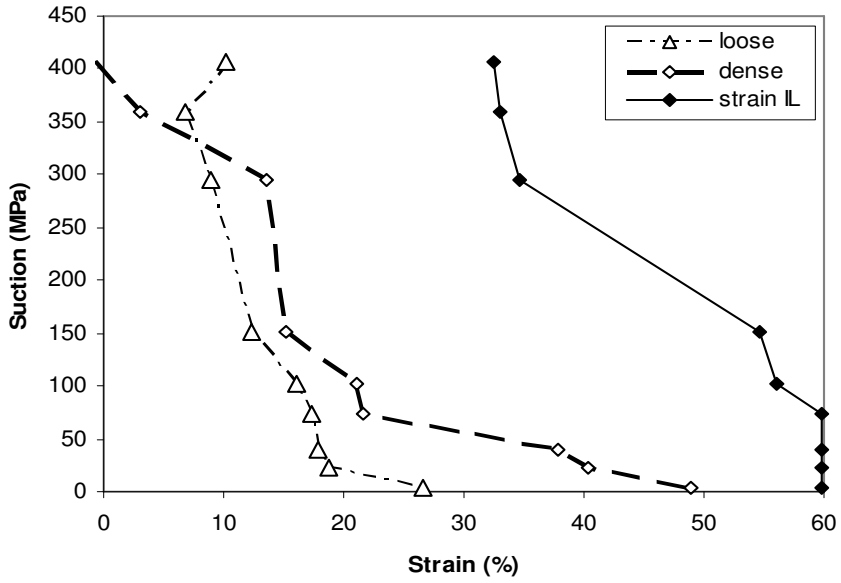

(b)

Figure 5.30. Microstructural and macrostructural swelling deformation for loose and dense a) Na-smectite, b) Ca-smectite.

Reversible and irreversible components of swelling deformation are studied in Figures 5.31 and 5.32 using loose and dense Na-smectite specimens as examples. Initial yield curves for the specimen are defined as LC_i and NL_i. When suction decreases, the stress Point 1 moves to Point 2. At this point, the yield locus NL_i has reached its final position NL_f. Microstructural swelling caused by the suction reduction produces a softer structure displacing LC_i towards its final position LC_f. Then, the soil cake followed a drying path 2 to 3 back to 405 MPa of suction. Only reversible strains occur, which means LC stays in its final position. Corresponding deformation and the variation of reversible and irreversible strains for both dense and loose samples is shown in Figure 5.32. Once again macrostructural strains are larger for the dense specimen because during wetting and drying paths the horizontal p distance to the LC curve is larger. In both cases, reversible strains are about 50% of the total strains.

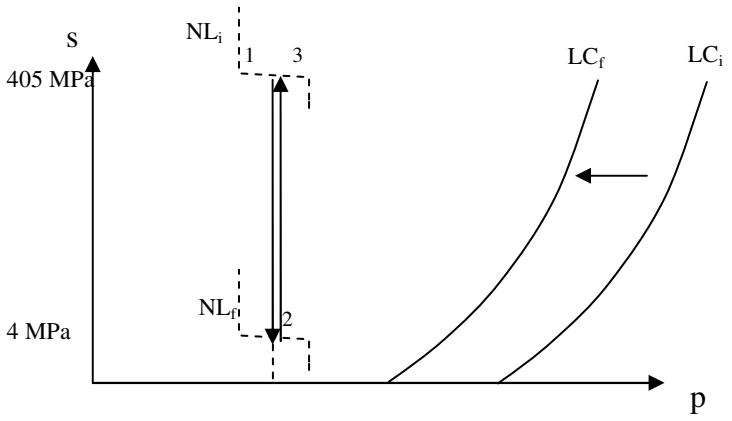

Figure 5.31. Stress paths in a wetting-drying cycle.

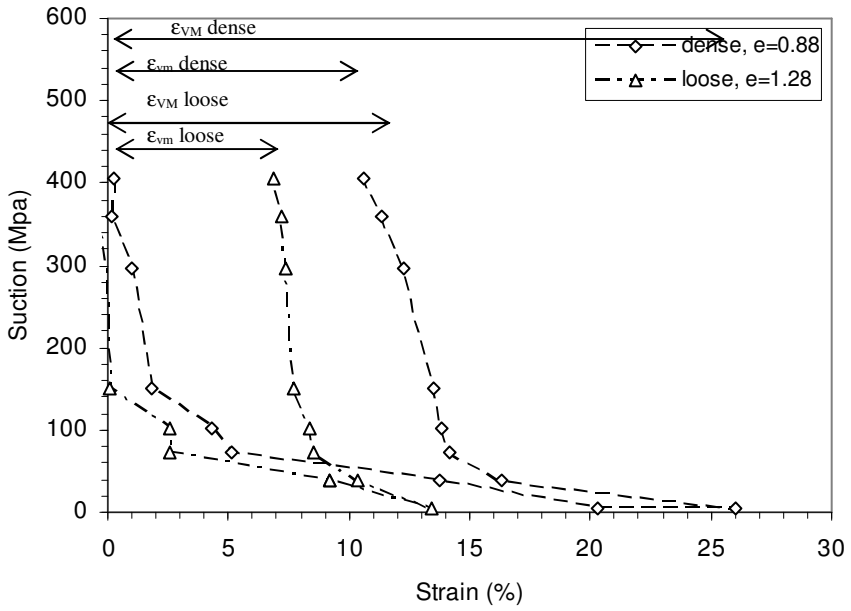

Figure 5.32. Swelling strains due to wetting/drying cycle for loose and dense Na-smectite samples.

Bulk volume changes in a sample are highly dependent on its stress history. Gens and Alonso (1992) postulated that at a given suction, the ratio of macrostructural / microstructural strains ($\varepsilon^P_{VM}/\varepsilon_{vm}$) is larger for $p/p_o = 0$ and it decreases to zero when p/p_o equal to 1 for a very open macrostructure. However, results from the free swelling tests indicate that although the overconsolidation ratio certainly affects the total strain in the sample, the initial density of the soil is also an important variable. For free swelling tests, loose and dense soil samples were tested at zero normal stress and different preconsolidation stress p_o. The ratio p/p_o is zero for both cases, but as it was observed, the $\varepsilon^P_{VM}/\varepsilon_{vm}$ ratio is significantly larger for the dense sample. This disagreement in the framework will probably occur also at low applied normal stresses. A specimen compacted at 400 kPa (loose) and tested at 40 kPa does not behave in the same way than a specimen compacted at 400 kPa (dense) and tested at 400 kPa, even though both have the same p/p_o ratio. In addition, other important variables that determine $\varepsilon^P_{VM}/\varepsilon_{vm}$ is the

interlayer cation and the clay fabric (i.e. number and length of mineral layers per quasicrystal).

The ratio $\varepsilon^{P}_{VM}/\varepsilon_{vm}$, which is equivalent to $\Delta e_T/\Delta e_{IL}$, is plotted as a function of the preconsolidation stress for the specimens tested under free swelling conditions. Results for Na and Ca-smectite at different suctions are presented in Figure 5.33. The ratio of macro and micro-structural strain decreases with lower values of p_o for all suction values during wetting; thus specimens with a more open structure exhibit lower $\varepsilon^{P}_{VM}/\varepsilon_{vm}$ ratio. It is also observed that as suction decreases, the $\varepsilon^{P}_{VM}/\varepsilon_{vm}$ ratio is larger in magnitude, and the ratio becomes more sensitive to the yield compaction stress p_o. During drying, the microstructural strain decreases while the macro-structure remains open, leading to higher $\varepsilon^{P}_{VM}/\varepsilon_{vm}$. In the case of Ca-smectite, the magnitude of $\varepsilon^{P}_{VM}/\varepsilon_{vm}$ is lower than for sodium smectite. In addition, the $\varepsilon^{P}_{VM}/\varepsilon_{vm}$ does not vary too much for dense and medium compacted samples, but a significant drop is observed for loosely compacted samples. Finally, $\varepsilon^{P}_{VM}/\varepsilon_{vm}$ during drying decreases, which indicates that the micro-structural strain in Ca-smectite has a larger contribution to the overall bulk volume change than that of Na-smectite.

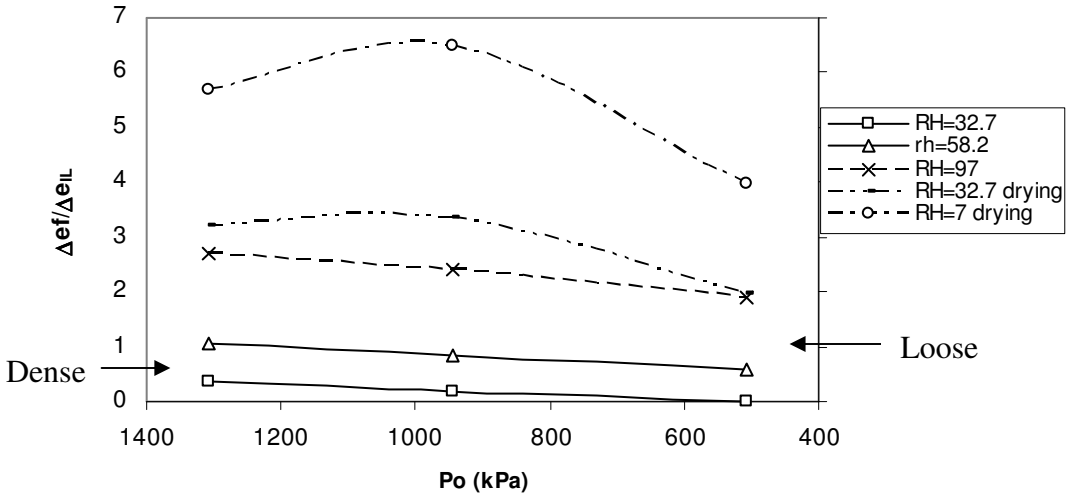

(a)

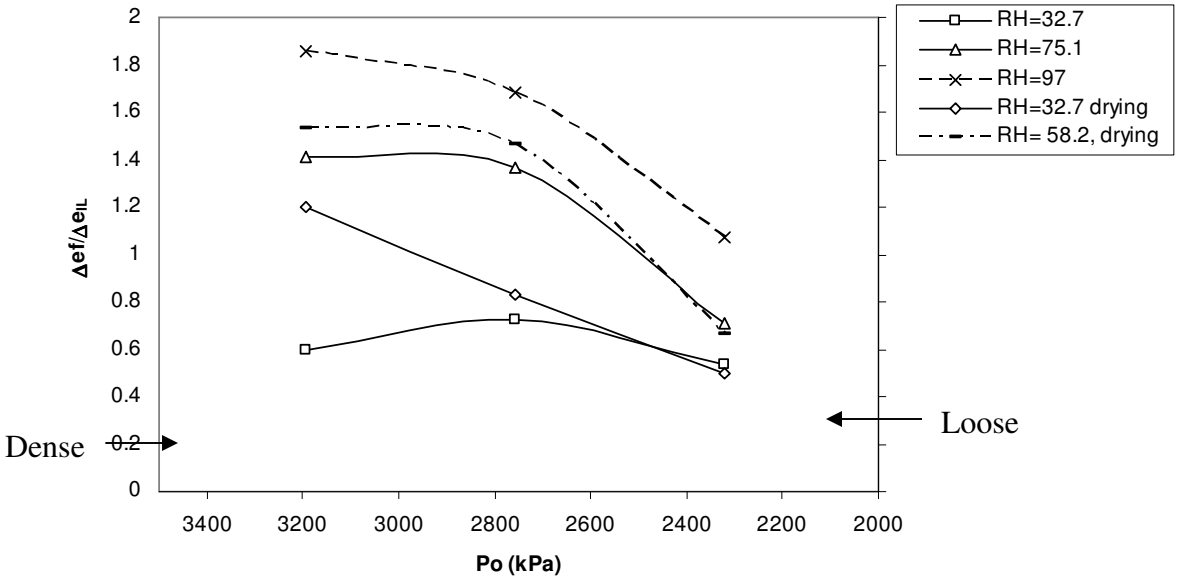

(b)

Figure 5.33. Dependence of the ratio between $\varepsilon^{P}_{VM}/\varepsilon_{vm}$ and the yield pressure p_o for a) Na-smectite, b) Ca-smectite

5.4.5. Bulk swelling pressure

Stress paths for specimens undergoing wetting under constant total volume boundary conditions are presented in Figures 5.34 and 5.35. Suction was reduced while at the same time an external load on the sample was continuously modified so no volumetric deformation occurs. Stress paths are plotted in the p,s space.

Figure 5.34 presents the data for loose and dense Na-smectite samples, where the maximum normal stress at compaction (p_o) was 1,332 kPa and 7,860 kPa for the loose and dense specimens respectively. The LC curves plotted with dotted lines are qualitatively drawn, since only one point in those curves is known. In this case the LC yield surface was not crossed by the stress paths but rather is located to the right in the p axis. When a suction decrement Δs is applied to the sample, a pressure increment Δp develops to maintain the constant volume. At higher suction values, larger decrements in suction are necessary to induce some change in swelling pressure, indicating a more rigid structure. The path followed is the result of deformations in the micro and macro structures. If only the microstructure was affected, the path followed would be the same as the NL. Larger swelling pressures were measured for the sample with an LC curve further away to the right (dense sample).

Data obtained for loose and dense Ca-smectite specimens exhibit a decrease in swelling pressure for suctions lower than 100 MPa (Figure 5.35.) Loading-collapse curves were qualitatively estimated, only the yield points of 1,332 kPa and 8,216 kPa during specimen compaction are known. The decrease in swelling pressure at 100 MPa suction is probably due to the stress path reaching the yield surface; at this point, collapsing strains dominate in magnitude other volume expansion contributions and the

stress paths follow the LC curve.

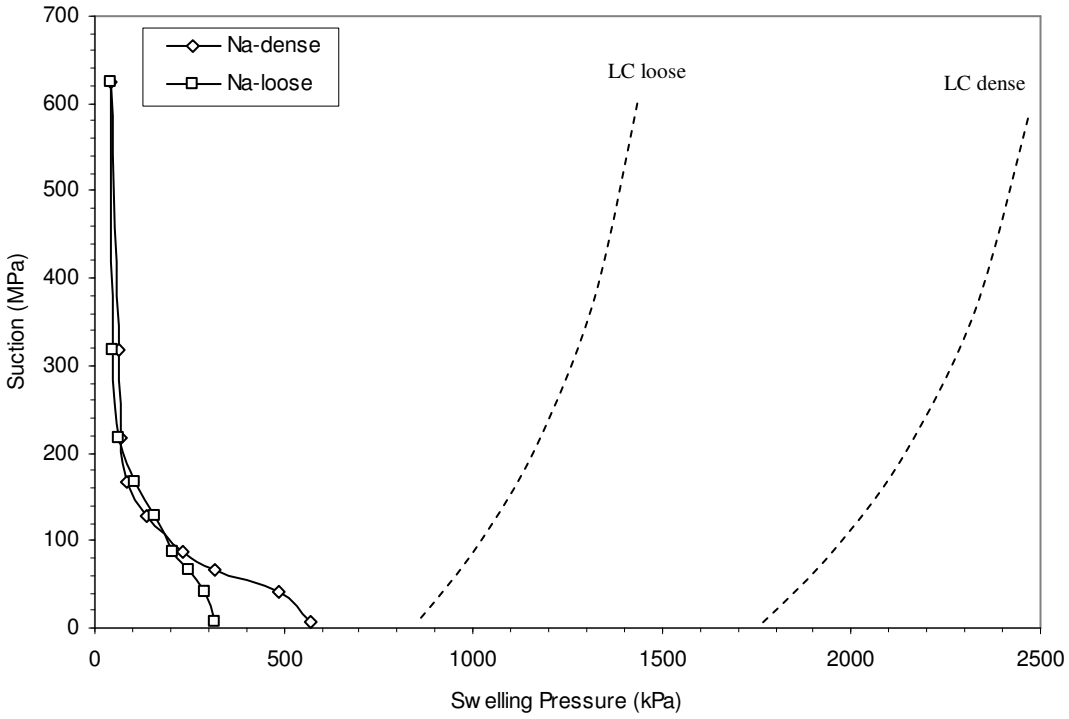

Figure 5.34. Stress path during constant volume wetting for Na-smectite

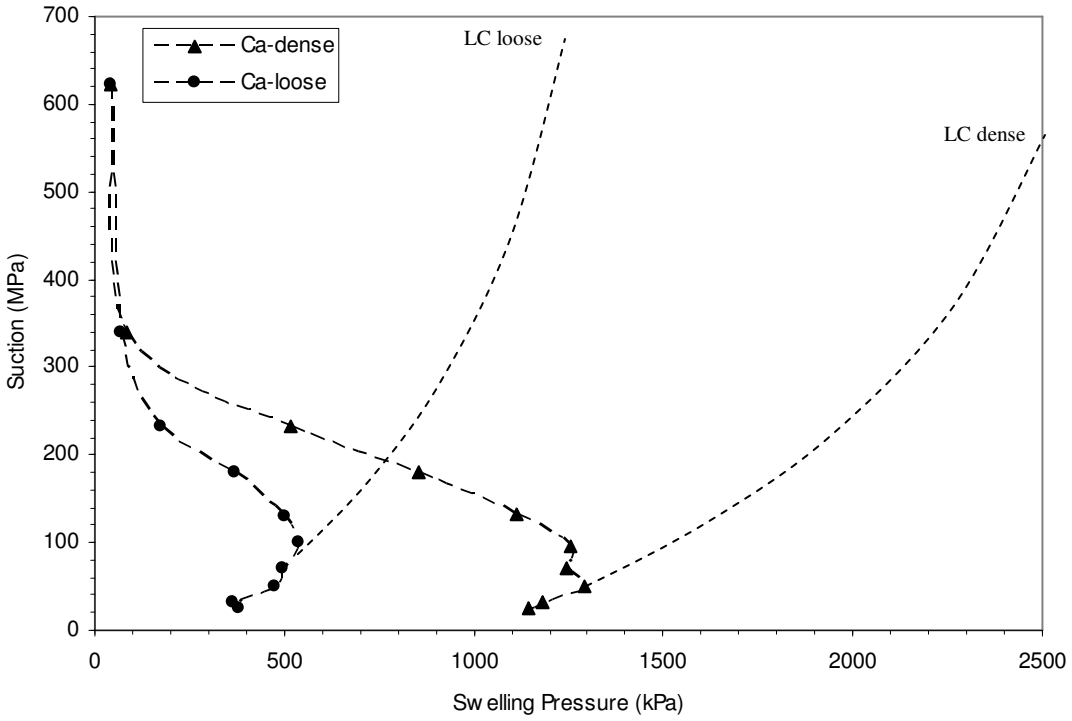

Figure 5.35. Stress path during constant volume wetting for Ca-smectite

Swelling deformations and pressures are highly dependent on the stress path followed by the sample (Justo et. al, 1984, Gens & Alonso, 1992). Interaction between two yield curves at different structural levels provides a tool to analyze and predict swelling clay behavior depending on the stress history of the sample. However, the fabric and chemistry of the clays are not accounted in the framework, both being very important variables in the translation from interlayer swelling to bulk volume changes or swelling pressures.

CHAPTER VI

SUMMARY, CONCLUSIONS AND RECOMMENDATIONS

6.1. Major observations and conclusions

This work contributes to the understanding of the effects that stress paths, initial density, clay mineralogy and exchange cation identity have in the effectiveness of how crystalline interlayer swelling upscales to macroscopic volume change and swell pressure response under controlled boundary stress conditions. Three types of clays were used in the experimental portion of the work: Na-smectite, Ca-smectite, and a calcium exchanged form of the sodium clay. Laboratory systems were developed to control suction (RH) conditions and to impose either free swelling or constant strain (zero volume change) boundary conditions. Experimental results were interpreted within the framework of three models: a fabric model for upscaling volume change (developed in this work), a multiscale porosity evolution model (Likos & Lu, 2006), and the Barcelona Basic Model (Gens & Alonso, 1992). A quantitative analysis was performed by defining curves describing constitutive curves for the behavior of smectite in the crystalline swelling regime. The major contributions, observations, and conclusions resulting from the research are summarized as follows:

1. An automated experimental system was designed and mobilized that is capable of controlling suction in a compacted clay specimen while maintaining boundary conditions that could be free swelling, constant stress, or constant strain. Suction control was achieved through regulation of RH in a closed environmental chamber. Axial deformation and water content change were measured for tests performed under free swelling conditions. Swelling pressure was measured for

tests performed under constant strain conditions. No tests under constant stress conditions were performed.

2. SEM imaging of sodium and calcium smectite provided qualitative information of particle size and pore fabric. Void space at scales of about 0.5μm and 5μm were observed, thus a multiscale porosity structure is evident.
3. Specimens compacted at initial pressures of 500 to 6400 kPa had initial void ratios of 1.34 to 0.68. Gravimetric water content at RH of 97% for Na-smectite specimens tested under free swelling conditions is around 32%. Axial strain at RH=97% is in the range of 12% to 25% for loose to dense samples. Measured swelling pressures range from 317 kPa to 573 kPa. In the case of Ca-smectite, gravimetric water corresponding to 85%RH is about 20%; this value increases to 30% for RH=97%. Axial strain for loose and dense Ca-smectite compacted samples range from 26% to 49%. Maximum swelling pressures measured were 538 kPa to 1294 kPa for "loose" and "dense" samples. Finally, the Ca-ion-exchange clay had 20% water content at 80%RH, with 8.1% axial strain. This information is valuable in geotechnical engineering; for example, the fact that smectite hydrates to about 30% of gravimetric water content indicates that packing and transporting geosynthetic clay liners (GCL) must be done under controlled low RH conditions for maintaining low water contents in the bentonite.
4. Sorption isotherms follow a wavy behavior corresponding to the one and two layer hydration states. Steeper portions in the curve for Na-smectite occurred at RH=10-30% and 60%-80%, corresponding to the 0-to-1 and 1-to-2 hydration layer transitions respectively. In the case of Ca-smectite, sorption isotherms

presented a steeper portion at RH of 5%-30% corresponding to the 1-to-2 hydration layer state.

5. Bulk volume change and swelling pressure behavior reflect the wavy behavior of the sorption isotherms. Results of Na-smectite specimens tested under free swelling conditions and analyzed in the context of the microstructural fabric model revealed that the internal acute angle of the parallelepiped (α) remains relatively constant until RH is greater than 33% (first hydration layer), whereupon the angle decreases by 1.6^{o} to 2.9^{o}. The next significant change in alpha occurs at RH=75%, corresponding to the second hydration layer. Likewise, $\Delta\alpha$ calculated for calcium-smectite undergoes greater change for RH=35%-45% coinciding with the 1-to-2 hydration layer state for Ca-smectite. For the three clays, changes in the interlayer and interparticle void space were observed at RH values corresponding to the hydration layer states. Significant increase in pressure was observed at these RH values.
6. Compaction density does not have significant effect on water vapor sorption behavior within the range of RH examined. A suite of ten sodium smectite specimens compacted at different initial densities was tested under free swelling conditions; sorption isotherms obtained for all ten samples are almost identical. Ten calcium smectite soil cakes were tested under similar conditions with similar results.
7. Compaction density has an appreciable effect on the behavior of bulk volume change under free swelling conditions. In general, the trend for both Na and Ca^{+2} smectite indicates that smaller bulk volume changes occur for specimens with

lower initial densities. The effect of compaction density is more evident for higher hydration layer states (larger RH values). These results are explained by considering that during the first layer transition most of the crystalline swelling was absorbed into the inter-particle void space, which may not be the case any more for the second layer hydration. Considering the microstructural model, the initial angle alpha was smaller for denser structures, but had the largest increment after hydration of the second layer. These observations are also consistent with the BBM, where the distance between the neutral loading line and the Load-Collapse is larger for denser specimens, implying larger deformations will occur when undergoing wetting. This information can be applied when the bulk volume change in clays needs to be minimized; for example, shallow foundations placed on expansive soils will undergo lower deformation if the clay underneath the foundation is loosely compacted.

8. Quantitatively, sodium smectite was evaluated for dense (e= 0.88), moderately dense (e=1.1), and loose (e=1.3) specimens at RH of 32.7%, 58%, and 97%. Results indicate that the effect of initial density for RH < 60% is minimal. Bulk volume change at RH=97% reflects a strong dependency between measured axial strain and initial void ratio. Axial strains for specimens with initial void ratios of 0.88 and 1.28 are 23% and 13%; thus the denser specimen undergoes about 40% more axial strain than the “loose” specimen. A similar analysis for calcium smectite specimens was performed. Results indicate that volume change response for Ca-smectite is more sensitive to initial void ratio than that of Na-smectite,

with a difference in axial strain deformation of up to 18% between the dense and loose specimens.

9. Hysteresis was observed in Na and Ca smectite results and was more evident for the Na-smectite. In general, denser specimens had larger hysteresis. This may be explained in the context of the microstructural fabric model where it was shown that during wetting, denser specimens undergo larger changes in α; however, the angle remains fairly constant during drying, leading to larger plastic strains. Thus, if a specimen follows a drying path, e_{IL} decreases corresponding to 2-to-1 and 1-to-0 hydration layer transitions, but e_{IP} remains fairly constant. Consideration of hysteresis is important in geotechnical engineering because most soils close to the surface are subjected to significant changes in RH.
10. Swelling pressure was measured for specimens undergoing wetting under constant strain boundary conditions. In general, swelling pressures were larger for Ca-smectite that those for Na-smectite. This was interpreted to result because Ca-smectite has more mineral layers per quasicrystal, implying larger interlayer swelling. Steeper portions in the swelling pressure vs RH curves were observed to correspond well with transitions in hydration layers.
11. The effect of initial compaction density on bulk swell pressure generation was investigated by conducting sorption tests under zero-volume-change boundary conditions. In the Na-smectite case, initial density becomes significant for RH>50%. Thus, during the first interlayer hydration, most of the increase in the interlayer void ratio (e_{IL}) is absorbed by the interparticle void ratio (e_{IP}) for both dense and loose specimens. A difference in macroscopic swelling between dense

and loose specimens was measured at RH corresponding to the second hydration layer state; crystalline swelling translates more effectively to macroscopic behavior for denser specimens due to their lower e_{IP}. Swelling pressures measured for Ca-smectite dense and loose specimens indicate that initial compaction density has a larger effect on Ca-smectite than on Na-smectite; this effect is apparent for RH>8%. Decrease in swelling pressure was observed for the Ca-smectite samples compacted to "dense" and "loose" specimens for RH>50%. This was explained in the context of the BBM by considering that the stress path reached the yield surface LC and so, at this point, collapsing strains dominate in magnitude over other volume expansion contributions and the stress paths follow the LC curve.

12. Clay mineralogy and exchange cation identity have a large effect on swelling and swelling pressures resulting from crystalline interlayer swelling. In general, Ca-smectite exhibits larger bulk volume changes and swelling pressures than Na-smectite for tests under the same stress and suction conditions. This behavior may be the result of higher number of mineral layers composing a quasicrystal in the Ca-smectite. It was also observed from the Ca-exchanged clay free swell test that the RH intervals corresponding to the hydration layer states depend on the interlayer cation. When comparing the axial deformations for the three clays compacted at e=0.88, results indicate that the Ca-exchanged specimen undergoes the least amount of macroscopic swelling. The exchange cation affects sorption response but it does not affect the volume change response. Thus, soils with

larger percentages of Ca-smectite are more likely to have larger bulk volume changes or swelling pressures for RH values lower than 95%.

13. Stress paths were considered at microstructural and macrostructural levels. Microstructural deformations are considered reversible and independent of the macrostructure, although the reverse is not true. In the normal stress-suction space, neutral loading paths (zero volumetric strain) for the microstructure follow a stepwise pattern corresponding to the 0-to-1 and 1-to-2-hydration layer states. The ratio of macrostructural strains to microstructural strains ($\varepsilon^{P}_{VM}/\varepsilon_{vm}$) decreases with lower values of maximum past pressure (p_o) for all suction values during wetting; thus specimens with a more open structure exhibit lower $\varepsilon^{P}_{VM}/\varepsilon_{vm}$ ratio. As suction decreases, the $\varepsilon^{P}_{VM}/\varepsilon_{vm}$ ratio is larger in magnitude, and it becomes more sensitive to the yield compaction stress p_o. During drying, the microstructural strain decreases while the macro-structure remains open, leading to higher $\varepsilon^{P}_{VM}/\varepsilon_{vm}$. This ratio has lower magnitude for Ca-smectite than that for Na-smectite. Thus, heavily overconsolidated clays will most likely undergo larger deformations with the increase of RH.
14. The behavior of more complicated natural soils and sediments with significant percentage of smectite will likely follow similar patterns than those of the pure smectite samples.

6.2. Recommendations for additional research

The following are topics that should be studied in future research:

1. Investigate swelling pressure for sodium and calcium, dense and loose specimens undergoing drying in RH=10% decrements. It is hypothesized that hysteresis will

be observed as well as steeper portions in the curve corresponding to the 2-to-1 and 1-to-0 transition layers. Data from these experiments would give more information on the elastic and plastic zones in the normal stress-suction plane.

2. Investigate axial strain deformation for sodium, calcium, and calcium-ion-exchanged smectite under constant stress (controlled stress) boundary conditions. The effect of initial density on these tests should also be examined by preparing specimens compacted to dense and loose conditions. The magnitude of the constant stress applied should be within the range of 500 kPa for the sodium smectite and 1200 kPa for the calcium smectite. It would be best if two sets of specimens were performed, with different constant stress boundary conditions. Results from these experiments would help complete a constitutive surface in the space of "e-normal stress-suction" for smectite in the crystalline swelling regime.
3. Obtain the Loading-Collapse (LC) curve for "dense" and "loose" sodium and calcium smectite specimens. Currently only one point in the LC curve is known. This new information would help quantify expected swelling in a sample by taking into account the distance between the given stress state of the sample and its corresponding yield curve.
4. At present, there is no framework that incorporates initial density, stress paths, and exchange cation identity into predicting the macroscopic effects of crystalline swelling. A new model that will help incorporate all these new data should be developed.
5. Iterative cycles (wetting and drying) for specimens tested under controlled stress boundary conditions should be investigated. This information would increase the

understanding of the role of stress paths in the macroscopic effects of interlayer swelling.

6. Investigate the behavior of non-ideal mixtures of multiple minerals, and compare their behavior with the obtain results. Adding some silt should have an effect as should adding clay-size particle of materials like quartz.

REFERENCES

Alonso, E.E., et. al., 1990, "A constitutive model for partially saturated soils," *Geothechnique,* Vol 40, pp 405-430.

ASTM, 2000, *Annual Book of ASTM Standards,* D-4318, Committee on Soils and Rock, West Conshohocken, PA.

Barshad, I., 1949, "The Nature of Lattice Expansion and Its Relation to Hydration in Montmorillonite and Vermiculite," *American Mineralogist*, Vol. 34, pp.675-684.

Berend, I., Cases, et. al., 1995, "Mechanism of adsorption and desorption of water vapor by homoionic montmorillonites," *Clays and Clay Minerals*, Vol, 43, pp. 324-336.

Bernier et. al., 1997, "Suction-controlled experiments on Boom clay", *Engineering Geology,* Vol 47, pp.325-328.

Bolt, G.H., 1956, "Physico-chemical Analysis of the Compressibility of Pure Clays," *Geotechnique*, Vol. 6, No. 2, pp.86-93.

Chen, F. H., 1988, *Foundations on Expansive Soils*. New York: American Elsevier Science Publishers.

Chipera, S.J., Carey, J.W., and Bish, D.L., 1997, "Controlled-Humidity XRD Analyses: Application to the Study of Smectite Expansion/Contraction," in *Advances in X-Ray Analysis*, J.V. Gilfrich *et al.* ed., p.713.

Collis-George, N. (1955) The hydration and dehydration of Na-montmorillonite (Belle Fourche). Journal of Soil Science, 6(1)

Cui, Y.J. et. al., 2002, "A model for the volume change behavior of heavily compacted swelling clays," *Engineering Geology*, Vol 54, pp.233-250.

Delage, P., Howat, M.D. and Cui, Y.J., 1998, "The relationship between suction and swelling properties in a heavily compacted unsaturated clay," *Engineering Geology*, Vol. 50, pp. 31-48.

Delville, A and Laszlo, P., 1990, "The origin of the swelling of clays by water," Am. Chem. Soc. Langmuir, 6(7), 1289-1294

Hunt, R.E., 1986, *Geotechnical Engineering Techniques and Practices,* McGraw Hill.

Gens A, Alonso EE., 1992, "A framework for the behaviour of unsaturated expansive clays," Canadian Geotechnical Journal; 29:1013–1032.

Israelachvili, J., 1992, *Intermolecular & Surface Forces*, Second Edition, Academic Press.

Justo, J.L., Delgado, A., and Ruiz, J., 1984, "The influence of stress-path in the collapse-swelling of soils at the laboratory," *Proceedings, 5th International Conference on Expansive Soils, Adelaide*, pp. 67-71.

Karaborni, S., Smit, B., Heidug, W., and van Oort, E., 1996, "The Swelling of Clays: Molecular Simulations of the Hydration of Montmorillonite," *Science*, Vol. 271, p.1102.

Kjellander, R., et. al., 1988, "Double-layer ion correlation forces restrict calcium-clay swelling," *J. Phy. Chem.*, 92, 6489-6492.

Likos, W.J., 2000, "Total suction – moisture content relationships for expansive clay," *Ph.D. Dissertation*, Colorado School of Mines, Golden, CO.

Likos, W. J. and Lu, N., 2003, "Automated Humidity System for Measuring Total Suction Characteristics of Clay," *Geotechnical Testing Journal*, Vol. 26, No. 2, pp. 179–190.

Likos, W.J., 2004, "Measurement of crystalline swelling in expansive clay." *Geotechnical Testing Journal*, **27**(6), 540-546.

Likos, W.J., and Lu, N., 2006, "Pore scale analysis of bulk volume change from crystalline swelling in Na^{+}- and Ca^{2+}-smectite," *Clays and Clay Minerals*, Vol. 54, No. 4, pp. 516 – 529.

Lloret A, Villar MV, Sa´ nchez M, Gens A, Pintado X, Alonso EE., 2003, " Mechanical behaviour of heavily compacted bentonite under high suction changes," *Ge´otechnique* 2003; 53(1):27–40.

Lu, N. and Likos, W.J., 2004, *Unsaturated Soil Mechanics*, John Wiley & Sons, Inc., Hoboken, New Jersey.

Marshall, C.E., 1949, "The Colloid Chemistry of the Silicate Minerals," *New York: Academic Press*, P. 54.

McKeen, R.G., 1992, "A Model for Predicting Expansive Soil Behavior," In *Proceedings of the 7th International Conference on Expansive Soils*, August 3-5, 1992, Dallas, Texas, Vol. 1, pp.1-6.

Miller, D. J., 1996, "Osmotic Suction as a Valid Stress State Variable in Unsaturated Soils." *Ph.D. dissertation*, Colorado State University, Fort Collins, CO.

Mitchell, J.K., 1993, "Fundamentals of Soil Behavior," *John Wiley*.

Mooney, R.W., Keenan, A.G., and Wood, L.A., 1952, "Adsorption of Water Vapour by Montmorillonite, I.," *J. Amer. Chem. Soc*., 74:1367.

Marshall, C. E.,1949, "*The colloid chemistry of the silicate mineral," New York: Academic Press*.

Madsen, F. T., and M.Muller-Vonmoos.,1989, "The swelling behavior of clays,". *Applied Clay Science*4:143–56.

McKeen, R.G., 1992, "A Model for Predicting Expansive Soil Behavior," In *Proceedings of the 7th International Conference on Expansive Soils*, August 3-5, 1992, Dallas, Texas, Vol. 1, pp.1-6.

Miller, D.J., 1996, "Osmotic suction as a valid stress state variable in unsaturated soils," Ph.D. dissertation, Colorado State University, Fort Collins, CO.

Moore, D.M., and Reynolds, R.C., 1997, "X-ray Diffraction and the Identification and Analysis of Clay Minerals," Oxford University Press.

Newman, A.C.D., ed., 1987, "Chemistry of Clays and Clay Minerals," *Wiley and Sons*.

Nishimura, T., and Fredlund, D. G., 2000, "Unconfined Compressive Strength of a Silty Soil and Kaolin below the Residual State," *Advances in Unsaturated Geotechnics*, ASCE Geotechnical Special Publication No. 99, pp. 262–274.

Norrish, K., 1954, "The Swelling of Montmorillonite," *Trans. Faraday Soc*. 18: pp.120-134.

Push R., 1982, "Mineral water-interaction and their influence on the physical behaviour of highly compacted Na bentonite," Canadian Geotechnical Journal; 19:381–387.

Quirk, J.P., and Aylmore, L.A.G., 1971, "Domains and Quasi-Crystalline Regions in Clay Systems", *Soil Science Society American Journal*, Vol. 35, pp.652-654.

Quirk, J.P., 1986, "Soil permeability in relation to sodicity and salinity." *Philosophical Transactions of the Royal Society of London*. A. 316, 297-317.

Romero E., 1999, "Characterisation and thermal-hydro-mechanical behaviour of unsaturated Boom clay: an experimental study," *Ph.D. Thesis*, Technical University of Catalonia, Spain, 1999.

Rizzi E, Giulio M, Willam K., 1996, " On failure indicators in multi-dissipative materials," *International Journal of Solids and Structures*; 33(20–22):3187–3214.

Rouquerol, F.,1999, "Adsorption by powders and porous solids: principles, methodology, and applications.," Academic Press, San Diego, California.

Saiyouri N, Hicher PY, Tessier D., 2000, " Microstructural approach and transfer water modelling in highly compacted unsaturated swelling clays," *Mechanics of Cohesive-Frictional Materials* ; 5:41–60.

Snethen, D.R., Johnson, L.D., and Patrick, D.M., 1977, "An Investigation of the Natural Microscale Mechanisms That Cause Volume Change in Expansive Clays," Federal Highway Administration Report No. FHWA-RD-77-75.

Tessier, D. (1990) "Behaviour and microstructure of clay minerals." in De Boodt, M. F., Hayes, M.H.B., Herbillon, A. (Eds). *Soil Colloids and their Associations in Aggregates*, Plenum Press, New York.

Tessier, D., 1991, "Electron microscope studies of clay microstructures," *Proceedings, NATO Advanced Research Workshop on Clay Swelling and Expansive Soils*, Cornell University, Ithaca, N.Y.

Tuller, M. and Or, D., 2003, "Hydraulic functions for swelling soils: pore scale considerations." *Journal of Hydrology*, 272, 50-71.

Van Olphen, H., 1963, "Compaction of Clay Sediments in the Range of Molecular Particle Distances," *Clays and Clay Minerals*, Vol. 11, pp.178-187.

Van Olphen, K., 1965, "Thermodynamics of Interlayer Adsorption of Water In Clays," *Journal of Colloid Science*, Vol. 20, pp.822-837.

Van Olphen, H.1977. *An introduction to clay colloid chemistry*. 2d ed.New York: John Wiley and Sons.

Villar, M.V., 2004, "Influence of temperature on the hydro-mechanical behaviour of a compacted bentonite," *Applied clay science*, Vol 26, Issues 1-4, pp. 337-350.

Wayllace, A., and Likos, W.J., 2007, "Microstructural model for up-scaling interlayer volume changes in expansive clay," *Proceedings of GeoDenver 2007*, ASCE, Denver, Colorado, in press.

Warketin, B.P. et. al., 1957, "*Swelling pressure of montmorillonite,"* Soil Sci. Soc. Proc.

Xie, M. et. al., 2004, "An upscaling method and a numerical analysis of swelling/shrinking processes in a compacted bentonite/sand mixture," *International Journal for Numerical and Analytical Methods in Geomechanics; 28:1479-1502.*

Xie, M. et. al., 2006, "Numerical Modelling of Swelling Pressure in Unsaturated Expansive Elasto-Plastic Porous Media," Center for Applied Geoscience Geohydrology/Hydroinformatics University of T¨ubingen, Germany.

Yong, R. N., & Mohamed, O. M., 1992, "A study of particle interaction energies in wetting of unsaturated expansive clays," *Geotechnical Research Center*, McGILLS University, Montreal.

Yong, R.N., "Soil suction and soil-water potentials in swelling clays in engineered clay barriers," *Geoenvironmental Engineering Research Centre*, Cardiff School of Engineering, University of Wales, Cardiff, UK

Young, J.F., 1967, "Humidity Control in the Laboratory Using Salt Solutions – A Review," *J. Appl. Chem.*, Vol. 17, pp.241-245.

VITA

Alexandra Wayllace obtained her B.S. in Civil Engineering and her Masters of Science in Systems Engineering with emphasis in Geotechnical Engineering from the Colorado School of Mines (CSM). Her Ph.D. in Geotechnical Engineering was obtained at the University of Missouri-Columbia (UMC) under the guidance of Dr. William Likos.

She is a Young Member of the Committee of Eng. Behavior of Unsaturated Soils in the Transportation Research Board, member of ASCE, she is recipient of one of six 2006 PCA Education Foundation Fellowships, received the Outstanding Graduate Student award at UMC and the Outstanding Graduating Senior Award in Civil Engineering from CSM. She was also a recipient of the Andes Scholarship for academic excellence.